

67

REPRINTED FROM

HANDBOOK ON SYNCHROTRON RADIATION

VOLUME 2

Edited by

GEOFFREY V. MARR

*Department of Physics, Natural Philosophy Building,
Aberdeen University, Aberdeen AB9 2UE, Scotland*



1987

NORTH-HOLLAND
AMSTERDAM · OXFORD · NEW YORK · TOKYO

CHAPTER 5

RESONANCES IN MOLECULAR PHOTOIONIZATION*

J.L. DEHMER

Argonne National Laboratory, Argonne, IL 60439, USA

A.C. PARR

*Synchrotron Ultraviolet Radiation Facility, National Bureau of Standards,
Gaithersburg, MD 20899, USA*

S.H. SOUTHWORTH

Los Alamos National Laboratory, Los Alamos, NM 87545, USA

Contents

| | |
|---|-----|
| 1. Introduction | 243 |
| 2. Shape resonances | 245 |
| 2.1. Overview | 245 |
| 2.2. Basic properties | 248 |
| 2.3. Eigenchannel plots | 255 |
| 2.4. Connections between shape resonances in electron–molecule scattering and in molecular photoionization | 260 |
| 3. Autoionization | 263 |
| 3.1. Overview | 263 |
| 3.2. MQDT treatment of H ₂ photoionization | 268 |
| 4. Triply differential photoelectron measurements – experimental aspects | 275 |
| 5. Case studies | 280 |
| 5.1. Shape-resonance-induced non-Franck–Condon effects in N ₂ 3σ _g photoionization | 280 |
| 5.2. Autoionization via the Hopfield series in N ₂ | 287 |
| 5.3. Continuum–continuum coupling effects in N ₂ 2σ _u photoionization | 294 |
| 5.4. Resonance effects in photoionization of the 1π _u level of C ₂ H ₂ | 297 |

Contents continued overleaf

* Work supported in part by the U.S. Department of Energy and the Office of Naval Research.

Handbook on Synchrotron Radiation, Vol. 2, edited by G.V. Marr
© Elsevier Science Publishers B.V., 1987

Contents continued

| | |
|---|-----|
| 5.5. Valence-shell photoionization of SF ₆ | 305 |
| 5.6. Valence-shell photoionization of BF ₃ | 318 |
| 6. Survey of related work | 330 |
| 7. Prospects for future progress | 334 |
| Appendix. A bibliography on shape resonances in molecular photoionization through early 1985 | 336 |
| References | 342 |

1. Introduction

Molecular photoionization is a rich source of information on fundamental intramolecular interactions. This is apparent when photoionization is viewed as a half-collision in which a collision complex, prepared by dipole excitation, decays by ejection of an electron from the field of the target. In the molecular case, the escaping electron must traverse the anisotropic molecular field and can undergo interactions with its nuclear modes. Hence, the photoelectron carries to the detector dynamical information on the two central aspects of molecular behavior – motion of an electron in a multicenter field and interplay among rovibronic modes.

Attention is invariably drawn to resonant photoionization mechanisms, such as shape resonances and autoionization. These resonant processes are important probes of photoionization for various reasons, the most obvious one being that they are usually displayed prominently against nonresonant behavior in such observables as the total photoionization cross section, photoionization branching ratios, and photoelectron angular distributions. More importantly, resonances temporarily trap the excited complex in a quasibound state, causing the excited electron to traverse the molecular core many times before its escape by tunneling or by exchange of energy with the core. In this way, resonances amplify the subtle dynamics of the electron–core interactions for more insightful analysis.

The last decade has witnessed remarkable progress in characterizing dynamical aspects of molecular photoionization. From among the great variety of successful streams of work, one can identify four broad classes which together have propelled the recent activities in this field. *First*, the extensive measurements of total photoabsorption/photoionization cross sections from the VUV to the X-ray range by a variety of means (see, e.g., Koch and Sonntag 1979 and a bibliography of inner-shell spectra by Hitchcock 1982, and original literature cited below) have continually provided fresh impetus to account for novel features displayed in molecular oscillator strength distributions. *Second*, shape resonances have emerged as a major focal point in the study of molecular photoionization dynamics. Initially stimulated by observations of intense, broad peaks in inner-shell spectra, beginning in the late sixties, the study of shape resonances in molecular photoionization has grown into a vigorous subfield. (A bibliography of papers discussing shape resonances in molecular photoionization is presented in the Appendix, along with an indication of the molecule(s) treated in each.) Benefitting greatly from the timely development of realistic, independent-electron models (Dehmer and Dill 1979b, Langhoff 1979, Raseev et al. 1980, Lucchese et al. 1982, Levine and Soven 1983, Collins and Schneider 1984, Levine and Soven 1984, Lynch et al. 1984b, Schneider and Collins 1984, Dill and Dehmer 1974, Lucchese et al. 1980, Lucchese and McKoy 1981c, Richards and Larkins 1984) for treating molecular photoionization, studies in this area have not only accounted

for the features in the total photoionization spectra of both inner and outer shells, but also have predicted and confirmed several manifestations in other physical observables as discussed below. *Third*, multichannel quantum defect theory (MQDT) was adapted (Fano 1970, Dill 1972, Herzberg and Jungen 1972, Atabek et al. 1974, Fano 1975, Jungen and Atabek 1977, Dill and Jungen 1980, Guisti-Suzor and Lefebvre-Brion 1980, Jungen 1980, Jungen and Dill 1980, Raoult et al. 1980, Jungen and Raoult 1981, Raoult and Jungen 1981, Giusti-Suzor 1982, Lefebvre-Brion and Giusti-Suzor 1983, Raoult et al. 1983, Raseev and Le Rouzo 1983, Giusti-Suzor and Fano 1984a,b, Giusti-Suzor and Jungen 1984, Giusti-Suzor and Lefebvre-Brion 1984, Jungen 1984a,b, Mies 1984, Mies and Julienne 1984, Lefebvre-Brion et al. 1985) to molecular photoionization, providing a framework for the quantitative and microscopic analysis of autoionization phenomena. This powerful theoretical framework has been successfully applied to a number of prototype diatomic molecules, yielding both insight into the detailed dynamics of resonant photoionization and some specific predictions for experimental testing by means discussed in the next item. *Fourth*, technical advances, especially the development of intense synchrotron radiation sources (Kunz 1979, Winick and Doniach 1980, Koch 1983), have made it feasible to perform triply differential photoelectron measurements (see, e.g., Marr et al. 1979, White et al. 1979, Parr et al. 1980, Krause et al. 1981, Derenbach et al. 1983, Morin et al. 1983, Parr et al. 1983, 1984) on gas phase atoms and molecules. By this we mean that photoelectron measurements are made as a function of three independent variables – incident photon wavelength, photoelectron energy, and photoelectron ejection angle. Variable wavelength permits the study of photoionization at and within spectral features of interest. Photoelectron energy analysis permits separation and selection of individual (ro)vibronic ionization channels. Measurement of photoelectron angular distributions accesses dynamical information, i.e., relative phases of alternative degenerate ionization channels, that is not present in integrated cross sections. This level of experimental detail approaches that at which theoretical calculations are done and, hence, permits us to isolate and study dynamical details which are otherwise swamped in integrated or averaged quantities. We emphasize that, although the current trend is toward use of synchrotron radiation for variable wavelength studies, a variety of light sources have been successfully used to study photoionization dynamics. For example, in the shape resonance literature cited in the Appendix, many of the pioneering measurements were carried out with laboratory sources. Likewise, although most current measurements of vibrational branching ratios and angular distributions within autoionizing resonances employ synchrotron radiation (see, e.g., Morin et al. 1982a,b, Carlson et al. 1983b, Marr and Woodruff 1976, Woodruff and Marr 1977, Baer et al. 1979, Codling et al. 1981, Ederer et al. 1981, Parr et al. 1981, West et al. 1981, Parr et al. 1982b, Truesdale et al. 1983b, Hubin-Franskin et al. 1984), many early and ongoing studies with traditional light sources have made significant observations of the effects of autoionization on vibrational branching ratios (Doolittle and Schoen 1965, Price 1968, Berkowitz and Chupka 1969, Collin and Natalis 1969, Blake et al. 1970, Bahr et al. 1971a,b,

Carlson 1971, Collin et al. 1972, Kleimenov et al. 1972, Gardner and Samson 1973, Tanaka and Tanaka 1973, Gardner and Samson 1974a,b, Caprace et al. 1976, Natalis et al. 1977, Gardner and Samson 1978, Eland 1980, Kumar and Krishnakumar 1981, 1983) and angular distributions (Carlson 1971, Carlson and Jonas 1971, Morgenstern et al. 1971, Carlson and McGuire 1972, Carlson et al. 1972, Niehaus and Ruf 1972, Hancock and Samson 1976, Mintz and Kuppermann 1978, Katsumata et al. 1979, Kibel et al. 1979, Sell et al. 1979, Kreile and Schweig 1980).

Here we review recent progress in this field with emphasis on resonant mechanisms and on the interplay between experiment and theory. Sections 2 and 3 discuss elementary aspects of shape resonances and autoionization, respectively. Section 4 describes experimental aspects of triply differential photoelectron measurements which are currently the major source of new data in this field. Section 5 describes particular case studies of molecular photoionization, chosen to focus on a variety of basic resonant mechanisms that are both under active study currently and likely to form main themes in the future. Whereas these case studies draw heavily upon results of the authors' program at the National Bureau of Standards' SURF-II Facility, section 6 surveys related work with a much broader perspective, stressing aspects which are often unique to other groups. Finally, section 7 offers some thoughts about future directions of research within and beyond the present limitations of this field.

2. Shape resonances

2.1. Overview

Shape resonances are quasibound states in which a particle is temporarily trapped by a potential barrier, through which it may eventually tunnel and escape. In molecular fields, such states can result from so-called "centrifugal barriers", which block the motion of otherwise free electrons in certain directions, trapping them in a region of space with molecular dimensions. Over the past few years, this basic resonance mechanism has been found to play a prominent role in a variety of processes in molecular physics, most notably in photoionization and electron scattering. As discussed more fully in later sections, the expanding interest in shape resonant phenomena arises from a few key factors:

First, shape resonance effects are being identified in the spectra of a growing and diverse collection of molecules and now appear to be active somewhere in the observable properties of most small (nonhydride) molecules. Examples of the processes which can exhibit shape resonant effects are X-ray and VUV absorption spectra, photoelectron branching ratios and photoelectron angular distributions (including vibrationally resolved), Auger electron angular distributions (Dill et al. 1980), elastic electron scattering (Bardsley and Mandl 1968, Schulz 1973, 1976, Lane 1980, Shimamura and Takayanagi 1984), vibrational excitation by electron impact (Dehmer and Dill 1980, Bardsley and Mandl 1968, Schulz 1973, 1976,

Lane 1980, Shimamura and Takayanagi 1984), and so on. Thus concepts and techniques developed in any of these contexts can be used extensively in molecular physics.

Second, being quasibound inside a potential barrier on the perimeter of the molecule, such resonances are localized, have enhanced electron density in the molecular core, and are uncoupled from the external environment of the molecule. This localization often produces intense, easily studied spectral features, while suppressing the nearby continuum and/or Rydberg structure and, as discussed more fully below, has a marked influence on vibrational behavior. In addition, localization causes much of the conceptual framework developed for shape resonances in free molecules to apply equally well (Dehmer and Dill 1979a) to photoionization and electron scattering and to other states of matter such as adsorbed molecules (Davenport 1976a,b, Dill et al. 1976, Davenport et al. 1978, Gustafsson et al. 1978b, Gustafsson 1980b, Stöhr and Jaeger 1982, Gustafsson 1983, Stöhr et al. 1983, 1984, Koestner et al. 1984, Carr et al. 1985), molecular solids (Blechschmidt et al. 1972, Dehmer 1972, Lau et al. 1982, Fock 1983, Fock et al. 1984, Fock and Koch 1984, 1985), and ionic crystals (Åberg and Dehmer 1973, Pulm et al. 1985).

Third, resonant trapping by a centrifugal barrier often imparts a well-defined orbital momentum character to the escaping electron. This can be directly observed, e.g., by angular distributions of scattered electrons (Bardsley and Mandl 1968, Schulz 1973, 1976, Lane 1980, Shimamura and Takayanagi 1984) or photoelectron angular distributions from oriented molecules (Davenport 1976a,b, Dill et al. 1976, Gustafsson et al. 1978b, Gustafsson 1980b, 1983), and shows that the centrifugal trapping mechanism has physical meaning and is not merely a theoretical construct. Recent case studies have revealed trapping of $l = 1$ to $l = 5$ components of continuum molecular wavefunctions. The purely molecular origin of the great majority of these cases is illustrated by the prototype system N_2 discussed in section 2.2.

Fourth, the predominantly one-electron nature of the phenomena lends itself to theoretical treatment by realistic, independent-electron methods (Dehmer and Dill 1979b, Langhoff 1979, Raseev et al. 1980, Lucchese et al. 1982, Levine and Soven 1983, 1984, Collins and Schneider 1984, Lynch et al. 1984b, Schneider and Collins 1984, Dill and Dehmer 1974, Lucchese et al. 1980, Lucchese and McKoy 1981c, Richards and Larkins 1984), with the concomitant flexibility in terms of complexity of molecular systems, energy ranges, and alternative physical processes. This has been a major factor in the rapid exploration in this area. Continuing development of computational schemes also holds the promise of elevating the level of theoretical work on molecular ionization and scattering and, in doing so, to test and quantify many of the independent-electron results and to proceed to other circumstances, such as weak channels, coupled channels, multiply-excited states, etc., where the simpler schemes become invalid.

The earliest and still possibly the most dramatic examples of shape resonance effects in molecules are the photoabsorption spectra of the sulfur K- (LaVilla and Deslattes 1966, LaVilla 1972) and L-shells (Zimkina and Fomichev 1966, Zimkina

and Vinogradov 1971, Blechschmidt et al. 1972, LaVilla 1972) in SF_6 . The sulfur L-shell absorption spectra of SF_6 and H_2S are shown in fig. 1 to illustrate the type of phenomena that originally drew attention to this area. In fig. 1 both spectra are plotted on a photon energy scale referenced to the sulfur L-shell ionization potential (IP) which is chemically shifted by a few eV in the two molecular environments, but lies near $h\nu \sim 175$ eV. The ordinate represents relative photoabsorption cross section and the two curves have been adjusted so that the integrated oscillator strength for the two systems is roughly equal in this spectral range, since absolute calibrations are not known. The H_2S spectrum is used here as a "normal" reference spectrum since hydrogen atoms normally do not contribute appreciably to shape resonance effects and, in this particular context, can be regarded as weak perturbations on the inner-shell spectra of the heavy atom. Indeed, the H_2S photoabsorption spectrum exhibits a valence transition, followed by partially resolved Rydberg structure, which converges to a smooth continuum. The gradual rise at threshold is attributable to the delayed onset of the " $2p \rightarrow \epsilon d$ " continuum which, for second row atoms, will exhibit a delayed onset prior to the occupation of the 3d subshell. This is the qualitative behavior one might well expect for the absorption spectrum of a core level.

In sharp contrast to this, the photoabsorption spectrum of the same sulfur 2p subshell in SF_6 shows no vestige of the "normal" behavior just described. Instead, three intense, broad peaks appear, one below the ionization threshold and two above, and the continuum absorption cross section is greatly reduced elsewhere.

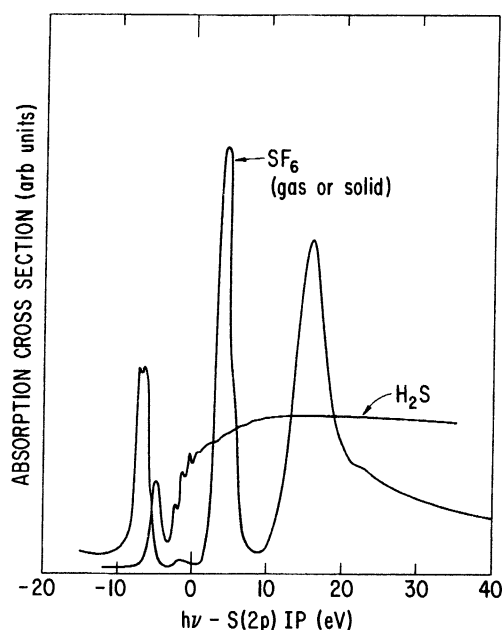


Fig. 1. Photoabsorption spectra of H_2S (from Zimkina and Vinogradov 1971) and SF_6 (from Blechschmidt et al. 1972) near the sulfur $L_{2,3}$ edge.

Moreover, no Rydberg structure is apparent, although an infinite number of Rydberg states must necessarily be associated with any positively charged molecular ion. Actually, Rydberg states superimposed on the weak bump below the IP were detected (Nakamura et al. 1971) using photographic detection, but obviously these states are extremely weak in this spectrum. This radical reorganization of the oscillator strength distribution in SF_6 was interpreted (Nefedov 1970, Dehmer 1972) in terms of potential barrier effects, resulting in three shape-resonantly enhanced final-state features of a_{1g} , t_{2g} , and e_g symmetry, in order of increasing energy. Another shape resonant feature of t_{1u} symmetry is prominent in the sulfur K-shell spectrum (LaVilla and Deslattes 1966) and, in fact, is believed to be responsible for the weak feature just below the IP in fig. 1 owing to weak channel interaction. Hence, four prominent features occur in the photoexcitation spectrum of SF_6 as a consequence of potential barriers caused by the molecular environment of the sulfur atom. Another significant observation (Blechschmidt et al. 1972) is that the SF_6 curve in fig. 1 represents both gaseous and solid SF_6 , within experimental error bars. This is definitive evidence that the resonances are eigenfunctions of the potential well inside the barrier, and are effectively uncoupled from the molecule's external environment.

2.2. Basic properties

The central concept in shape resonance phenomena is the single-channel, barrier-penetration model familiar from introductory quantum mechanics. In fact, the name "shape resonance" means simply that the resonance behavior arises from the "shape", i.e., the barrier and associated inner and outer wells, of a local potential. The basic shape resonance mechanism is illustrated schematically (Child 1974) in fig. 2. In the figure an effective potential for an excited and/or unbound electron is shown to have an inner well at small distances, a potential barrier at intermediate distances, and an outer well (asymptotic form not shown) at large separations. In the context of molecular photoionization, this would be a one-dimensional abstraction of the effective potential for the photoelectron in the field of a molecular ion. Accordingly, the inner well would be formed by the partially screened nuclei in the molecular core and would therefore be highly anisotropic and would overlap much of the molecular charge distribution, i.e., the initial states of the photoionization process. The barrier, in all well-documented cases, is a so-called centrifugal barrier. (Other forces such as repulsive exchange forces, high concentrations of negative charge, etc., may also contribute, but have not yet been documented to be pivotal in the molecular systems studied to date.) This centrifugal barrier derives from a competition between repulsive centrifugal forces and attractive electrostatic forces and usually resides on the perimeter of the molecular charge distribution where the centrifugal forces can compete effectively with electrostatic forces. Similar barriers are known for d- and f-waves in atomic fields (Fano and Cooper 1968), however, the l (orbital angular momentum) character of resonances in molecular fields can be higher than those of constituent atoms owing to the larger spatial extent of the molecular charge

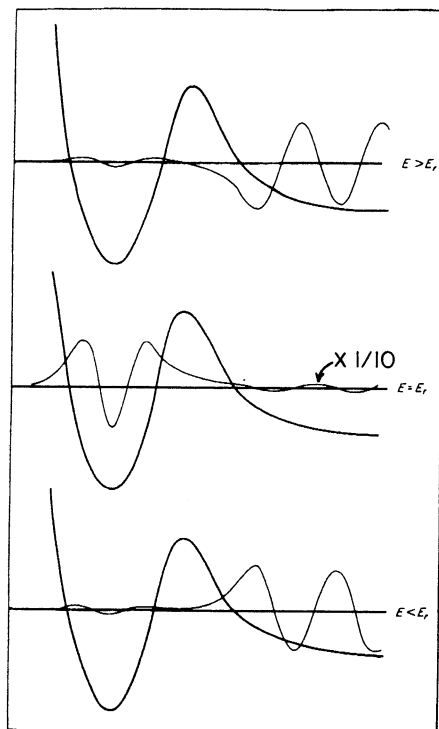


Fig. 2. Schematic of the effect of a potential barrier on an unbound wavefunction in the vicinity of a quasibound state at $E = E_r$ (adapted from Child 1974). In the present context, the horizontal axis represents the distance of the excited electron from the center of the molecule.

distribution, e.g., see the discussion in connection with N_2 photoionization below. The outer well lies outside the molecule where the Coulomb potential ($\sim -r^{-1}$) of the molecular ion again dominates the centrifugal terms ($\sim r^{-2}$) in the potential. We stress that this description has been radically simplified to convey the essential aspects of the underlying physics. In reality effective barriers to electron motion in molecular fields occur for particular l components of particular ionization channels and restrict motion only in certain directions. Specific examples which illustrate alternative types of centrifugal barriers in molecular fields are discussed below in connection with N_2 , BF_3 , and SF_6 .

Focusing now on the wavefunctions in fig. 2, we see the effect of the potential barrier on the wave mechanics of the photoelectron. For energies below the resonance energy, $E < E_r$ (lower part of fig. 2), the inner well does not support a quasibound state, i.e., the wavefunction is not exponentially decaying as it enters the classically forbidden region of the barrier. Thus the wavefunction begins to diverge in the barrier region and emerges in the outer well with a much larger amplitude than that in the inner well. When properly normalized at large r , the amplitude in the molecular core is very small, so we say this wavefunction is

essentially an eigenfunction of the outer well although small precursor loops extend inside the barrier into the molecular core.

At $E = E_r$, the inner well supports a quasibound state. The wavefunction exhibits exponential decay in the barrier region so that if the barrier extended to $r \rightarrow \infty$, a true bound state would lie very near this total energy. Therefore the antinode that was not supported in the inner well at $E < E_r$, has traversed the barrier to become part of a quasibound waveform which decays monotonically until it re-emerges in the outer well region, much diminished in amplitude. This "barrier penetration" by an antinode produces a rapid increase in the asymptotic phase shift by $\sim \pi$ radians and greatly enhances the amplitude in the inner well over a narrow band of energy near E_r . Therefore at $E = E_r$, the wavefunction is essentially an eigenfunction of the inner well although it decays through the barrier and re-emerges in the outer well. The energy halfwidth of the resonance is related to the lifetime of the quasibound state and to the energy derivative of the rise in the phase shift in well-known ways. Finally, for $E > E_r$, the wavefunction reverts to being an eigenfunction of the outer well as the behavior of the wavefunction at the outer edge of the inner well is no longer characteristic of a bound state.

Obviously this resonant behavior will cause significant physical effects: the enhancement of the inner-well amplitude at $E \sim E_r$ results in good overlap with the initial states which reside mainly in the inner well. Conversely, for energies below the top of the barrier but not within the resonance halfwidth of E_r , the inner amplitude is diminished relative to a more typical barrier-free case. This accounts for the strong modulation of the oscillator strength distribution in fig. 1. Also, the rapid rise in the phase shift induces shape resonance effects in the photoelectron angular distribution. Another important aspect is that eigenfunctions of the inner well are localized inside the barrier and are substantially uncoupled from the external environment of the molecule. As mentioned above, this means that shape resonant phenomena often persist in going from the gas phase to the condensed phase (e.g., fig. 1), and, with suitable modification, shape resonances in molecular photoionization can be mapped (Dehmer and Dill 1979a) onto electron-scattering processes and vice versa. Finally, note that this discussion has focussed on total energies from the bottom of the outer well to the top of the barrier, and that no explicit mention was made of the asymptotic potential, which determines the threshold for ionization. Thus valence or Rydberg states in this energy range can also exhibit shape resonant enhancement, even though they have bound state behavior at large r , beyond the outer well.

We will now turn, for the remainder of this section, to the specific example of the well-known σ_v shape resonance in N_2 photoionization, which was the first case for which shape resonant behavior was demonstrated (Dehmer and Dill 1975) in a diatomic molecule and has since been used as a prototype in studies of various shape resonance effects as discussed below. To identify the major final-state features in N_2 photoionization at the independent-electron level, we show the original calculation (Dehmer and Dill 1975, 1976a) of the K-shell photoionization spectrum performed with the multiple-scattering model. This calculation agrees

qualitatively with all major features in the experimental spectrum (Wight et al. 1972/73, 1976, Kay et al. 1977, Hitchcock and Brion 1980a), except a narrow band of double excitation features, and with subsequent calculations, using more accurate techniques (Langhoff 1984, Lynch et al. 1984b, Schneider and Collins 1984). The four partial cross sections in fig. 3 represent the four dipole-allowed channels for K-shell (IP = 409.9 eV) photoionization. Here we have neglected the localization (Bagus and Schaefer 1972, Lozes et al. 1979) of the K-shell hole since it does not greatly affect the integrated cross section, and the separation into u and g symmetries both helps the present discussion and is rigorously applicable to the subsequent discussion of valence-shell excitation. (Note that the identification of shape resonant behavior is generally easier in inner-shell spectra, since the problems of overlapping spectra, channel interaction, and zeros in the dipole matrix element are reduced relative to valence-shell spectra.)

The most striking spectral feature in fig. 3 is the first member of the π_g sequence, which dominates every other feature in the theoretical spectrum by a factor of ~ 30 . (Note that the first π_g peak has been reduced by a factor of 10 to fit in the frame.) The concentration of oscillator strength in this peak is a centrifugal

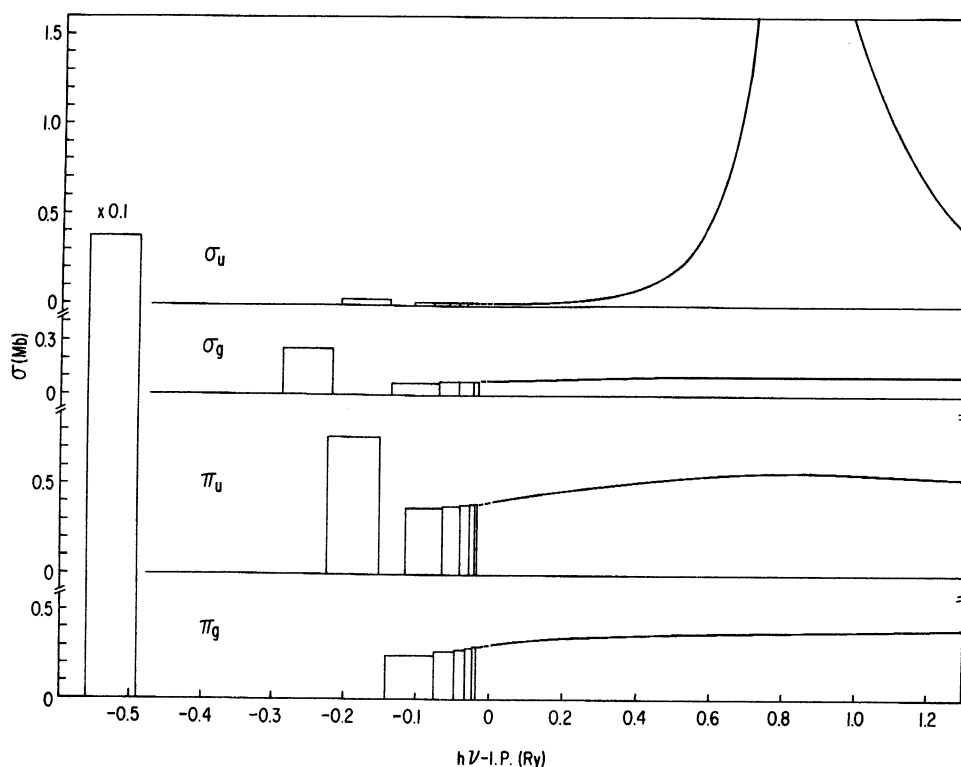


Fig. 3. Partial photoionization cross sections for the four dipole-allowed channels in K-shell photoionization of N_2 . Note that the energy scale is referenced to the K-shell IP (409.9 eV) and is expanded twofold in the discrete part of the spectrum.

barrier effect in the d-wave component of the π_g wavefunction. The final state in this transition is a highly localized state, about the size of the molecular core, and is the counterpart of the well-known (Bardsley and Mandl 1968, Schulz 1973, 1976, Lane 1980, Shimamura and Takayanagi 1984) π_g shape resonance in e-N₂ scattering at 2.4 eV. For the latter case, Krauss and Mies (1970) demonstrated that the effective potential for the π_g elastic channel in e-N₂ scattering exhibits a potential barrier due to the centrifugal repulsion acting on the dominant $l = 2$ lead term in the partial-wave expansion of the π_g wavefunction. In the case of N₂ photoionization, there is one less electron in the molecular field to screen the nuclear charge so that this resonance feature is shifted (Dehmer and Dill 1979a) to lower energy and appears in the discrete. It is in this sense that we refer to such features as “discrete” shape resonances. The remainder of the π_g partial cross section consists of a Rydberg series and a flat continuum. The π_u and σ_g channels both exhibit Rydberg series, the initial members of which correlate well with partially resolved transitions in the experimental spectrum below the K-shell IP.

The σ_u partial cross section, on the other hand, was found to exhibit behavior rather unexpected for the K shell of a first-row diatomic. Its Rydberg series was extremely weak, and an intense, broad peak appeared at ~ 1 Ry above the IP in the low-energy continuum. This effect is caused by a centrifugal barrier acting on the $l = 3$ component of the σ_u wavefunction. The essence of the phenomena can be described in mechanistic terms as follows: the electric dipole interaction, localized within the atomic K shell, produces a photoelectron with angular momentum $l = 1$. As this p-wave electron escapes to infinity, the anisotropic molecular field can scatter it into the entire range of angular momentum states contributing to the allowed σ and π ionization channels ($\Delta l = 0, \pm 1$). In addition, the spatial extent of the molecular field, consisting of two atoms separated by 1.1 Å, enables the $l = 3$ component of the σ_u continuum wavefunction to overcome its centrifugal barrier and penetrate into the molecular core at a kinetic energy of ~ 1 Ry. This penetration is rapid, a phase shift of $\sim \pi$ occurring over a range of ~ 0.3 Ry. These two circumstances combine to produce a dramatic enhancement of photoelectron current at ~ 1 Ry kinetic energy, with predominantly f-wave character.

The specifically molecular character of this phenomenon is emphasized by comparison with K-shell photoionization in atomic nitrogen and the united-atom case, silicon. In contrast to N₂, there is no mechanism for the essential p-f coupling, and neither atomic field is strong enough to support resonant penetration of high- l partial waves through their centrifugal barriers. (With substitution of “d” for “f”, this argument applies equally well to the d-type resonance in the discrete part of the spectrum.) Note that the π_u channel also has an $l = 3$ component but does not resonate. This underscores the directionality and symmetry dependence of the trapping mechanism.

To place the σ_u resonance in a broader perspective and show its connection with high energy behavior, we show, in fig. 4, an extension of the calculation in fig. 3 to much higher energy. Again, the four dipole-allowed channels in D_{∞h} symmetry are shown. The dashed line is two times the atomic nitrogen K-shell

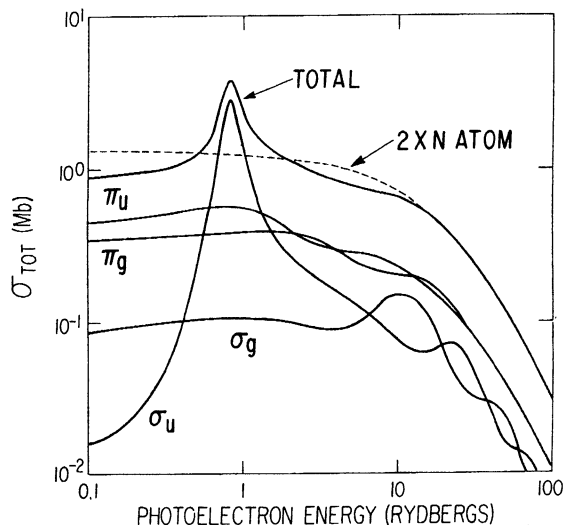


Fig. 4. Partial photoionization cross sections for the K-shell of N_2 over a broad energy range. The dashed line represents twice the K-shell photoionization cross section for atomic nitrogen, as represented by a Hartree-Slater potential.

cross section. Note that the modulation about the atomic cross section, caused by the potential barrier, extends to ~ 100 eV above threshold before the molecular and atomic curves seem to coalesce.

At higher energies, a weaker modulation appears in each partial cross section. This weak modulation is a diffraction pattern, resulting from scattering of the photoelectron by the neighboring atom in the molecule, or, more precisely, by the molecular field. Structure of this type was first studied over 50 years ago by Kronig (Kronig 1931, 1932, Azaroff 1963) in the context of metal lattices. It currently goes by the acronym EXAFS (extended X-ray absorption fine structure) and is used extensively (Kunz 1979, Winick and Doniach 1980, Koch 1983, Teo and Joy 1981, Lee et al. 1981) for local structure determination in molecules, solids, and surfaces. The net oscillation is very weak in N_2 , since the light atom is a weak scatterer. More pronounced effects are seen, e.g., in K-shell spectra (Kincaid and Eisenberger 1975) of Br_2 and $GeCl_4$. Our reason for showing the weak EXAFS structure in N_2 is to show that the low-energy, resonant modulation (called "near-edge" structure in the context of EXAFS) and high-energy EXAFS evolve continuously into one another and emerge naturally from a single molecular framework, although the latter is usually treated from an atomic point-of-view.

Figure 5 shows a hypothetical experiment which clearly demonstrates the l character of the σ_u resonance. In this experiment, we first fix the nitrogen molecule in space and orient the polarization direction of a photon beam, tuned near the nitrogen K-edge, along the molecular axis. This orientation will cause photoexcitation into σ final states, including the resonant σ_u ionization channel. The figure shows the angular distribution of photocurrent as a function of both

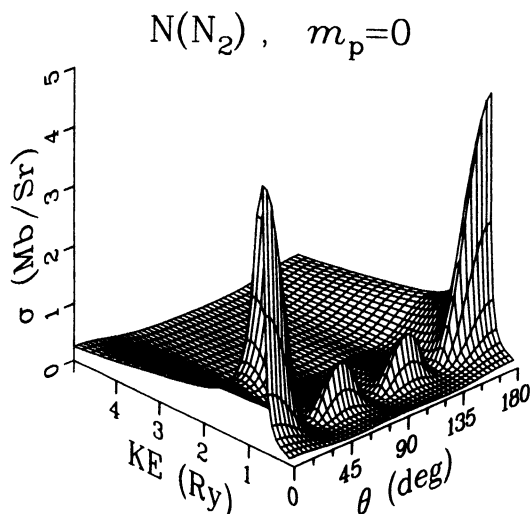


Fig. 5. Fixed-molecule photoelectron angular distribution for kinetic energies 0–5 Ry above the K-shell IP of N_2 . The polarization of the ionizing radiation is oriented along the molecular axis in order to excite the σ continua and the photoelectron ejection angle, θ , is measured relative to the molecular axis.

excess energy above the K-shell IP and angle of ejection, θ , relative to the molecular axis. Most apparent in fig. 5 is the enhanced photocurrent at the resonance position, $KE \sim 1$ Ry. Moreover the angular distribution exhibits three nodes, with most of the photocurrent exiting the molecule along the molecular axis and none at right angles to it. This is an f-wave ($l=3$) pattern and indicates clearly that the resonant enhancement is caused by an $l=3$ centrifugal barrier in the σ_u continuum of N_2 . Thus the centrifugal barrier has observable physical meaning and is not merely a theoretical construct. Note that the correspondence between the dominant asymptotic partial wave and the trapping mechanism is not always valid, especially when the trapping is on an internal or off-center atomic site where the trapped partial wave can be scattered by the anisotropic molecular field into alternative asymptotic partial waves, e.g., BF_3 (Swanson et al. 1981a) and SF_6 . Finally, note that the hypothetical experiment discussed above has been approximately realized by photoionizing molecules adsorbed on surfaces. The shape resonant features tend to survive adsorption and, owing to their observable l -character, can even provide evidence (Gustafsson et al. 1978b, Gustafsson 1980b, 1983) as to the orientation of the molecule on the surface. A related family of measurements on adsorbed molecules record total absorption/ionization measurements as a function of the polarization direction of the light (see, e.g., Stöhr and Jaeger 1982, Stöhr et al. 1983, 1984, Koestner et al. 1984, Carr et al. 1985). This utilizes the symmetry properties of shape-resonance-enhanced absorption features to indicate the relative orientation of the molecular axis and the polarization direction. In the example cited above, the large enhancement above the K-edge of N_2 will occur only when the polarization is parallel to the molecular axis.

In this section, we have utilized the σ_u ($l=3$) shape resonance in N_2 to illustrate the basic concepts underlying shape resonance phenomena. This resonance is supported by a barrier on the perimeter of the molecular charge distribution, which acts on the $l=3$ component of the σ_u continuum wavefunction. It is important to realize that potential barriers in molecular fields can also take different forms. For instance, the t_{2g} and e_g shape resonances in SF_6 (sections 2.1 and 5.5) result from the trapping of $l=2$ waves on the central sulfur atom. Although the trapping is associated with an atomic site, the molecular field plays a crucial role in modifying the potential in the vicinity of the barrier, relative to the free atom. This is manifested in two ways. First, in an isolated sulfur atom, the $l=2$ wave will penetrate its potential barrier over a much broader energy range centered at higher kinetic energy, thus greatly diminishing the resonance effect. Second, the symmetry of the molecular field splits the $l=2$ resonance into the crystal-field pair of t_{2g} and e_g quasibound states. In such a case, the d-wave trapping may not be clearly manifested in the asymptotic wave function, i.e., at the detector, since the departing d-wave may be rescattered into other partial waves by the anisotropic molecular field containing six fluorine atoms. Another type of potential barrier in molecules is illustrated by the e' shape resonance in BF_3 (section 5.6). In this case, the essential trapping mechanism was found (Swanson et al. 1981a) to involve the $l=1$ component on the fluorine site. This off-center trapping site also causes rescattering of the trapped wave before it reaches the detector. In addition, the off-center trapping mechanism permits the trapping of a p wave in photoionization, for which the Coulomb potential would dominate the $l=1$ centrifugal potential, were they centered on the same origin. These are only three examples, intended to create a broader perspective with which to approach new cases, which are likely to produce yet other types of barriers to photoelectron motion in molecular fields.

Finally, we would like to emphasize an intimate connection which exists between shape resonances and unoccupied valence states in quantum chemistry language (Langhoff 1984). This was dramatically demonstrated over ten years ago, when Gianturco et al. (1972) interpreted the shape resonances in SF_6 photoionization using unoccupied virtual orbitals in an LCAO-MO calculation. This connection is a natural one since shape resonances are localized within the molecular charge distribution and therefore can be realistically described by a limited basis set suitable for describing the valence MOs. However, the scattering approach used in the shape resonance picture is necessary for analysis of various dynamical aspects of the phenomena discussed above.

2.3. Eigenchannel plots

The next topic in the discussion on basic properties of shape resonances involves eigenchannel contour maps (Loomba et al. 1981), or "pictures" of unbound electrons. This is the continuum counterpart of contour maps of bound-state electronic wavefunctions which have proven so valuable as tools of quantum chemical visualization and analysis. Indeed, the present example helps achieve a

physical picture of the σ_u shape resonance, and the general technique promises to be a useful tool for analyzing resonant trapping mechanisms and other observable properties in the future (see also Hermann and Langhoff 1981). The key to this visualization, given in eq. (5) below is the construction of those particular combinations of continuum orbital momenta that diagonalize the interaction of the unbound electron with the anisotropic molecular field. These combinations, known as eigenchannels, are the continuum analogues of the eigenstates in the discrete spectrum, i.e., the bound states.

The electronic eigenvalue problem in the molecular continuum is inhomogeneous, i.e., there is a solution at every energy. Moreover, there are, in general, alternative solutions possible at a given energy, depending on how the inhomogeneity is chosen. Typically, calculations are done in terms of real, oscillatory radial functions for the alternative possible orbital momenta. The result is the K -matrix-normalized partial-wave expansion of the continuum electronic wavefunction, which takes the asymptotic form (Dehmer and Dill 1979b, Dill and Dehmer 1974, Newton 1966)

$$\Psi_L \sim (\pi k)^{-1/2} r^{-1} \sum_{L'} (\sin \theta_L \delta_{LL'} + K_{LL'} \cos \theta_L) Y_{L'}(\hat{r}), \quad (1)$$

where $L = (l, m)$ is the photoelectron orbital momentum and its projection along the molecular z axis, and k^2 is the electron kinetic energy in rydberg. The electron distance r from the molecular center is given in bohr; $\theta_L = kr - l\pi/2 + \omega$, where the Coulomb phase, $\omega = -(Z/k) \ln(2kr) + \arg \Gamma[l + 1 - i(Z/k)]$ and the molecular ion charge, $Z = 1$. The coefficients $K_{LL'}$ of the cosine terms form a real, symmetric matrix known as the K matrix. The K matrix reflects the coupling between different angular momenta due to the nonspherical molecular potential, and, as such, summarizes in a compact way the electron-molecule interaction. That single orbital momentum L (we refer here to l and m collectively as orbital momentum) for which there occurs a sine term specifies the inhomogeneity, and each choice of L gives a row of the K matrix. By determining all rows in this way we obtain the full K matrix and thereby a complete set of functions at the given energy.

The wavefunction (1) specifies what might be called a calculational boundary condition. Its form allows us to obtain the K matrix while working in terms of real radial functions. There are two other types of boundary conditions (Dehmer and Dill 1979b, Dill and Dehmer 1974, Newton 1966) however: physical boundary conditions, appropriate for representing physical observables, and eigenchannel boundary conditions, appropriate for analysis of the continuum wavefunction itself. The sets of wavefunctions for these alternative three types of boundary conditions are interrelated by unitary transformations.

Physical boundary conditions are introduced to obtain physical observables. One transforms to complex radial functions so that the directional character of the continuum electron at large distances, where it is detected, can be represented. This so-called S matrix boundary condition and its use in representing electron-molecule scattering and molecular photoionization is discussed by, e.g., Dill and

Dehmer (1974) and by Dehmer and Dill (1976b). Physical boundary conditions are not well suited, however, for analysis of the continuum wavefunction itself. What is needed, rather, are the “normal modes” of the interaction of the continuum electron with the molecule, the eigenchannels of the electron–molecule complex. These are obtained by diagonalizing the K matrix, viz.

$$\tan(\pi\mu_\alpha)\delta_{\alpha\alpha'} = \sum_{LL'} U_{\alpha L} K_{LL'} U_{L'\alpha'}, \quad (2)$$

to give the eigenvectors Ψ_α and eigenphases μ_α . The coefficients $U_{L\alpha}$ give the composition of the alternative eigenvectors Ψ_α in terms of the K matrix normalized functions Ψ_L , viz.

$$\Psi_\alpha = \sum_L \Psi_L U_{L\alpha}. \quad (3)$$

Using eq. (2) and the fact that the matrix U is unitary, i.e.,

$$\delta_{LL'} = \sum_\alpha U_{L\alpha} U_{\alpha L'}, \quad (4)$$

we can rewrite the eigenvectors as (Newton 1966)

$$\Psi_\alpha \sim (\pi k)^{-1/2} r^{-1} \sum_L [\sin \theta_l + \tan(\pi\mu_\alpha) \cos \theta_l] Y_L(\hat{r}) U_{L\alpha}. \quad (5)$$

This equation is the key result of this discussion. Because molecules are not spherical, an electron of a particular angular momentum is in general “rescattered” into a range of angular momenta. This rescattering is indicated in eq. (1) by the sum over L' , and the coefficients $K_{LL'}$ give the relative amplitudes of the various rescatterings. The eigenchannel functions (5), on the other hand, correspond to those special combinations of incident angular momenta which are unchanged by the anisotropic potential of the molecule, i.e., the normal (eigen)-modes of the electron–molecule interaction.

Comparison of eq. (5) with eq. (1), then, shows why the eigenchannel representation (5) is more suitable for analysis of the continuum molecular electronic wavefunction. *First*, as we have seen, the mixing of different orbital momenta is greatly simplified. *Second*, the radial wavefunctions for different angular momenta all have the same mixing coefficient $\tan(\pi\mu_\alpha)$. *Third*, if an eigenchannel is dominated by a particular orbital momentum, then the eigenchannel wavefunction (5) has the characteristic angular pattern of the corresponding spherical harmonic. *Last*, and perhaps most important, because quasibound shape-resonant states generally resonate in a single eigenchannel α , the eigenchannel representation gives us the most direct image of these resonant states.

As discussed earlier, the σ_u resonance is accompanied by a corresponding rise by about π radians in one component of the eigenphase sum,

$$\mu_{\text{sum}} = \sum_\alpha \mu_\alpha. \quad (6)$$

This resonant component is in turn composed almost entirely of the single partial wave $l = 3$,

$$U_{L\alpha_{\text{res}}} \approx \delta_{l3} . \quad (7)$$

At these kinetic energies only one other orbital momentum, $l = 1$, contributes appreciably to the photoelectron wavefunction. (Orbital momenta $l = 0, 2, 4$, etc. do not contribute because they are of even parity, and $l = 5$ and higher odd orbital momenta are kept away from the molecule by centrifugal repulsion.) This means that there is only one other appreciable eigenchannel. Its eigenphase component, primarily $l = 1$, is nearly constant throughout the resonant region. Thus, within about 20 eV above the ionization threshold, the N_2 odd-parity continuum can be analyzed in terms of just two eigenchannels, a nonresonant p-like channel and a resonant f-like channel.

In fig. 6 we have plotted the p-like eigenchannel wavefunction for two kinetic energies, one below (top) and one at (bottom) the resonance, which in this calculation falls at ~ 1.2 Ry. The molecule is in the y - z plane, along the z axis. The surface contours have been projected onto the plane to show more clearly the angular variation of the wavefunction. The single nodal plane characteristic of p waves is clearly seen in this projection. It is remarkable that, despite the complex l -mixing induced by the anisotropic molecular potential, this eigenchannel has such a well-defined ($l = 1$) orbital-momentum character. The cusps in the surface mark the positions of the nuclei. The only apparent change from one surface to the other is the slight shortening of wavelength as the kinetic energy increases. This smooth contraction of nodes continues monotonically through the resonance energy to higher energies. We conclude from fig. 6 that the p eigenchannel is indeed nonresonant.

The f-like eigenchannel, plotted in fig. 7, shows a strikingly different behavior. Now the surfaces whose contours have at large distance the three nodal planes characteristic of f orbitals, show clearly the resonant nature of the f eigenchannel. Again note the clear emergence of a single ($l = 3$) orbital-momentum character over the whole wavefunction. Below and above (not shown) the resonance energy, the probability amplitude is roughly similar to that of the p-wave-dominated eigenchannel. But at the resonance energy there is an enormous enhancement of the wavefunction in the molecular interior; the wavefunction now resembles a molecular bound-state probability amplitude distribution. It is this enhancement, in the region occupied by the bound states, that leads to the very large increase in oscillator strength indicative of the resonance, and to the other manifestations discussed earlier and in subsequent sections.

These eigenchannel plots are discussed more fully elsewhere (Loomba et al. 1981); however, before leaving the subject, several points should be noted. *First*, the N_2 example that we have chosen is somewhat special in that there is a near one-to-one correspondence between the eigenchannels and single values of orbital angular momentum. Orbital angular momentum is, however, not a "good" quantum number in molecules and more generally we should not always expect

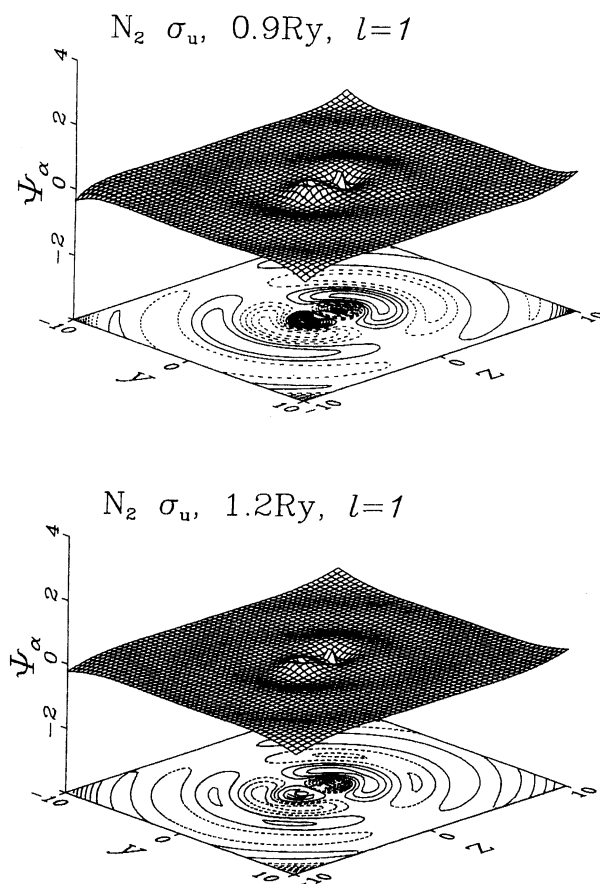


Fig. 6. The p-wave-dominated eigenchannel wavefunctions for two electron kinetic energies in the σ_u continuum of N_2 . The molecule is in the y - z plane, along the z axis, centered at $y = z = 0$. Contours mark steps of 0.03 from 0.02 to 0.29; solid: positive, dashed: negative.

such clear nodal patterns. Frequently, several angular momenta contribute to the continuum eigenchannels (although a barrier in only one l component will be primarily responsible for the temporary trapping that causes the enhancement in that and coupled components) and this means that the resulting eigenchannel plots will be correspondingly richer. *Second*, eqs. (1) and (5) are asymptotic expressions. The orbital momentum composition of these wavefunctions is more complicated in the molecular interior, as seen, e.g., in figs. 6 and 7. Nonetheless, continuity and a dominant l may, as in the case of N_2 , cause the emergence of a distinct l pattern, even into the core region. *Third*, while these ideas were developed (Loomba et al. 1981) in the context of molecular photoionization, the continuum eigenchannel concept carries over without any fundamental change to electron-molecule scattering. This is a further example of the close connection (Dehmer and Dill 1979a) between shape resonances in molecular photoionization

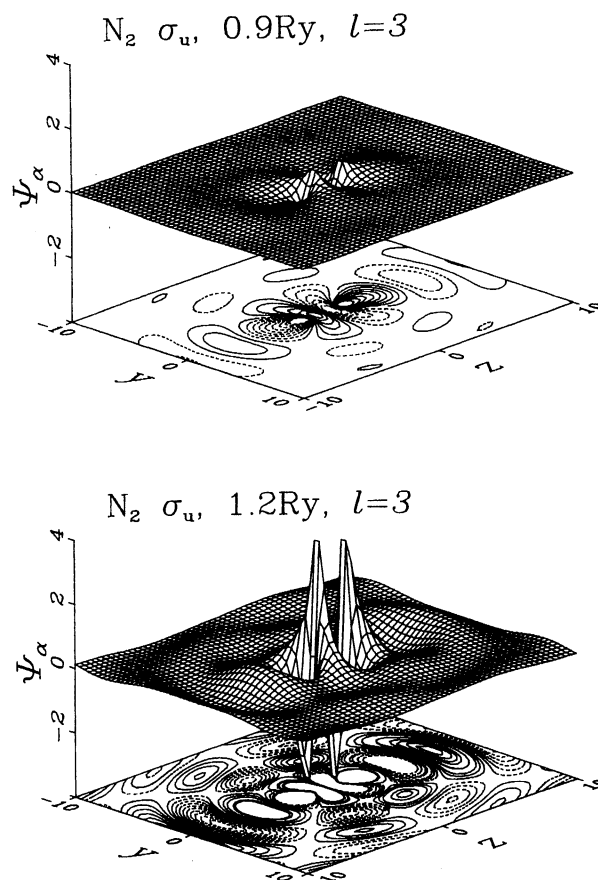


Fig. 7. The f-wave-dominated eigenchannel wavefunctions for nonresonant (top) and resonant (bottom) electron kinetic energies in the σ_u continuum of N_2 . The molecule is in the y - z plane, along the z axis, centered at $y = z = 0$. Contours mark steps of 0.03 from 0.02 to 0.29; solid: positive, dashed: negative. The lack of contour lines for 1.2 Ry near the nuclei is because of the 0.29 cutoff.

and electron-molecule scattering. *Finally*, while we have used one-electron wavefunctions here, obtained with the multiple-scattering model, the eigenchannel concept is a general one and we may look forward to its use in the analysis of more sophisticated, many-electron molecular continuum wavefunctions.

2.4. Connections between shape resonances in electron-molecule scattering and in molecular photoionization

At first glance, there is little connection between shape resonances in electron-molecule scattering ($e + M$) and those in molecular photoionization ($h\nu + M$). The two phenomena involve different numbers of electrons and the collision velocities are such that all electrons are incorporated into the collision complex.

Hence, we are comparing a neutral molecule and a molecular negative-ion system. However, although the long-range part of the scattering potential is drastically different in the two cases, the strong short-range potential is not drastically different since it is dominated by the interactions among the nuclei and those electrons common to both systems. Thus, shape resonances which are localized in the molecular core substantially maintain their identity from one system to another, but are shifted in energy owing to the difference caused by the addition of an electron to the molecular system. This unifying property of shape resonances thus links together the two largest bodies of data on the molecular electronic continuum: $h\nu + M$ and $e + M$, and although these resonances shift in energy in going from one class to another and manifest themselves in somewhat different ways, this link permits us to transfer information between the two. This can serve to help interpret new data and even to make predictions of new features to look for experimentally. Actually, this picture (Dehmer and Dill 1979a) was surmised empirically from evidence contained in survey calculations on $e + M$ and $h\nu + M$ systems and, in retrospect, from data. These observations can be summarized as follows: By and large, the systems $h\nu + M$ and $e + M$ display the same manifold of shape resonances, only those in the $e + M$ system are shifted ~ 10 eV to higher electron energy. Usually, there is one shape resonance per symmetry for a subset of the symmetries available. The shift depends on the symmetry of the state, indicating, as one would expect, that the additional electron is not uniformly distributed. Finally, there is substantial proof that the l -character is preserved in this process, although interaction among alternative components in a scattering eigenchannel can vary and thus alter the l mixing present.

There are several good examples available to illustrate this point – N_2 , CO, CO_2 , BF_3 , SF_6 , etc. In general, one can start from either the neutral or the negative ion system, but, in either case, there is a preferred way to do so: In the $h\nu + M$ case, it is better to examine the inner-shell photoabsorption and photoionization spectra. Shape resonances almost invariably emerge most clearly in this context. Additional effects, discussed briefly at the end of this section, frequently make the role of shape resonances in valence-shell spectra more complicated to interpret. In the $e + M$ case, a very sensitive indicator of shape resonance behavior is the vibrational excitation channel. Vibrational excitation is enhanced by shape resonances (Bardsley and Mandl 1968, Schulz 1973, 1976, Lane 1980, Shimamura and Takayanagi 1984) and is typically very weak for nonresonant scattering. Hence, a shape resonance, particularly at intermediate energy (10–40 eV) (Dehmer and Dill 1980, Dill et al. 1979b) may be barely visible in the vibrationally and electronically elastic scattering cross section, and yet be displayed prominently in the vibrationally inelastic electronically elastic cross section.

Two examples will help illustrate these points. In $e-SF_6$ scattering, the vibrationally elastic scattering cross section has been calculated theoretically (Dehmer et al. 1978) and shown to have four shape resonances of a_{1g} , t_{1u} , t_{2g} , and e_g symmetry at approximately 2, 7, 13, and 27 eV, respectively. The absolute total cross section measured by Kennerly et al. (1979) shows qualitative agreement,

although the evidence for the e_g resonance is marginal. (This resonance might be more evident in a vibrational excitation spectrum, which is not available.) Hence, using the guidelines given above, one would expect shape resonance features in the $h\nu + M$ case at -8 , -3 , 3 , and 17 eV (on the kinetic energy scale) to a very crude, first approximation. Indeed, the K- and L-shell photoabsorption spectra of SF_6 show such intense features, as discussed in an earlier section. This correlation is indicated (Fock and Koch 1985) in fig. 8, along with approximate resonance positions in the valence-shell spectra, for which the evidence is more fragmentary (see section 5.5).

Using N_2 , we reverse the direction of the mapping, and start with $h\nu + N_2$, which was discussed extensively in earlier sections. Here a "discrete" shape resonance of π_g symmetry and a shape resonance of σ_u symmetry are apparent in the K-shell spectrum (Wight et al. 1972/73, 1976, Kay et al. 1977, Hitchcock and Brion 1980a) (see fig. 3). These occur at ~ -9 and 10 eV on the kinetic energy scale (relative to the ionization threshold). Hence, one would look for the same set of resonances in $e-N_2$ scattering at ~ 1 and ~ 20 eV incident electron energies. The well-known π_g shape resonance (Bardsley and Mandl 1968, Schulz 1973, 1976, Lane 1980, Shimamura and Takayanagi 1984) is very apparent in the vibrationally elastic cross section; however, there is only a very broad bump at ~ 20 eV (Kennerly 1980). As noted above, the vibrationally inelastic cross section is much more sensitive to shape resonances, and, indeed, the σ_u shape resonance in $e-N_2$ scattering has been established theoretically and experimentally by looking in this channel (Dehmer and Dill 1980, Pavlovic et al. 1972, Truhlar et al.

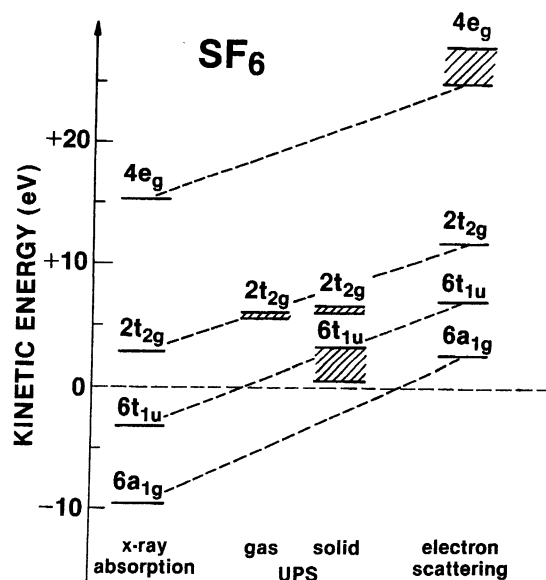


Fig. 8. Systematics of shape resonance positions in different measurements on SF_6 . (Adapted from Fock and Koch 1984, 1985.)

1972, Dehmer et al. 1980, Rumble et al. 1981). Several other excellent examples exist, but we will conclude by pointing out that the connections between $e\text{-CO}_2$ and $h\nu + \text{CO}_2$ resonances have been recently discussed (Dittman et al. 1983) in detail, including a study of the eigenphase sums in the vicinity of the σ_u shape resonance in the two systems.

Finally, we note similar connections and additional complications upon mapping from inner-shell to valence-shell $h\nu + M$ spectra. On going from deep inner-shell spectra to valence-shell spectra, shape resonances in $h\nu + M$ also shift approximately 1–4 eV toward higher kinetic energy, due to differences in screening between localized and delocalized holes as well as other factors. As mentioned above, several complications arise in valence-shell spectra which can tend to obscure the presence of a shape resonance compared to their more straightforward role in inner-shell spectra. These include greater energy dependence of the dipole matrix element, interactions with autoionizing levels (Morin et al. 1982a, Collins and Schneider 1984), strong continuum–continuum coupling (Dehmer et al. 1982, Stephens and Dill 1985) between more nearly degenerate ionization channels, strong particle–hole interactions (Krummacher et al. 1980, Langhoff et al. 1981a, Krummacher et al. 1983, Bagus and Viinikka 1977, Cederbaum and Domcke 1977, Cederbaum et al. 1977, 1978, 1980, Schirmer et al. 1977, Wendin 1981, Schirmer and Walter 1983) etc. So, for the most transparent view of the manifold of shape resonance features in $h\nu + M$, one should always begin with inner-shell data.

3. Autoionization

3.1. Overview

Autoionization is an intrinsically multichannel process in which a resonantly excited discrete state from one channel couples to the underlying electronic continua of one or more other channels to effect ionization. It has been known since Fano's original work (Fano and Cooper 1968, Fano 1935, 1961) almost fifty years ago, that this process produces characteristic asymmetric Fano–Beutler profiles in the photoionization cross section. Since then, there have been extensive studies of autoionization structure in the total photoionization cross sections of atoms (Fano and Cooper 1968) and molecules (see, e.g., Koch and Sonntag 1979, Hayaishi et al. 1982, Dibeler and Walker 1967, Dibeler and Liston 1968, Chupka and Berkowitz 1969, Dibeler and Walker 1973, McCulloh 1973, Dehmer and Chupka 1975, 1976, Berkowitz and Eland 1977, Gurtler et al. 1977, Berkowitz 1979, Ono et al. 1982, Wu and Ng 1982, P.M. Dehmer et al. 1984). In addition, the manifestations of autoionization in such dynamical parameters as photoionization branching ratios and photoelectron angular distributions have been recognized and have recently developed into a major focal point for current studies of molecular photoionization dynamics (see, e.g., Morin et al. 1980,

Tabché-Fouhailé et al. 1981, Unwin et al. 1981, Hayaishi et al. 1982, Keller et al. 1982, Morin et al. 1982a,b, Parr et al. 1982a, Carlson et al. 1983b, Levine and Soven 1983, Morin 1983, Collins and Schneider 1984, Levine and Soven 1984, Fano 1970, Dill 1972, Herzberg and Jungen 1972, Atabek et al. 1974, Fano 1975, Jungen and Atabek 1977, Dill and Jungen 1980, Giusti-Suzor and Lefebvre-Brion 1980, Jungen 1980, Jungen and Dill 1980, Raoult et al. 1980, Jungen and Raoult 1981, Raoult and Jungen 1981, Giusti-Suzor 1982, Lefebvre-Brion and Giusti-Suzor 1983, Raoult et al. 1983, Raseev and Le Rouzo 1983, Giusti-Suzor and Fano 1984a,b, Giusti-Suzor and Jungen 1984, Giusti-Suzor and Lefebvre-Brion 1984, Jungen 1984a,b, Mies 1984, Mies and Julienne 1984, Lefebvre-Brion et al. 1985, Marr and Woodruff 1976, Woodruff and Marr 1977, Baer et al. 1979, Codling et al. 1981, Ederer et al. 1981, Parr et al. 1981, West et al. 1981, Parr et al. 1982b, Truesdale et al. 1983b, Hubin-Franskin et al. 1984, Doolittle and Schoen 1965, Price 1968, Berkowitz and Chupka 1969, Collin and Natalis 1969, Blake et al. 1970, Bahr et al. 1971a,b, Carlson 1971, Collin et al. 1972, Kleimenov et al. 1972, Gardner and Samson 1973, Tanaka and Tanaka 1973, Gardner and Samson 1974a,b, Caprace et al. 1976, Natalis et al. 1977, Gardner and Samson 1978, Eland 1980, Kumar and Krishnakumar 1981, 1983, Carlson and Jonas 1971, Morgenstern et al. 1971, Carlson and McGuire 1972, Carlson et al. 1972, Niehaus and Ruf 1972, Hancock and Samson 1976, Mintz and Kuppermann 1978, Katsumata et al. 1979, Kibel et al. 1979, Sell et al. 1979, Kreile and Schweig 1980, Berry and Nielsen 1970a,b, Duzy and Berry 1976).

A more physical description of the autoionization process is helpful in discussing the alternative decay mechanisms possible in molecules: In most cases, autoionizing states consist of an excited Rydberg electron bound to an excited ion (also called core) primarily by Coulomb attraction. [The case of two highly correlated electrons bound to an ion is another important case which requires special treatment (Fano 1983) and will not be discussed here.] A necessary condition for decay of this state by ionization is that the excitation energy of the ion must be greater than the binding energy of the Rydberg electron. Then, barring alternative decay paths, autoionization will take place by means of a close collision, between the Rydberg electron and the ion, in which excitation energy of the ion is transferred to the excited electron to overcome its binding energy and permit its escape from the ionic field. Notice that, although a Rydberg electron spends only a very small fraction of time within the molecular ion, such close encounters are essential for autoionization since, only when the Rydberg electron is nearby can it participate fully in the dynamics of the core and exchange energy efficiently with it.

A molecular ion core can store the energy needed to ionize a Rydberg electron in any of its three modes – electronic, vibrational, or rotational. The most direct means of storing electronic energy is to produce a hole in a molecular orbital (MO) other than the outermost occupied MO, e.g., by promoting one of the inner electrons into a Rydberg orbital. In addition, various degrees of vibrational and rotational excitation can accompany photoexcitation of Rydberg states con-

verging to any state of the ion. It is the existence and interplay among the alternative energy modes which lead to the unique properties of molecular autoionization.

As a concrete example of rotational and vibrational autoionization we will discuss photoionization of H_2 . The alternative rovibrational ionization channels for para- H_2 ($J=0$) are shown schematically in fig. 9. The ground ionic state, $\text{H}_2^+ \text{X } ^2\Sigma_g^+$, is the only bound electronic state in this spectral range so that the possibility of electronic autoionization is eliminated. In fig. 9, the vertical, shaded bars represent various vibrational channels of $\text{H}_2^+ ^2\Sigma_g^+$, labeled by $v^+ = 0-5$. Pairs of continua are associated with each v^+ reflecting the two rotational continua $N^+ = 0, 2$ produced by photoionization of para- H_2 . Converging to each of these (and higher) rovibrational thresholds are Rydberg series, supported by the Coulomb field of the H_2^+ ion. A small subset of these Rydberg states is indicated, for later reference, by horizontal lines at their observed spectral location and placed directly under the threshold to which they converge. Any of these optically

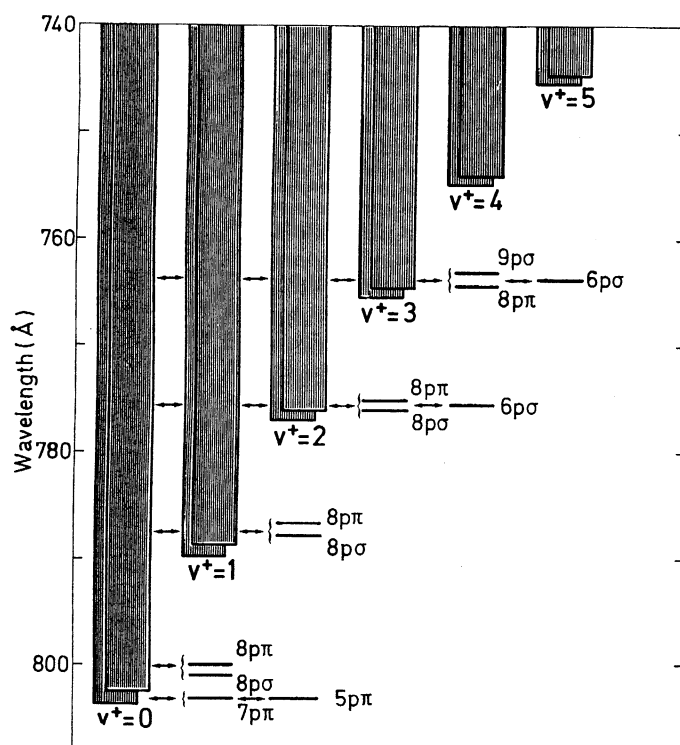


Fig. 9. Schematic illustration of vibrational/rotational autoionization in cold para- H_2 ($J=1$, negative parity final states). Continua are indicated by vertical hatching. For each given v^+ of the ion H_2^+ there are two continua corresponding to rotational quantum number $N^+ = 0$ and 2 of the ion ($J=1$). Selected discrete Rydberg levels are indicated below the vibrational ionization limit with which they are associated. (From Raoult and Jungen 1981.)

allowed Rydberg states can autoionize by coupling with accessible open channels. In this case, autoionization would proceed by transferring energy stored in rotation or vibration of the ion core to the photoelectron. If more than one continua is available the decay will proceed into each with a branching ratio determined by the detailed dynamics of the decay process. Moreover, the angular distribution of the photoelectrons escaping in each channel will reflect further

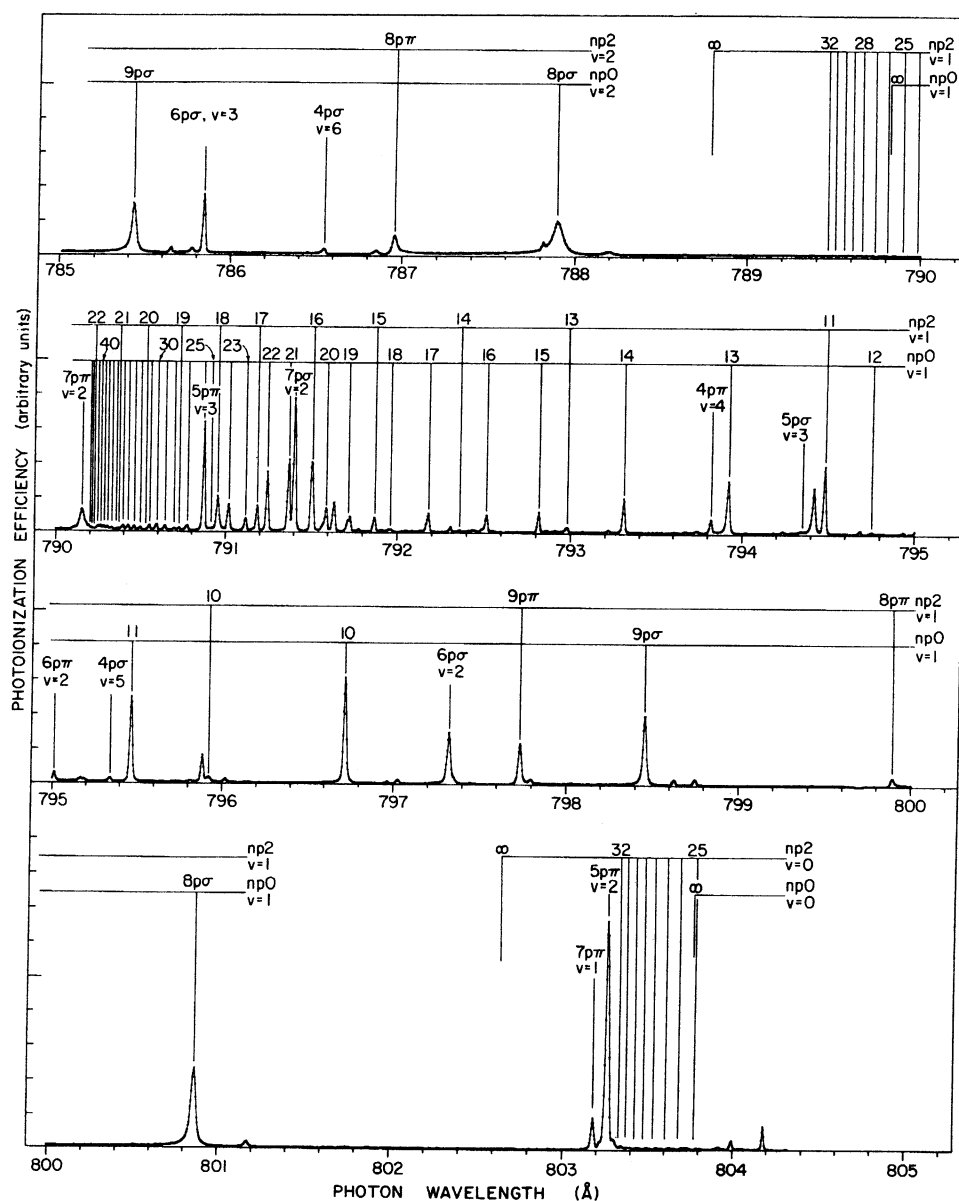


Fig. 10. A portion of the photoionization cross section of para-H₂ at 78 K. (From Dehmer and Chupka 1976.)

details of the dynamics including relative phases of degenerate photoelectron wavefunctions.

Based on the picture, so far, of a set of rovibrational thresholds and Rydberg series converging to each, one might expect a dense pattern of autoionizing levels, but one which would straightforwardly yield to spectroscopic analysis in terms of characteristic rovibrational spacings and known behavior of Rydberg series. However, this simple picture of a rich but fundamentally uncomplicated spectrum ignores all interaction between the Rydberg electron and molecular core, and is

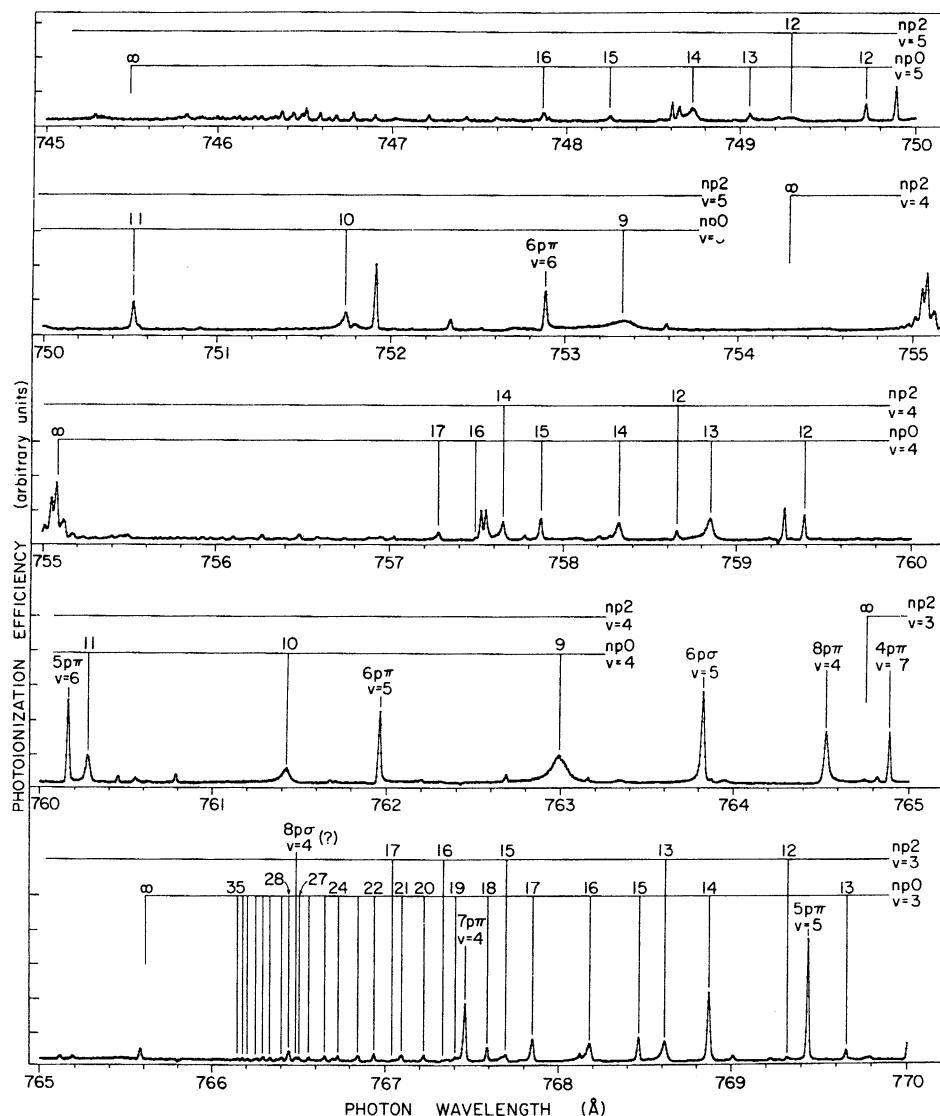


Fig. 11. A portion of the photoionization cross section of para- H_2 at 78 K. (From Dehmer and Chupka 1976.)

wrong. This is shown dramatically in figs. 10 and 11 which show the total photoionization spectrum (Dehmer and Chupka 1976) in two spectral regions (chosen for later discussion) covered in fig. 9, one from the first IP to 785 Å and the other covering 770–745 Å. Careful inspection will reveal that, for any Rydberg series, the spacings, intensities, and profiles will deviate strongly from a simple Rydberg pattern. This is especially true near “interlopers”, i.e., Rydberg states falling in the midst of a Rydberg series, but converging to a higher limit. For such cases level shifts and intensity redistribution frequently modify the entire host Rydberg series. These modifications arise from mutual interactions mediated by short range forces and have been accounted for in detail in this prototype system.

In the following two sections we use two examples which represent the state-of-the-art in theoretical and experimental studies of molecular autoionization dynamics. The most accurate and penetrating theoretical analysis (Fano 1970, Dill 1972, Herzberg and Jungen 1972, Dill and Jungen 1980, Jungen 1980, Jungen and Dill 1980, Raoult et al. 1980, Jungen and Raoult 1981, Raoult and Jungen 1981, Giusti-Suzor 1982, Raseev and Le Rouzo 1983, Jungen 1984a,b) has been carried out on parts of the H_2 spectrum using MQDT. Two representative cases will be discussed including rotational autoionization and a prediction of vibrational branching ratios and photoelectron angular distributions resulting from vibrational autoionization above the $v^+ = 3$ limit at ~ 764.8 Å. These predictions have not yet been tested, although equivalent experiments on electronic autoionization in N_2 have recently been performed (Parr et al. 1981, West et al. 1981). The latter case will be discussed in section 5.2.

3.2. MQDT treatment of H_2 photoionization

Multichannel quantum defect theory and its application to molecular photoionization have been described in detail elsewhere (Fano 1970, Dill 1972, Herzberg and Jungen 1972, Atabek et al. 1974, Fano 1975, Jungen and Atabek 1977, Dill and Jungen 1980, Giusti-Suzor and Lefebvre-Brion 1980, Jungen 1980, Jungen and Dill 1980, Raoult et al. 1980, Jungen and Raoult 1981, Raoult and Jungen 1981, Giusti-Suzor 1982, Lefebvre-Brion and Giusti-Suzor 1983, Raoult et al. 1983, Raseev and Le Rouzo 1983, Giusti-Suzor and Fano 1984a,b, Giusti-Suzor and Jungen 1984, Giusti-Suzor and Lefebvre-Brion 1984, Jungen 1984a,b, Mies 1984, Mies and Julienne 1984, Lefebvre-Brion et al. 1985). Hence we will only briefly summarize the important attributes of MQDT and will then turn to two examples of its application to photoionization of H_2 .

MQDT is a theoretical framework which *simultaneously* treats the interactions between and within *whole* excitation channels. The input to an MQDT calculation consists chiefly of a small set of physically meaningful parameters (quantum defects and dipole amplitudes) which characterize the short range interactions between the excited electron and the core, are slowly varying functions of energy relative to rovibronic structure in the spectrum, and can generally be obtained from the positions and intensities of low-lying states in the spectrum. Also used

are known transformation properties of molecular wavefunctions, e.g., between Hund's coupling cases, and the asymptotic boundary conditions pertinent to a particular spectral range. Given these, straightforward matrix mechanics yields, at each excitation energy, the spectral composition of the total final state wavefunction in terms of the short-range, body-frame basis set, known dipole strengths, and the asymptotic eigenphase shifts of the observable ionization channels. These quantities are then related to such observables as the total photoionization cross section, vibrational branching ratios, and photoelectron angular distributions by now standard formulas.

We wish to emphasize that this theoretical framework is not only elegant, but also reflects very accurately the internal mechanics of the excited complex. Hence, the quality of the computed observable depends solely upon the quality of the input. When accurate empirical quantum defects are used, adiabatic and non-adiabatic corrections to the Born–Oppenheimer approximation are included automatically, to all orders. Hence, given physical input from low-lying excited states, one can use MQDT to generate accurate predictions for experiments throughout the extremely complex high-excitation regions. This is to be contrasted to the normal perturbation approach which would require treating each state separately, with explicit adiabatic and non-adiabatic corrections, and with little hope of treating higher order interactions within and between whole excitation channels.

A striking example of the power and accuracy of MQDT in a complex situation is provided by the rich rotational/vibrational autoionization structure in the 174.3 cm^{-1} spectral range between the $N^+ = 0$ and 2 rotational thresholds associated with the lowest $v^+ = 0$ ionization potential of H_2 (Dehmer and Chupka 1976). The results of a calculation (Jungen and Dill 1980) of this structure is given in fig. 12. Across the top of the figure are indicated the level positions one obtains with discrete boundary conditions, i.e., by eliminating open channels from the linear system. This level of analysis determines the initial assignments of spectral features. Alternatively, photoabsorption directly into the continuum is shown across the bottom of fig. 12. This is the single-channel level of approximation used throughout the discussion of shape resonances in section 2. If rotational autoionization only is introduced, then the levels $np2$ of the Rydberg series converging to the upper ($N^+ = 2$) threshold of $\text{H}_2^+ X^2\Sigma_g^+ (v^+ = 0)$ autoionize and distort the continuum into a Rydberg series of Fano–Beutler profiles. This is shown in the middle frame in fig. 12. Finally, if vibrational autoionization channels are also introduced, then the $5p\pi$, $v = 2$ and $7p\pi$, $v = 1$ levels autoionize and strongly distort the rotationally autoionizing levels as well, shifting intensity from above to below the vibrational interlopers.

It is seen that the effect of vibrational autoionization on the ionization cross section is profound and that it affects the whole range shown, corresponding to about 100 cm^{-1} . Indeed, if the fine variations of the cross section are neglected, the whole spectrum can be viewed as one “giant” resonance of about 50 cm^{-1} width which causes a global transfer of intensity from the high-energy to the low-energy side of the vibrational peaks. This transfer leads to further modifica-

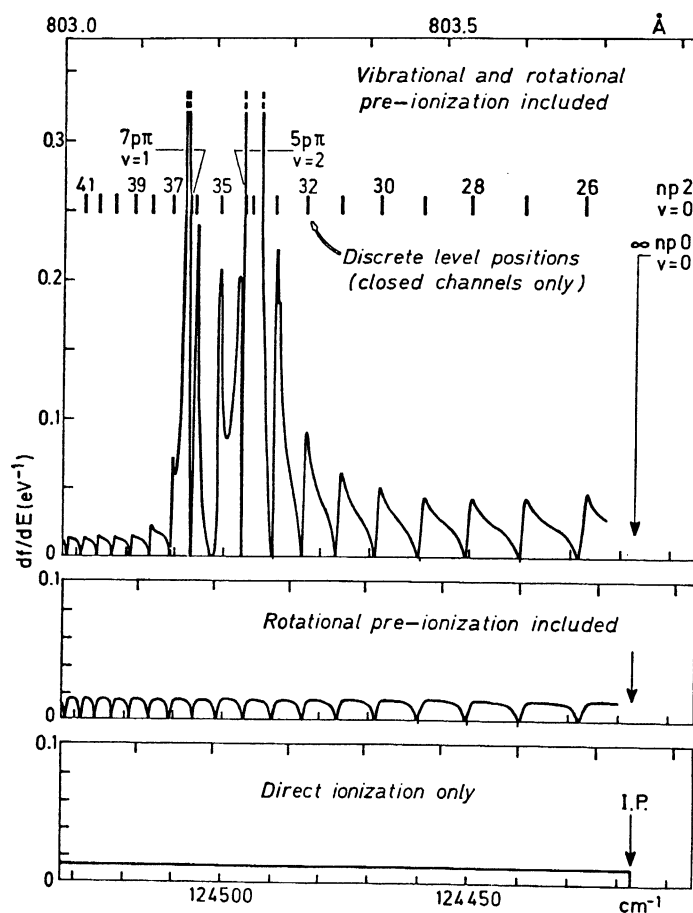


Fig. 12. MQDT calculation of photoionization of $\text{H}_2\text{X } ^1\Sigma_g^+$ ($J''=0$, $v''=0$) near the ionization threshold. (From Jungen and Dill 1980.)

tions of the fine structure. For example, for $n = 26$ and 27 the intensity minima still correspond nearly to the discrete $np2$ levels, but for higher n the profiles become progressively distorted until near $n = 32-35$, it is the intensity maxima which coincide with the discrete level positions. In other words, there exists no longer a simple relationship between the extrema in the ionization curve and the positions of the autoionizing levels. In view of these complexities it is clear that vibrational and rotational autoionization cannot be meaningfully treated as separate processes in this spectral region. A key feature of the MQDT is that it is based on no such assumed separability, i.e., it is applicable independently of coupling strengths between alternative decay mechanisms.

In fig. 13 the calculated spectrum (Jungen and Dill 1980) is compared with the high-resolution photoionization spectrum (Dehmer and Chupka 1976). The calculated spectrum from fig. 12 was convoluted with a triangular apparatus function of

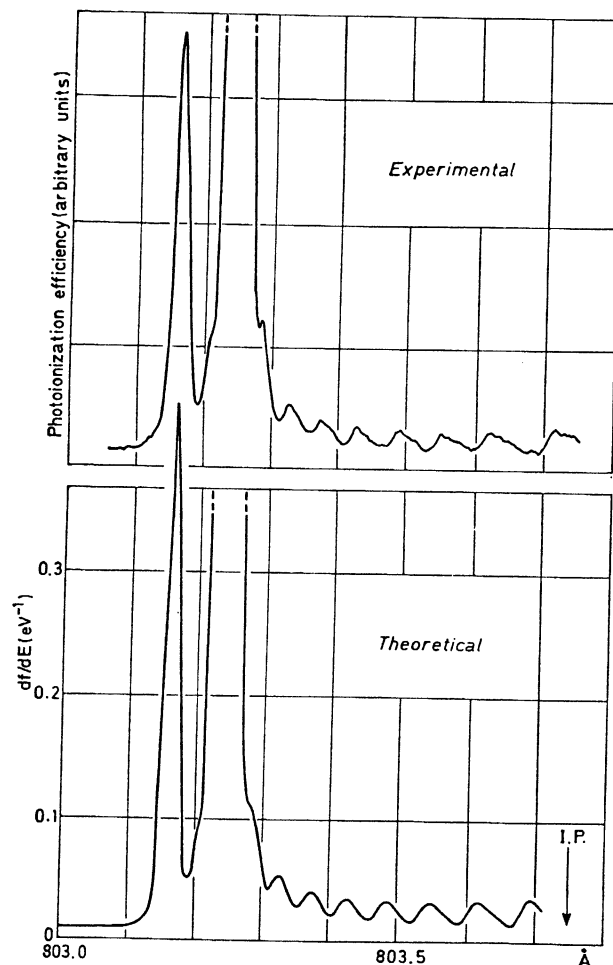


Fig. 13. MQDT results from fig. 12 broadened to a resolution of 0.022 \AA and compared with data from Dehmer and Chupka (1976). (Figure from Jungen and Dill 1980.)

halfwidth 0.022 \AA to mimic the finite experimental resolution. The comparison in fig. 13 shows essentially exact agreement and reflects more clearly than words the state-of-the-art in computational simulation of detailed photoionization dynamics.

Triply differential cross sections have also been computed (Raoult and Jungen 1981) near each of the levels explicitly shown in fig. 9. We will skip to the highest set of levels, above the $v^+ = 3$ limit, to discuss MQDT predictions of vibrational branching ratios and β 's. This spectral range, between 762.5 and 765 \AA in fig. 11, is most attractive for future experimental examination since it produces four photoelectron peaks, i.e., corresponding to $v^+ = 0-3$, with sufficiently large photoelectron energies to be measured with existing electron energy analyzers.

Figure 14 shows the calculated total and vibrational partial cross sections (the

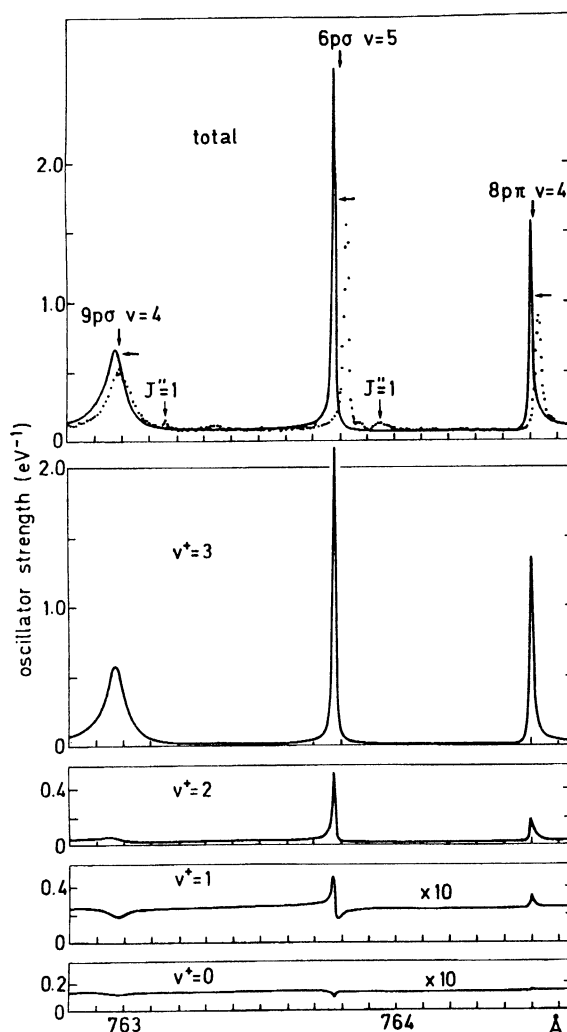


Fig. 14. Total and partial oscillator strengths for photoionization of H_2 near the $v^+ = 3$, $N^+ = 2$ ionization threshold (764.755 \AA). (Experimental points from Dehmer and Chupka 1976; figure adapted from Raoult and Jungen 1981.)

rotational sublevels have been summed over) in this spectral range, together with total photoionization data (Dehmer and Chupka 1976). In this case the calculations are not folded with the instrument function and are, accordingly, sharper and higher. The horizontal arrow indicates the height that would be obtained from such a convolution. Also the vertical arrows show more precise peak positions from the high-resolution absorption spectrum (Herzberg and Jungen 1972). Given these qualifications, the agreement in the total cross section is, again, quite satisfactory. The vibrational partial cross sections, for which no experimental data is available is shown in the lower frames of fig. 14. There, we

see that the widths of the vibrational autoionization peaks are the same as in the total cross section, as expected, but that the profiles vary drastically. Other details of the behavior of these partial cross sections are displayed more clearly in the vibrational branching ratios, discussed below.

Figure 15 again shows the total photoionization cross section, together with the total β (summed over v^+) and the vibrational branching ratio and β_{v^+} for each vibrational ionization channel v^+ . The total β curve is observed to dip strongly

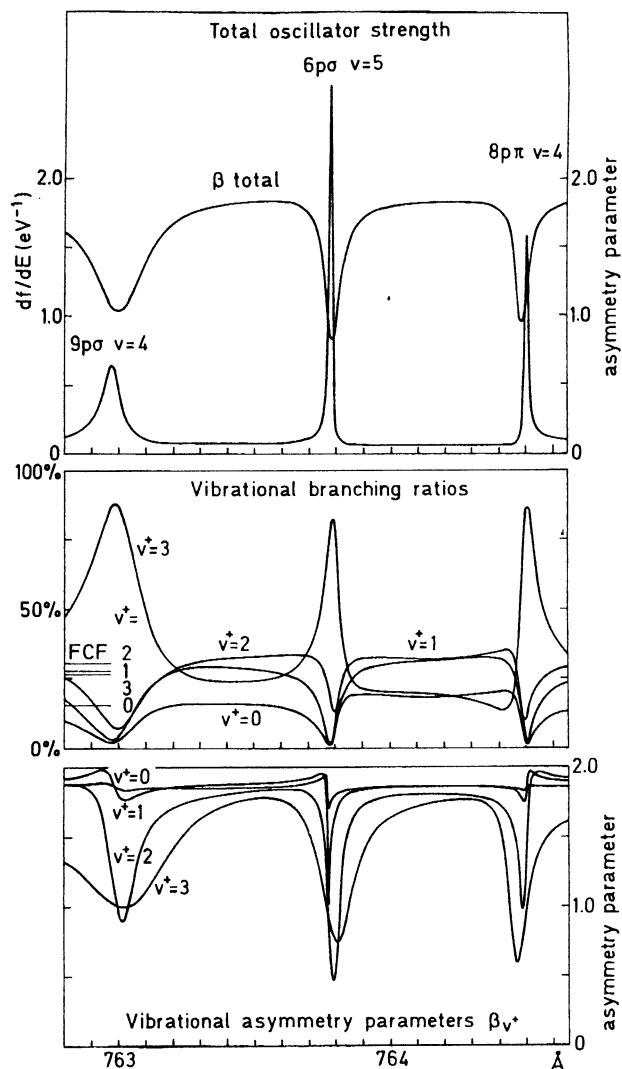


Fig. 15. Asymmetry parameter β (total and vibrationally resolved) and vibrational branching ratios for photoionization of H_2 near the $v^+ = 3$, $N^+ = 2$ ionization threshold (764.755 Å). (Figure adapted from Raoult and Jungen 1981.)

within the resonances. This is a consequence of the discrete wavefunction component mixing strongly into the ionization continuum. Classically speaking, one would say that the “quasibound” photoelectron spends more time near the core so that angular momentum exchange is enhanced. In this case the $N^+ = 2$ ionization channel becomes dominant near the center of the resonance and the value of β is depressed correspondingly, showing that directional information carried by the incoming photon is largely transferred to molecular rotation in the subsequent electron–core collisions. This general behavior is also reflected in the partial β_{v^+} curves although, in addition, a strong v^+ dependence in the magnitudes and shapes of the β_{v^+} is also observed. Note that the spectral extent of the variations induced in the β_{v^+} by vibrational autoionization is considerably larger than the halfwidths of the resonances themselves. This is a significant advantage in triply differential experimental studies which are difficult to perform with narrow photon bandwidth, for intensity reasons, and are only now being attempted with bandwidths of 0.1–0.2 Å.

The middle frame in fig. 15 shows the vibrational branching ratios in this region, along with the FC factors for direct ionization. As in the case of shape resonant photoionization (see, e.g., section 5.1), striking non-FC behavior is observed in the vicinity of the vibrationally autoionizing states. As in the case of β_{v^+} , the spectral extent of the autoionization effect is greater than the autoionizing resonance halfwidth when displayed as vibrational branching ratios, a significant consideration in the context of experimental tests of these predictions. These calculations also predict that the branching ratio in the open channel with the highest v^+ , corresponding to autoionization with the lowest possible $|\Delta v|$, is strongly enhanced at the expense of all other channels which are strongly depressed from their FC factors. Thus, the well-known propensity rule (Berry and Nielsen 1970a,b) stating that a vibrationally autoionized level decays preferentially with the smallest possible change of vibrational quantum number, is globally confirmed in these calculations, although for certain wavelengths (e.g., 764.4 Å in fig. 15) the exact opposite may be true.

The results just presented tend to lull one into the feeling that we understand photoionization of H_2 completely, needing only to extend the range of the above MQDT treatment to any region of interest. Nevertheless, it is imperative to perform experimental tests at the triply differential level, as it is in the more detailed quantities such as vibrational branching ratios and angular distributions that we are most likely to observe shortcomings in our detailed understanding of this most important prototype system. That such measurements have not been performed is often surprising to some. To emphasize the dearth of detailed data on this point, we show in fig. 16 a recent summary (Southworth *et al.* 1982b) of β measurements on H_2 (and D_2) together with other theoretical treatments. The gap between figs. 15 and 16 is enormous. Indeed, the measurements are difficult; however, optimization of current technology should make this goal attainable. This is one of the main motivations for the new generation instrument described in section 4. There is also another dimension to the problem, reflected in fig. 16: autoionization aside, there exists a glaring disagreement between theory and

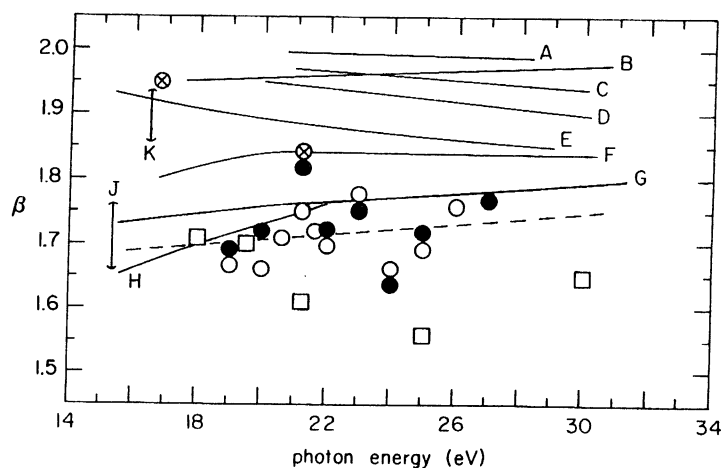


Fig. 16. Various experimental and theoretical results for the asymmetry parameter, β , for photoionization of H_2 and D_2 . (Complete citations for the various data are given in the article by Southworth et al. 1982b, from which this figure was taken.)

experiment for the β values in the open continuum of H_2 . The theoretical results tend to lie significantly (~ 0.2 β units) higher than measured values. Subsequent theoretical and experimental work shows that this difference is very persistent (see e.g., Itikawa et al. 1983, Hara and Ogata 1985, Raseev 1985, Hara 1985, Richards and Larkins 1986, and references therein), in spite of improvements on both sides. Thus, although great strides have been made during the last decade, the goal of understanding the photoionization dynamics of this most fundamental molecule presents several very contemporary challenges.

4. Triply differential photoelectron measurements – experimental aspects

In order to fully examine dynamical aspects of the resonant photoionization processes discussed above, it is essential to perform measurements of photoelectron intensity as a function of three independent variables – wavelength of the incident light, to select the spectral features; photoelectron kinetic energy, to select the ionization channel of interest; and ejection angle, to measure angular distributions. For convenience, we refer to this level of experiment as “triply differential” photoelectron measurements. Over the last few years, angle-resolved electron spectroscopy has been combined with synchrotron radiation sources to achieve successful triply differential measurements in molecules, including vibrational state resolution. Presently several groups (e.g., Marr et al. 1979, White et al. 1979, Parr et al. 1980, Krause et al. 1981, Derenbach et al. 1983, Morin et al. 1983, Parr et al. 1983, 1984) are involved in this type of experiment, each with

their own specific experimental configuration and special emphasis, but each fulfilling the requirements for full triply differential studies. Here we will review, as an example, the experimental aspects of a new instrument (Parr et al. 1983, 1984) presently at the Synchrotron Ultraviolet Radiation Facility (SURF-II) at the National Bureau of Standards, in order to focus on some of the experimental considerations in triply differential photoionization studies.

The new triply differential electron spectrometer system at NBS consists of a high-throughput normal-incidence monochromator (Ederer et al. 1980) (fig. 17) and a pair of 10 cm mean-radius hemispherical electron spectrometers in an experimental chamber (fig. 18). To avoid later confusion we note that an earlier configuration using the same monochromator with a single, rotatable 5 cm mean-radius spectrometer (Parr et al. 1980) has been used for the past several years in several triply differential photoionization studies and is, in fact, the instrument used to obtain the data presented later in sections 5.1, 5.2, and 5.4–5.6. The data in section 5.3 was taken with the new instrument (Parr et al. 1983). The special emphasis with both generations of instruments has been the same, namely, to optimize the photon and electron resolution in order to probe detailed dynamics within shape resonance and autoionization structure in the near-normal-incidence range ($h \leq 35$ eV). The new instrument further optimizes several aspects of the electron spectrometer system to greatly extend the sensitivity and/or resolution compared to earlier measurements, for reasons discussed in section 7.

The high-flux, 2 meter monochromator shown in fig. 17 has been specifically

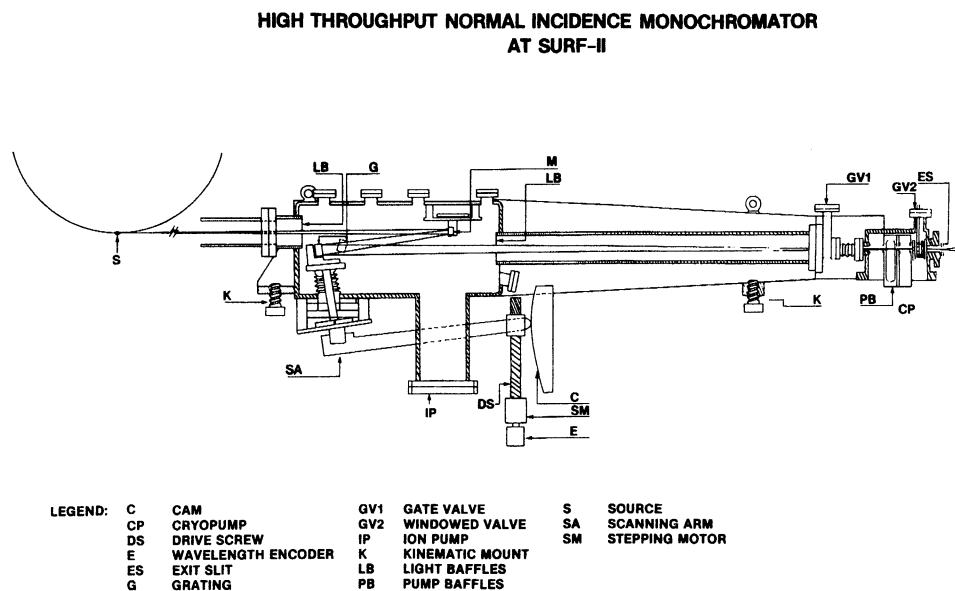


Fig. 17. Schematic diagram of high-throughput, normal-incidence monochromator. (From Ederer et al. 1980.)

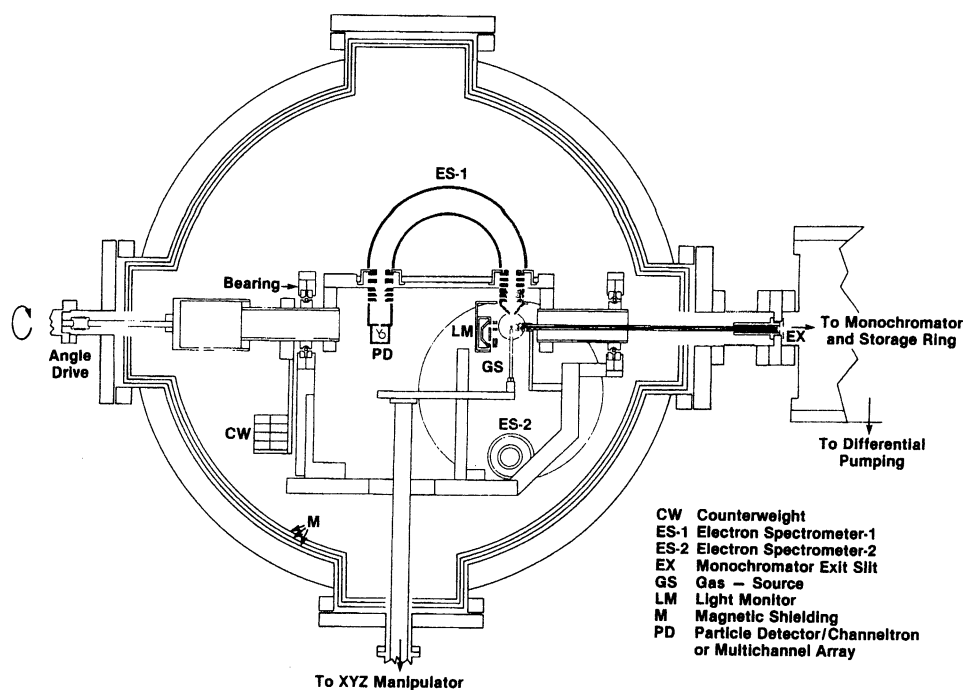


Fig. 18. Schematic diagram of dual electron spectrometer system. (From Parr et al. 1983, 1984.)

matched to the characteristics of the SURF-II storage ring: First and foremost, it uses the small vertical dimension of the stored electron beam ($\sim 100 \mu\text{m}$) as the entrance aperture of the monochromator, an important feature which eliminates loss of incident flux on the entrance slit. Second, it is attached directly to the exit port of the storage ring, resulting in the very large capture angle of 65 mrad in the horizontal plane. This arrangement produces approximately $10^{10} \text{ photons s}^{-1} \text{ \AA}^{-1}$ per mA of circulating current (typical initial current presently $\sim 50 \text{ mA}$) at 1000 \AA and has been used for triply differential measurements out to $\sim 375 \text{ \AA}$. Together with a 1200 line/mm grating and a $200 \mu\text{m}$ ($100 \mu\text{m}$) exit slit, this configuration yields a photon resolution of $\sim 0.8 \text{ \AA}$ (0.4 \AA). Plans are made to improve the resolution with a higher dispersion grating. The dispersed light is channeled by a 2-mm-i.d. capillary tube for a distance of $\sim 40 \text{ cm}$ into the interaction region of the experimental chamber. The low pumping conductance of this capillary tube is very effective in reducing the gas load on the monochromator and storage ring during experiments in which the gas pressure in the experimental chamber can be as high as 10^{-4} Torr .

The new electron spectrometer system is shown schematically in fig. 18. The chamber is a 76 cm diameter, 92 cm long stainless steel vacuum chamber. It is pumped by a 500 liter/s turbomolecular pump and an 8000 liter/s closed-cycle helium cryopump to provide maximum flexibility in studying the whole range of

gaseous targets. Low magnetic fields of $<500 \mu\text{G}$ are maintained throughout the chamber by three layers of high-permeability magnetic shielding.

The system is designed to operate with either one rotating (ES-1) or two stationary (ES-1 and ES-2) electron spectrometers. In either configuration the electron spectra can be recorded as a function of ejection angle relative to the principle axis of polarization. This leads to the determination of the photoelectron branching ratios and angular distributions according to the following expression which applies to dipole excitation of free molecules with elliptically polarized light (Parr et al. 1973, Samson and Starace 1975):

$$\frac{d\sigma}{d\Omega} = \frac{\sigma}{4\pi} \left[1 + \frac{\beta}{4} (3P \cos 2\theta + 1) \right], \quad (8)$$

where β is the asymmetry parameter, σ is the integrated cross section, P is the polarization of the light with the horizontal component being the major axis, and θ is the angle of ejection of the photoelectron with respect to the horizontal direction. In general, each resolved ionization channel (each photoelectron peak) will have a characteristic set of dynamical parameters, β and σ .

The number of electrons ejected per unit light flux per unit solid angle, $dn/d\Omega$, is proportional to the differential cross section; hence we can write

$$\frac{dn}{d\Omega} = N \left[1 + \frac{\beta}{4} (3P \cos 2\theta + 1) \right]. \quad (9)$$

Measurement of P , θ and the number of electrons as a function of θ enables a determination of β and N . The relative quantity N , when normalized over a relevant set of possible alternative ionization channels, gives the branching ratio for the particular transition. The measurement of P is accomplished with a triple reflection polarizer based upon the considerations of Horton et al. (1969). The incoming light flux is monitored by a 90% transparent tungsten photocathode on the input aperture of the polarization analyzer. After three reflections the light is intercepted by a second tungsten photodiode. The ratios of these two photodiode signals at 0° and 90° with respect to the major polarization axis determine the polarization.

Each electron analyzer is a 10 cm mean-radius version of our previous instrument (Parr et al. 1980) and utilizes the same electron lens system – a three-aperture “zoom” lens (Harting and Read 1976) to focus the electrons into the hemispherical dispersive element, and a similar one to refocus the energy-analyzed electrons on the exit slit. There are no entrance or exit apertures in the equatorial plane of the hemispheres and therefore the aperture in the entrance cone determines the basic resolution. The resolution obtainable while yet maintaining good signal is expected to be on the order of 20 meV. Measurement of sub-10 meV resolution has been demonstrated. Thus, the resolving power of this instrument is a significant improvement over that typically used now with

synchrotron radiation, and will allow for the extension of studies of non-Franck-Condon effects to small polyatomic molecules.

The electrical aspects of the electron spectrometers are generally similar to those of the previously described apparatus (Parr et al. 1980). Briefly, the fixed voltages are controlled by highly regulated conventional power supplies and the variable voltages are under computer control. A 16-bit digital to analog converter (DAC) with a basic increment of 0.0005 V controls the ramping of offset voltages. The variable focus voltages are controlled by isolated power sources run by the computer. The computer (LSI-11/23) is interfaced to a CAMAC crate through which it controls the grating drive, angular position, light detection system, electron counting system, and other experimental chores. Both analyzers are ramped off the 16-bit DAC but have their own separately controlled power supplies for lens voltages. The two identical analyzers allow a determination of the branching ratios and asymmetry parameters without rotation, i.e., the electron intensity at two angles can be measured simultaneously. The instrument is calibrated by reference to gases with known cross sections (Marr and West 1976) and asymmetry parameters (Kreile and Schweig 1980, Dehmer et al. 1975, Holland et al. 1982). The calibration features for the two analyzers are incorporated into a computer program that corrects and analyzes the data. Area detectors have been purchased and will soon be integrated into the instrument, thus significantly increasing its sensitivity.

The gas jet is mounted on an XYZ manipulator in order to optimize signal intensity and resolution by external adjustment. Gas nozzles for the system are interchangeable and provide both effusive beams and supersonic jets by use of pinhole apertures of diameter 7–50 μm . The positioning of the supersonic source is of particular importance and necessitates the positioning capability of this inlet system. With the larger hemispherical dispersive element, the use of two analyzers, better gas source technology, incorporation of area detectors, and enhanced pumping, we expect a significant improvement in the basic sensitivity of the instrument (a very conservative estimate would be $>100\times$) as compared to our previous 5 cm radius single analyzer system (Parr et al. 1980).

The same LSI-11 computer that is used for automation is also used for the data reduction. The basic data consists of electron counts as a function of wavelength, ramp voltage, and angle. The ramp voltage is converted, using known quantities, to electron kinetic energy. The electron counts are then normalized for correction factors that depend upon kinetic energy, such as the transmission functions of the instruments and a small angular correction. Upon obtaining a suitably normalized set of data, the photoelectron spectra are typically fitted to a Gaussian basis set using spectroscopic values for vibrational energy spacings, while treating peak height, peak width, and overall position as free parameters. The calculated curve and normalized data are plotted to aid in the evaluation of the quality of fit. In addition, the fitting program outputs statistical parameters which can be used to estimate the accuracy of the fit. Finally, the areas of the respective peaks are used to infer the values of the branching ratios and asymmetry parameters which contain the dynamical information for the process.

5. Case studies

5.1. Shape-resonance-induced non-Franck-Condon effects in N_2 $3\sigma_g$ photoionization

Molecular photoionization at wavelengths unaffected by autoionization, predissociation, or ionic thresholds has been generally believed to produce Franck-Condon (FC) vibrational intensity distributions within the final ionic state and v -independent photoelectron angular distributions. We now discuss the prediction (Dehmer et al. 1979, Dehmer and Dill 1980) and confirmation (Carlson et al. 1980, Raseev et al. 1980, West et al. 1980, Lucchese and McKoy 1981b, Leal et al. 1984) that shape resonances represent an important class of exceptions to this picture. These ideas are illustrated with a calculation of the $3\sigma_g \rightarrow \epsilon\sigma_u$, $\epsilon\pi_u$ photoionization channel of N_2 , which accesses the same σ_u shape resonance discussed above at approximately $h\nu \sim 30$ eV, or ~ 14 eV above the $3\sigma_g$ IP. The potential energy curves for N_2 are shown in fig. 19 in order to orient this discussion and for later reference. The process we are considering involves

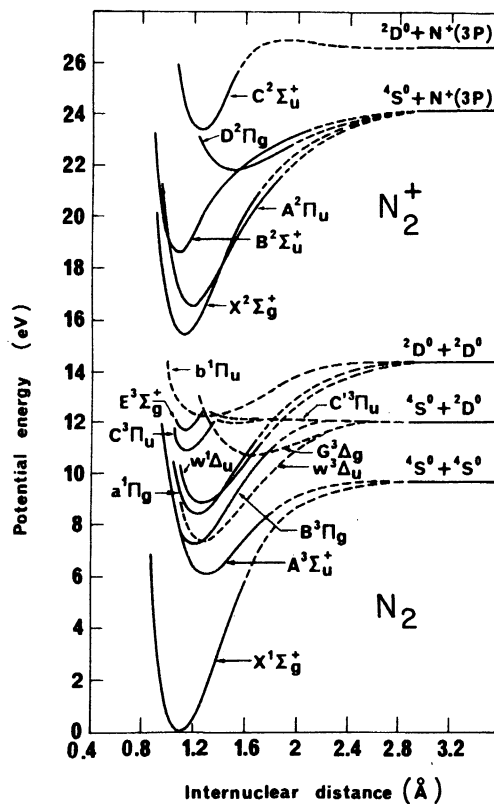


Fig. 19. Potential energy curves for N_2 and N_2^+ .

photoexcitation of $N_2 X^1\Sigma_g^+$ in its vibrational ground state with photon energies from the first IP to beyond the region of the shape resonance at $h\nu \sim 30$ eV. This process ejects photoelectrons leaving behind N_2^+ ions in energetically accessible states. Figure 20 shows a typical photoelectron spectrum taken at $h\nu = 21.2$ eV which exhibits photoelectron peaks corresponding to production of N_2^+ in its X, A, and B states, i.e., the three lowest ionic states in fig. 19. As we are interested in the ionization of the $3\sigma_g$ electron, which produces the $X^2\Sigma_g^+$ ground state of N_2^+ , we are concerned with the photoelectron band in the range $15.5 \text{ eV} \leq \text{IP} \leq 16.5 \text{ eV}$ in fig. 20. The physical effects we seek involve the relative intensities and angular distributions of the $v = 0-2$ vibrational peaks in the $X^2\Sigma_g^+$ electronic band, and, more specifically, the departures of these observables from behavior predicted by the FC separation.

The breakdown of the FC principle arises from the quasibound nature of the shape resonance, which, as we discussed in section 2, is localized in a spatial region of molecular dimensions by a centrifugal barrier. This barrier and, hence, the energy and lifetime (width) of the resonance are sensitive functions of internuclear separation R and vary significantly over a range of R corresponding to the ground-state vibrational motion. This is illustrated in the upper portion of figs. 21 and 22 where the dashed curves represent separate, fixed- R calculations of the partial cross section and asymmetry parameter for $N_2 3\sigma_g$ photoionization over the range $1.824 a_0 \leq R \leq 2.324 a_0$, which spans the N_2 ground-state vibrational wavefunction.

Of central importance in fig. 21 is the clear demonstration that resonance positions, strengths, and widths are sensitive functions of R . In particular, for larger separations, the inner well of the effective potential acting on the $l=3$ component of the σ_u wavefunction is more attractive and the shape resonance shifts to lower kinetic energy, becoming narrower and higher. Conversely, for lower values of R , the resonance is pushed to higher kinetic energy and is

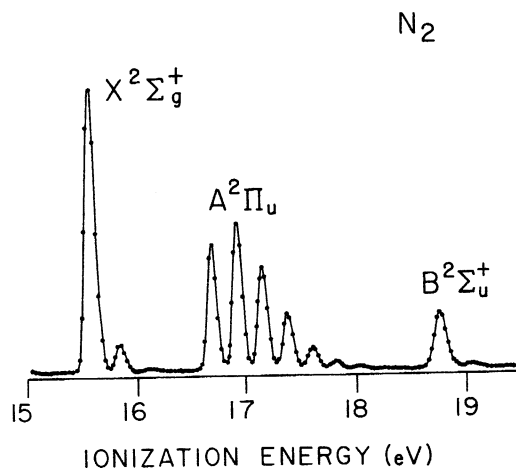


Fig. 20. Photoelectron spectrum of N_2 at $h\nu = 21.3$ eV.

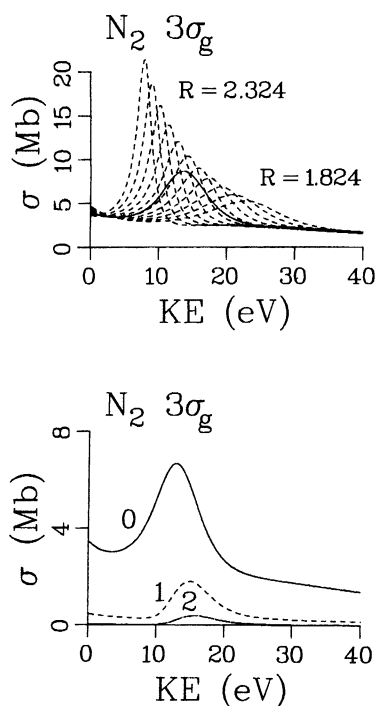


Fig. 21. Cross sections σ for photoionization of the $3\sigma_g$ ($v_i = 0$) level of N_2 . Top: fixed- R (dashed curves) and R -averaged, vibrationally unresolved (solid curve) results. Bottom: results for resolved final-state vibrational levels, $v_f = 0-2$.

weakened. This indicates that nuclear motion exercises great leverage on the spectral behavior of shape resonances, since small variations in R can significantly shift the delicate balance between attractive (mainly Coulomb) and repulsive (mainly centrifugal) forces which combine to form the barrier. In the present case, variations in R , corresponding to the ground-state vibration in N_2 , produce significant shifts of the resonant behavior over a spectral range several times the fullwidth at half maximum of the resonance calculated at $R = R_e$. By contrast, nonresonant channels are relatively insensitive to such variation in R , as was shown by results (Wallace 1980) on the $1\pi_u$ and $2\sigma_u$ photoionization channels in N_2 .

Thus, in the vicinity of a shape resonance, the electronic transition moment varies rapidly with R . This produces non-FC (parametric) coupling that was estimated (Dehmer et al. 1979, Chase 1956) by computing the net transition moment for a particular vibrational channel as an average of the R -dependent dipole amplitude, weighted by the product of the initial- and final-state vibrational wavefunctions at each R ,

$$D_{v_f v_i}^- = \int dR \chi_{v_f}^\dagger(R) D^-(R) \chi_{v_i}(R). \quad (10)$$

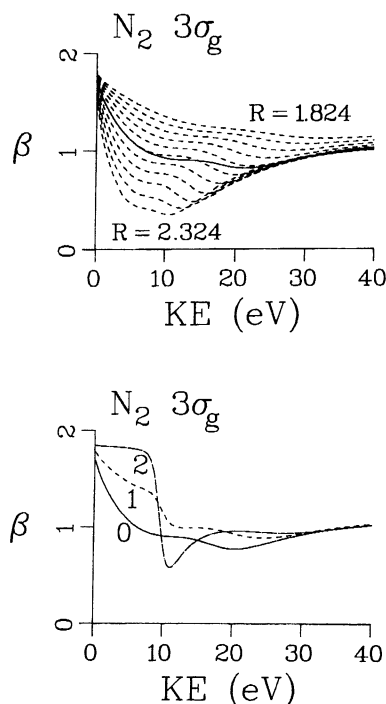


Fig. 22. Asymmetry parameters β for photoionization of the $3\sigma_g$ ($v_i = 0$) level of N_2 . Top: fixed- R (dashed curves) and R -averaged, vibrationally unresolved (solid curve) results. Bottom: results for resolved final-state vibrational levels, $v_f = 0-2$.

The vibrational wavefunctions were approximated by harmonic-oscillator functions and the superscript minus denotes that incoming-wave boundary conditions have been applied and that the transition moment is complex. Note that even when the final vibrational levels v_f of the ion are unresolved (summed over), vibrational motion within the initial state $v_i = 0$ can cause the above equation to yield results significantly different from the $R = R_e$ result, because the R -dependence of the shape resonance is highly asymmetric. This gross effect of R averaging can be seen in the upper half of fig. 21 by comparing the solid line (R -averaged result, summed over v_f) and the middle dashed line ($R = R_e$). Hence, even for the calculation of gross properties of the whole, unresolved electron band, it is necessary to take into account vibrational effects in channels exhibiting shape resonances. As we stated earlier, this is generally not a critical issue in nonresonant channels.

The resulting behavior of individual vibrational levels is shown in the bottom half of figs. 21 and 22. Looking first at the partial cross sections in fig. 21, we see that the resonance position varies over a few volt depending on the final vibrational state, and that higher levels are relatively more enhanced at their resonance position than is $v_f = 0$. This sensitivity to v_f arises because transitions to alternative final vibrational states preferentially sample different regions of R . In

particular, $v_f = 1, 2$ sample successively smaller R , governed by the maximum overlap with the ground vibrational state, causing the resonance in those vibrational channels to peak at higher energy than that for $v_f = 0$. The impact of these effects on branching ratios is clearly seen in fig. 23, where the ratio of the higher v_f intensities to that of $v_f = 0$ is plotted in the resonance region. There we see that the ratios are slightly above the FC factors (9.3%, $v_f = 1$; 0.6%, $v_f = 2$) at zero kinetic energy, go through a minimum just below the resonance energy in $v_f = 0$, then increase to a maximum as individual $v_f > 0$ vibrational intensities peak, and finally approach the FC factors again at high kinetic energy. Note that the maximum enhancement over the FC factors is progressively more pronounced for higher v_f , i.e., 340% and 1300% for $v_f = 1, 2$, respectively, in this calculation.

Equally dramatic are the effects on $\beta(v_f)$ shown in the lower portion of fig. 22. Especially at and below the resonance position, β varies greatly for different final vibrational levels. The $v_f = 0$ curve agrees well with the solid curve in the upper half, since the gross behavior of the vibrationally unresolved electronic band will be governed by the β of the most intense component. The $R = R_e$ curve has been found to agree well with wavelength-dependent measurements (Marr et al. 1979, Carlson et al. 1980), and the agreement is improved by the slight damping caused by R averaging. More significant for the present purposes is the v_f -dependence of β . Carlson first observed (Carlson 1971, Carlson and Jonas 1971) that, at 584 Å, the $v_f = 1$ level in the $3\sigma_g$ channel of N_2 had a much larger β than the $v_f = 0$ level even though there was no apparent autoionizing state at that wavelength. This is in semiquantitative agreement with the results in fig. 22 which give $\beta(v_f = 0) \sim 1.0$ and $\beta(v_f = 1) \sim 1.5$. Although the agreement is not exact, we feel this demonstrates that the "anomalous" v_f -dependence of β in N_2 stems mainly from the σ_u shape resonance which acts over a range of the spectrum many times its own ~ 5 eV width. The underlying cause of this effect is the shape-resonance-enhanced

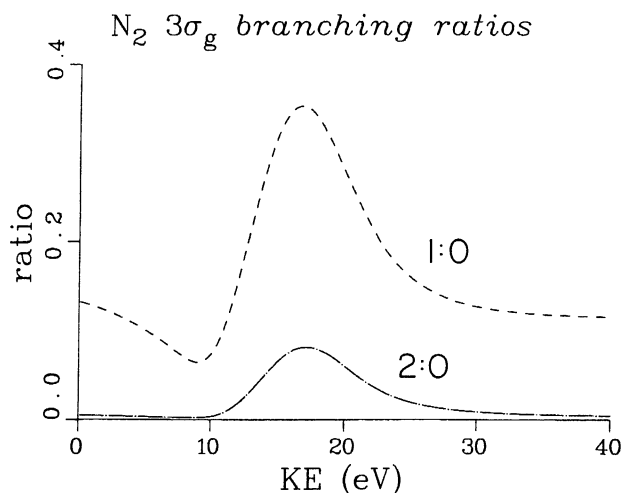


Fig. 23. Vibrational branching ratios $\sigma(v_f)/\sigma(v_f = 0)$ for photoionization of the $3\sigma_g$ level of N_2 .

R -dependence of the dipole amplitude, just as for the vibrational partial cross sections. In the case of $\beta(v_i)$, however, both the R -dependence of the phase and of the magnitude of the complex dipole amplitude play a crucial role, whereas the partial cross sections depend only on the magnitude.

This prototype study demonstrated several new aspects of photoionization channels exhibiting shape resonances: First, the localization and delay in photoelectron escape associated with a shape resonance enhances the sensitivity of photoelectron dynamics to nuclear separation, invalidating the FC factorization of the two modes. The resulting asymmetric and non-monotonic dependence of the transition amplitude on internuclear separation requires the folding of the transition amplitude with the vibrational motion of the molecule, at least at the level of eq. (10). Under certain circumstances, interference effects, analogous to those exhibited by the 2.4 eV π_g resonance in e-N₂ scattering (Bardsley and Mandl 1968, Schulz 1973, 1976, Lane 1980, Shimamura and Takayanagi 1984, Herzenberg and Mandl 1962, Birtwistle and Herzenberg 1971, Chandra and Temkin 1976, Schneider et al. 1979) may be important as well. Second, the effects are large in both vibrational intensities and angular distributions, but were largely overlooked in earlier work because shape resonance effects tend to lie in an inconvenient wavelength range for laboratory light sources. Synchrotron radiation has since solved this problem. Third, it is significant to note that the effects of the shape resonance described above act over tens of volts of the spectrum, several times the halfwidth of the resonance, and that σ and β probe the effects differently, i.e., have maximal effects in different energy regions. This underscores the well-known difference in dynamical information contained in the two physical observables. Fourth, a long-standing "anomalous" v_i -dependence in the photoelectron angular distributions of the $3\sigma_g$ channel of N₂ has been resolved. Finally, the phenomena described here for one channel of N₂ should be very widespread, as shape resonances now appear to affect one or more of the inner- and outer-shell channels in most small (nonhydride) molecules.

These theoretical predictions were soon tested in two separate experiments as indicated in figs. 24 and 25. In fig. 24, the branching ratio for production of the $v = 0$ and 1 vibrational levels of N₂⁺ X $^2\Sigma_g^+$ is shown. The dash-dot curve is the original prediction (Dehmer et al. 1979) from fig. 23. The solid dots are the measurements (West et al. 1980) in the vicinity of the shape resonance at $h\nu \sim 30$ eV. The conclusion drawn from this comparison is that the observed variation of the vibrational branching ratio relative to the FC factor over a broad spectral range qualitatively confirms the prediction; however, subsequent calculations (Raseev et al. 1980, Lucchese and McKoy 1981b, Leal et al. 1984) with fewer approximations have achieved better agreement based on the same mechanism for breakdown of the FC separation. The dashed and solid curves are results based on a Schwinger variational treatment (Lucchese and McKoy 1981b) of the photoelectron wavefunction. The two curves represent the length and velocity form of the transition matrix element, both of which are in excellent agreement with the data. This is an outstanding example of interaction between experiment and theory, proceeding as it did from a novel prediction, through

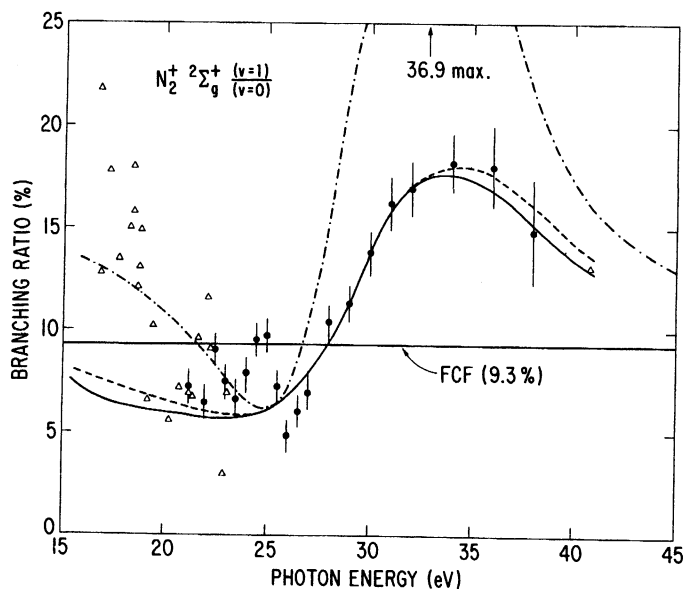


Fig. 24. Branching ratios for production of the $v=0, 1$ levels of $N_2^+ X^2\Sigma_g^+$ by photoionization of N_2 : \bullet , from West et al. (1980); Δ , from Gardner and Samson (1978); $-\cdot-\cdot-$, multiple scattering model prediction from Dehmer et al. (1979); $---$, frozen-core Hartree-Fock dipole length approximation from Lucchese and McKoy (1981b); $---$, frozen-core Hartree-Fock dipole velocity approximation from Lucchese and McKoy (1981b).

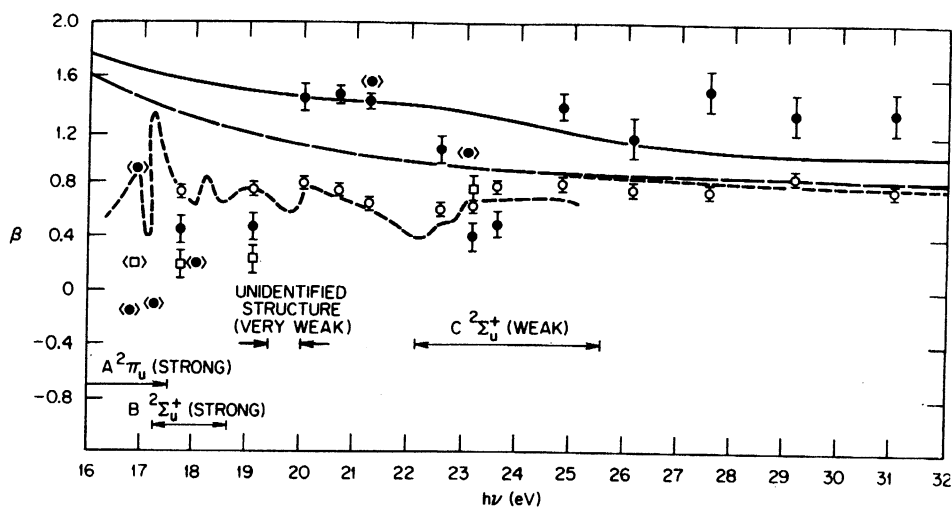


Fig. 25. Photoelectron asymmetry parameters for the $v=0, 1$ levels of $N_2^+ X^2\Sigma_g^+$: \circ , $v=0$ data from Carlson et al. (1980); \bullet , $v=1$ data from Carlson et al. (1980); long-dashed curve, $v=0$ prediction from Dehmer et al. (1979); solid curve, $v=1$ prediction from Dehmer et al. (1977); other data described by Carlson et al. (1980), from which this figure was taken.

experimental testing, and final quantitative theoretical agreement in a short time. Also shown in fig. 24 are data in the $15.5 \text{ eV} \leq h\nu \leq 22 \text{ eV}$ region which are earlier data (Gardner and Samson 1978) obtained using laboratory line sources. The apparently chaotic behavior arises from unresolved autoionization structure, whose detailed study is discussed in the next section.

Figure 25 shows angular distribution asymmetry parameters (β) for the $v = 0, 1$ levels of $\text{N}_2^+ \text{X } ^2\Sigma_g^+$ over roughly the same energy region. These data were taken at the Synchrotron Radiation Center at the University of Wisconsin by Carlson and coworkers (Carlson et al. 1980). In the region above $h\nu \sim 25 \text{ eV}$, this data also shows qualitative agreement with the predicted (Dehmer et al. 1979) v -dependence of β caused by the σ_v shape resonance. In this case the agreement is somewhat improved in later calculations (Lucchese and McKoy 1981b), mainly for $v = 1$; however, the change is less dramatic than for the branching ratios.

5.2. Autoionization via the Hopfield series in N_2

Recall the scattered data in the $15.5 \text{ eV} \leq h\nu \leq 20 \text{ eV}$ region of the vibrational branching ratio data for N_2 shown in fig. 24. As indicated in the discussion of that data, the scatter was produced by unresolved autoionization structure leading to the A and B states of N_2^+ (see fig. 19). The high-resolution total photoionization spectrum (P.M. Dehmer et al. 1984) of N_2 in that spectral range is given in figs. 26 and 27, showing the rich autoionization structure in the N_2 spectrum. This serves to emphasize the difference in precision needed in studying the two types of resonant photoionization processes, i.e., shape and autoionizing resonances. The relatively broad Hopfield absorption and emission Rydberg series (Hopfield 1930a,b) converging to the $v = 0$ level of $\text{N}_2^+ \text{B } ^2\Sigma_u^+$ at 661.2 \AA was chosen for the initial triply differential study (Parr et al. 1981) of molecular autoionization structure. The choice was guided by two considerations: First, the series represented a relatively isolated series whose lower members were sufficiently broad to permit systematic investigation within autoionization profiles with available instrumentation. Second, this was considered a good prototype system wherein the full rotational-vibrational-electronic autoionization process is in play. In this case, the autoionizing states consist of a Rydberg electron bound to an electronically-excited $\text{N}_2^+ \text{B } ^2\Sigma_u^+$, $v = 0$ core. Ionization occurs when the Rydberg electron collides with the core, enabling the exchange of the large electronic excitation energy from the core together with smaller amounts of energy to or from the nuclear modes.

Although several members of the Hopfield absorption and emission series have been studied (West et al. 1981) by triply differential photoelectron spectroscopy, we will focus here on the lowest (and broadest) $m = 3$ members of these series at $\lambda = 723.3$ and 715.5 \AA , respectively. The spectroscopic assignments for these series are summarized elsewhere (Parr et al. 1981). Here we note that the window and main absorption series, together with a weaker absorption series between them seem to be most consistent with the designation $nd\pi_g$, $nd\sigma_g$, and $ns\sigma_g$.

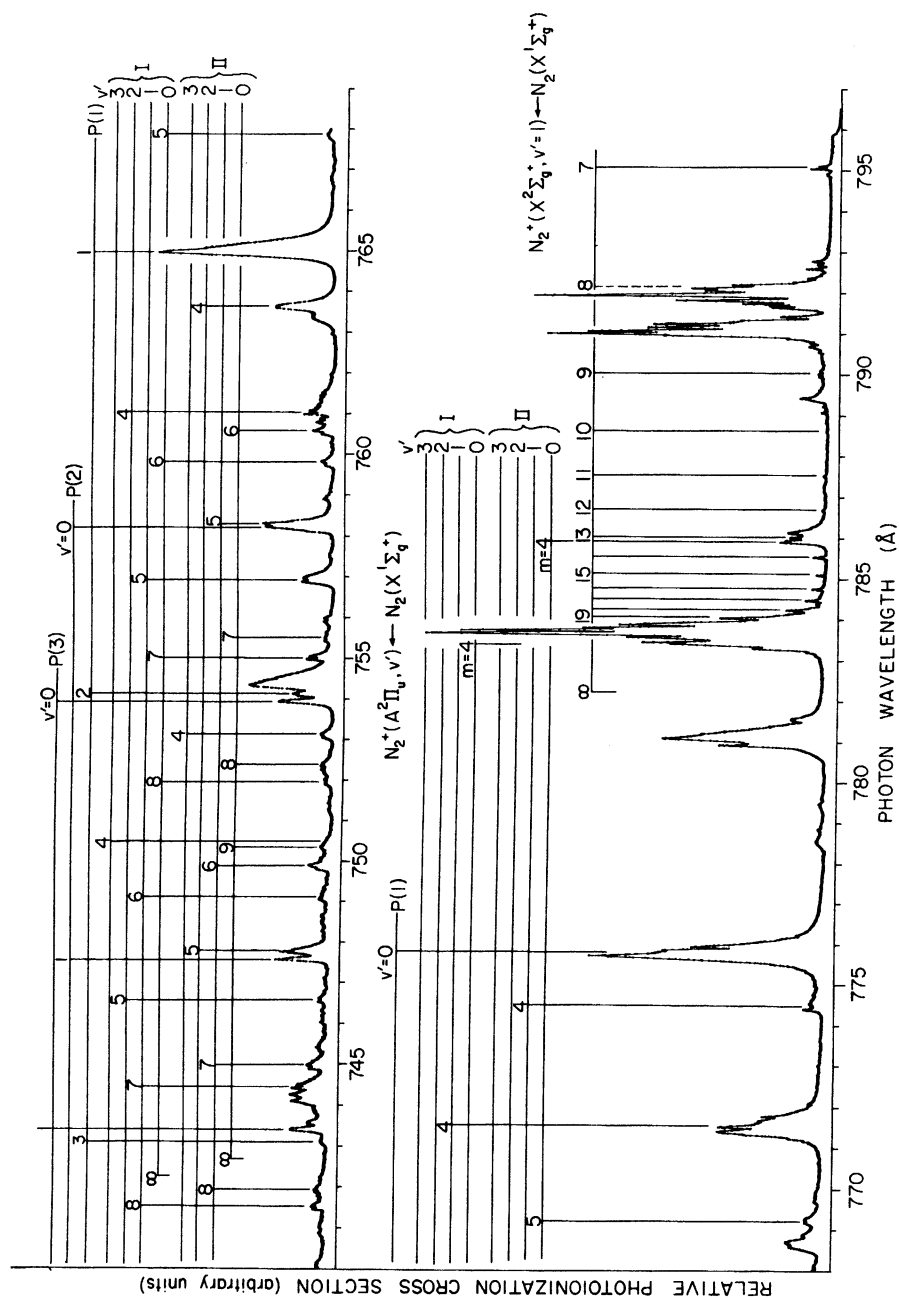


Fig. 26. A portion of the photoionization spectrum of N_2 at 78 K. (Taken from P.M. Dehmer et al. 1984.)

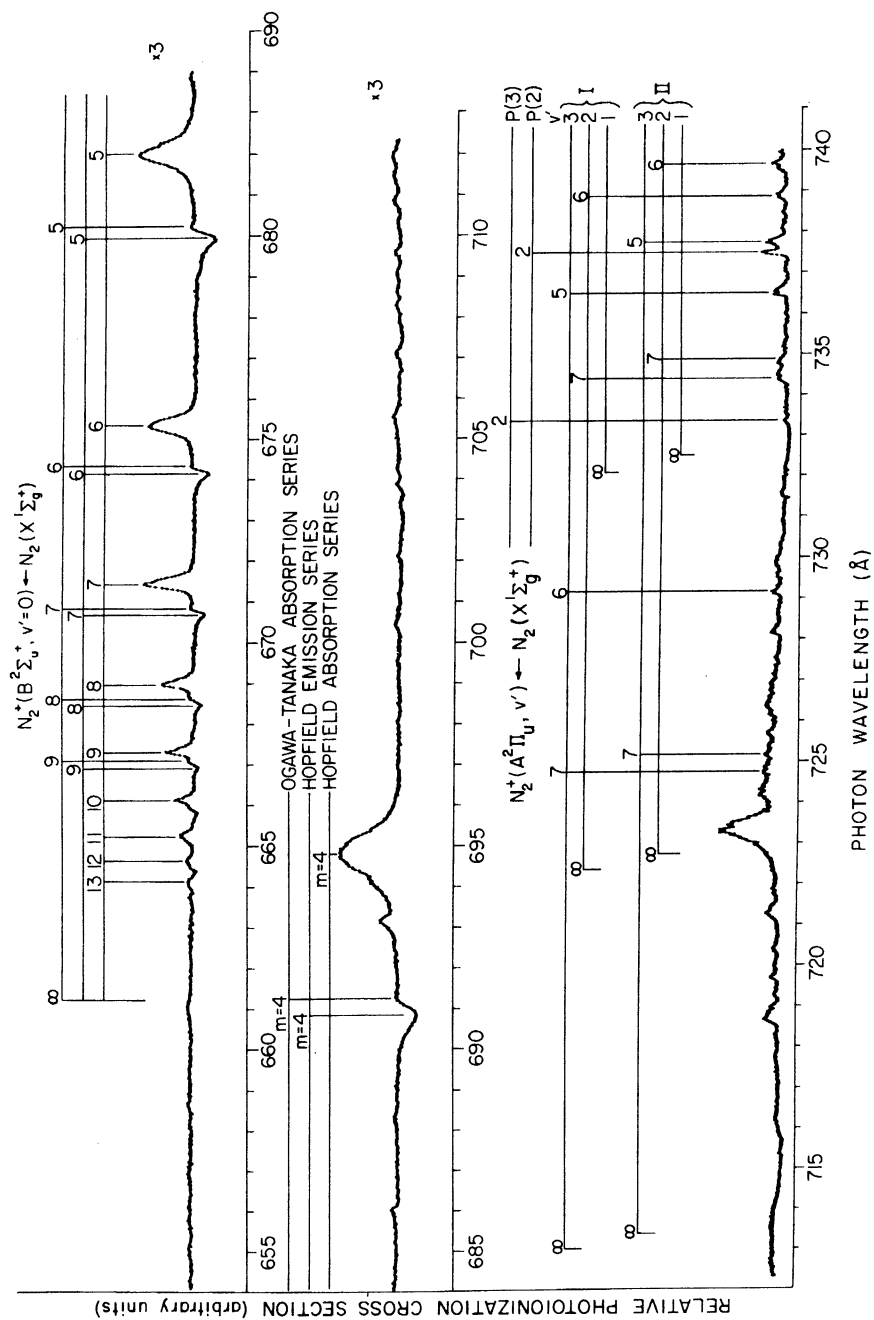


Fig. 27. A portion of the photoionization spectrum of N_2 at 78 K. (From P.M. Dehmer et al. 1980.)

These assignments have been confirmed in recent theoretical work (Raoult et al. 1983).

In fig. 28, we present the vibrational branching ratios for formation of the ground-state ion $N_2^+ X^2\Sigma_g^+$ by photoionization in the range $710 \text{ \AA} \leq \lambda \leq 730 \text{ \AA}$. Here we define the vibrational branching ratio as the ratio of the intensity of a particular vibrational level to the sum over the whole vibrational band. In fig. 29 the asymmetry parameter β is given for the same processes. In both figures the positions of the Hopfield emission and absorption features at 715.5 and 723.3 \AA , respectively, are indicated by solid lines joining the upper and lower frames. In the vicinity of these features, a hand-drawn dashed curve is constructed only to guide the eye, and should not be taken too seriously. In both figures, typical error bars for the data in each frame are shown on the last point. Duplicate branching ratio measurements (the open circles were taken at the magic angle and the solid dots were deduced from the angular distribution measurements) show the reproducibility of the data. Note that an early branching-ratio study of this region of the N_2 photoionization spectrum was reported by Woodruff and Marr (Marr and Woodruff 1976, Woodruff and Marr 1977) but without angle dependence and with insufficient wavelength resolution to characterize the profiles of the Hopfield resonances.

Focusing first on the vibrational branching ratios in fig. 28, we see three major qualitative features:

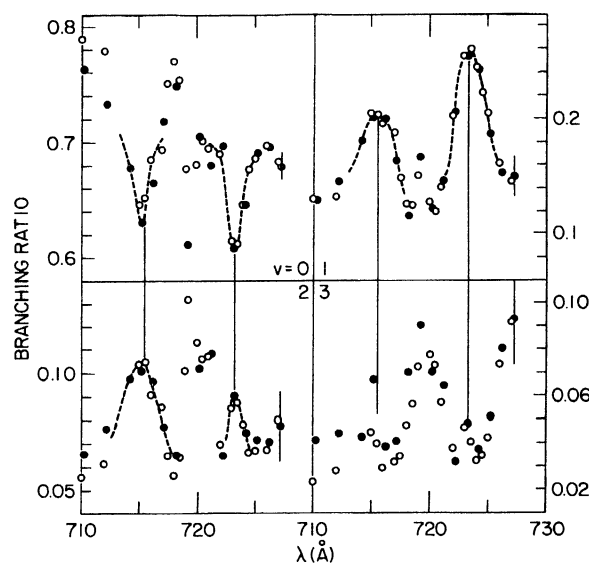


Fig. 28. Vibrational branching ratios for production of $N_2^+ X^2\Sigma_g^+$ ($v=0-3$ in the range $710 \text{ \AA} \leq \lambda \leq 730 \text{ \AA}$). Vertical lines at 715.5 and 723.3 \AA denote the positions of the first members of the Hopfield "emission" and absorption series approaching the $N_2^+ B^2\Sigma_u^+$ ($v=0$) limit. Typical error bars are indicated on the last point in each frame. The dashed line is hand drawn to guide the reader's eye.

Open and closed circles represent two independent runs. (Figure taken from Parr et al. 1981.)

(1) The $v = 0$ branching ratio exhibits pronounced dips at the locations of the two major autoionization features, whereas the higher vibrational channels, most notably $v = 1$, show enhancements. Hence, the quasibound autoionizing states mediate a transfer of dipole amplitude from the $v = 0$ channel to the much weaker $v = 1, 2$, and 3 channels, a transfer which involves simultaneous electronic de-excitation and vibrational excitation of the ion core. This transfer is primarily directed to the $v = 1$ channel and is much diminished by $v = 3$. This enhancement of vibrational channels with small Franck-Condon factors relative to the most intense channel is reminiscent of the effects of shape resonances in those few cases studied so far. Comparison with vibrational autoionization in H_2 , where ionization channels with the minimum (negative) Δv usually dominate (Raoult and Jungen 1981, Berry and Nielsen 1970a,b) is not straightforward since $\Delta v = 0$ is permitted in this case; and, anyhow, transitions in which vibrational excitation occurs are favored. Establishing the systematics of this diverse set of observations is obviously a most timely problem.

(2) Despite the great contrast between the window and absorption profiles in the photoabsorption and photoionization spectra, the profiles in fig. 28 are of similar shape and both exhibit either an enhancement or depletion, depending upon the channel.

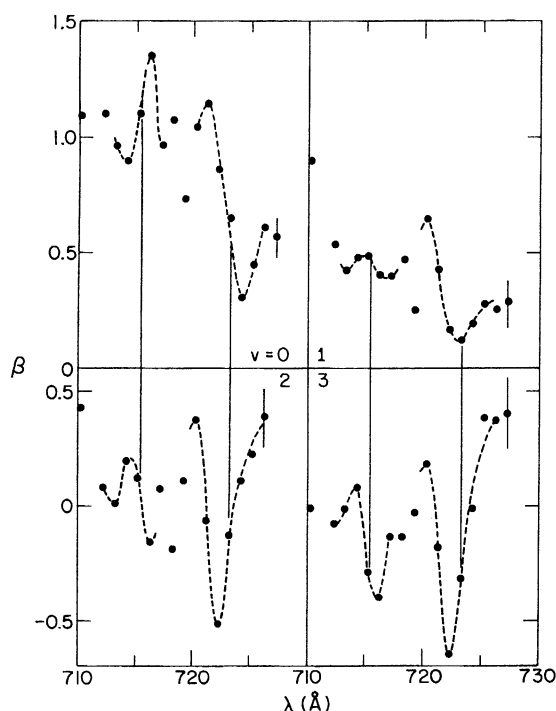


Fig. 29. Photoelectron asymmetry parameters corresponding to the production of $N_2^+ X^2\Sigma_g^+$ ($v = 0-3$) in the range $710 \text{ \AA} \leq \lambda \leq 730 \text{ \AA}$. Other conventions as in fig. 28. (Figure taken from Parr et al. 1981.)

(3) Definite "interloper" structure occurs between the two major resonances, with variable shape and strength. Both the weak absorption peak near the window resonance and other weak structures (one peak in the photoionization spectrum at 718.8 Å correlates well with the main interloper structures in fig. 28) may play a role here.

The angular distribution results in fig. 29 also exhibit structure at the positions of the two major resonances and in between. Implicit in the spectral variations in β is information on both the vibrational branching ratios and the relative phases of the alternative vibrational ionization channels. Specifically, the competition between asymptotic phases produces large asymmetric variations in β at the resonance positions, which vary from one final vibrational level to another. For instance, the β curve near the Hopfield "emission" line exhibits a peak for $v=0$ that evolves into a dip for $v=3$. Near the Hopfield absorption profile, the position of the minimum in β , although not extremely well defined by these data, shifts from the long-wavelength side of the resonance position to the short-wavelength side.

Following these measurements and the related partial cross section measurements by Morin et al. (Morin 1983, Morin et al. 1987, see also Nenner and Beswick 1987), Raoult et al. (1983) applied a two-step formulation of MQDT to the $m=3$ member of the Hopfield series in N_2 . This represented the first *ab initio* study of electronic autoionization profiles in molecules and was very successful in obtaining reasonable agreement with experiment, especially in light of the complexity of the calculation, which involved forty-seven electronic quantities corresponding to five electronic channels for Σ symmetry and six for Π symmetry.

Several approximations were utilized in order to treat such a complicated excited complex (e.g., fixed internuclear separation, neglect of correlation in the final continuum state). Nevertheless, this pioneering calculation succeeded in three important areas: It clearly established the assignments of the Hopfield absorption and emission series. It achieved reasonable agreement with the partial cross sections between 700 and 730 Å, measured by Morin et al. (Morin 1983, Morin et al. 1987, see also Nenner and Beswick 1987) and rationalized the cause for remaining differences. Finally, it achieved semiquantitative agreement for the asymmetry parameters measured by West et al. (1981) for the $X^2\Sigma_g^+$ and $A^2\Pi_u$ states in this same wavelength region.

Here we will highlight the calculation of the β results as they were found to be consistent with the partial cross section results and, furthermore, proved to be useful in revealing details which are hardly seen in the partial cross sections. This stresses the complementarity of the two types of dynamical parameters.

Figure 30 displays the variation of the asymmetry parameter with photon energy. The calculated β value is purely electronic and has been obtained for $R=2.068$ a.u. Raoult et al. (1983) compared their calculation to the vibrationally resolved experimental β values for the $v=0$ component of both the $X^2\Sigma_g^+$ and $A^2\Pi_u$ N_2^+ states. Indeed, the effect of electronic autoionization is expected to be the largest in the $X^2\Sigma_g^+$, $v=0$ and $A^2\Pi_u$, $v=0$ continua, because the corresponding vibrational wavefunctions have the largest overlap with the $B^2\Sigma_u^+$, $v=0$

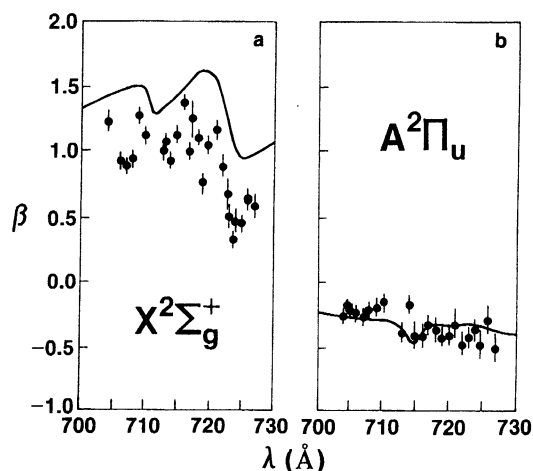


Fig. 30. Comparison of *ab initio* MQDT calculations with experimental results for the asymmetry parameter resulting from photoionization of N_2 in the $700 \text{ \AA} \leq \lambda \leq 730 \text{ \AA}$ region. Data points are from West et al. (1981) and the theoretical curve (solid line) and figure are taken from Raoult et al. (1983).

vibrational wavefunction. (One assumes that the Rydberg states and the corresponding ionic core have the same vibrational functions.)

The asymmetry parameter β calculated for the $X^2\Sigma_g^+$ core state is globally in agreement with the experimental results (see fig. 30a). The calculated off-resonance value results from an interference between outgoing p and f waves. If only the p wave (f wave) is considered, with the transition moments given by Raoult et al. (1983), the β value should be 1.7 (0.73). At 700 \AA , the calculated β value is 1.33, intermediate between these two single-wave values. The two dips around 712 and 725 \AA reproduce well the observed features. The β energy variation may be understood as follows. If a resonant state decays mainly in one specific channel $l\lambda$ at the energy corresponding to the maximum of the resonance in the cross section, only one term dominates the β expression, and β takes a geometrical value, $\beta_{l\lambda}$. These geometrical values are listed in table 1 in the article by Thiel (1982). Thus, the dip at 725 \AA may be understood when one looks at the different $l\lambda$ contributions to the $X^2\Sigma_g^+$ partial cross section. The $(B^2\Sigma_u^+)3'd'\sigma_g$ Rydberg state autoionizes preferentially in the $(X^2\Sigma_g^+)\epsilon f\sigma_u$ continuum and at 724 \AA , the maximum in the cross section, the β value must be $\beta_{f\sigma} = 0.53$. Indeed, this value is attained experimentally (see fig. 30a). The calculated value is larger because the resonance in the $f\sigma$ cross section was evaluated to be too small (Raoult et al. 1983). Nevertheless, this proves that the calculations are qualitatively consistent with experiment, since the continuum–continuum interaction $(B^2\Sigma_u^+)\epsilon d\sigma_g/(X^2\Sigma_g^+)\epsilon f\sigma_u$ is computed to be greater than the $(B^2\Sigma_u^+)\epsilon d\sigma_g/(X^2\Sigma_g^+)\epsilon p\sigma_u$ one (Raoult et al. 1983). The dip at 712 \AA is more difficult to interpret because the β value results from the combined effects of the $3d\pi_g$ and $4s\sigma_g$ resonances. Indeed, no single $l\lambda$ contribution is dominant in this region. Two experimental features are not reproduced. The feature at 719 \AA corresponds to

the peak which is seen in the total cross section of fig. 27. This state was previously assigned to the $(A^2\Pi_u, v^+ = 3)10s\sigma_g$ state by Ogawa and Tanaka (1962). It is difficult to be confident in this assignment, because the vibrational overlap between $A^2\Pi_u, v = 3$ and $X^2\Sigma_g^+, v^+ = 0$ is very weak. However, the appearance of this feature in fig. 30a confirms that this unknown state autoionizes electronically in the $(X^2\Sigma_g^+)\epsilon l\lambda$ continua as argued in the partial cross section discussion in the article by Raoult et al. (1983). Similarly, the dip around 705 Å is not assigned to a $(A^2\Pi_u, v^+ = 4)nl\lambda$ Rydberg state but rather to the $(B^2\Sigma_u^+, v^+ = 1)4's'\sigma_g$ and $(B^2\Sigma_u^+, v^+ = 1)3d\pi_g$ states which are expected in this spectral range. Comparison (Raoult et al. 1983) of the partial cross sections and asymmetry parameters shows that, for equivalent energy resolution, features which appear very weakly in the partial cross sections can be seen in the β measurements.

In contrast to the β for the $X^2\Sigma_g^+$ channel, the energy variation of β for the $A^2\Pi_u, v = 0$ channel is flat (fig. 30b). The MQDT calculation reproduces this behavior very well. The detailed dynamics in this channel are discussed further by Raoult et al. (1983).

In this section we have focused our attention on the Hopfield series. In principle, with *ab initio* electronic quantities, it should be straightforward to calculate, by an MQDT treatment, the photoionization spectrum throughout the spectral range between the $X^2\Sigma_g^+$ and $A^2\Pi_u$ ionization limits. But, in this region, in addition to the vibrational and dissociation effects, it would be important to include the perturbation by the valence states and the intensity borrowing of the $(A^2\Pi_u)^3\Pi_u$ states from the $^1\Pi_u$ states. Simultaneously with these improvements in the calculations, new measurements of the partial cross sections and of the photoelectron angular distributions would be useful to clarify the assignments of numerous unidentified bands in this region. In particular, the $(A^2\Pi_u)nd\delta_g$ series has not yet been identified in spite of its expected strong transition moment. Clearly, the results of this case study have marked the beginning of a significant advance in understanding the detailed dynamics of electronic autoionization in small molecules while indicating the need for further advances in both *ab initio* calculations and high-resolution triply differential photoelectron measurements.

5.3. Continuum–continuum coupling effects in $N_2\ 2\sigma_u$ photoionization

Our third case study concerns photoionization of the $2\sigma_u$ subshell in N_2 , i.e., the third band in fig. 20 with an IP of ~ 18.8 eV. This channel is presently the clearest example in molecular photoionization of continuum–continuum coupling and has been studied very recently by both theoretical (Stephens and Dill 1985) and experimental means (Southworth et al. 1986).

Coupling between molecular photoelectrons and residual electrons is usually weak, because continuum electrons are so diffuse that they have negligible amplitude in the molecular interior (see, e.g., section 2.3) where strong interaction can take place. By the same token, prominent structure in photoionization spectra can signal special dynamical circumstances which enhance electronic

amplitude in the core region, and which thereby may amplify many-electron effects. It was proposed (Stephens and Dill 1983) that the marked deviations from one-electron predictions seen in the 25–35 eV photon energy range in the photoionization spectra of the $2\sigma_u$ level of N_2 reflect just such amplification. The deviations coincide with the shape-resonant enhancement of $3\sigma_g^{-1}\epsilon\sigma_u$ f-wave ($l=3$) photoelectrons in the molecular core, (see, e.g., section 2.2) and they are particularly striking in the photoelectron asymmetry parameter β (Marr et al. 1979, Wallace et al. 1979, Lucchese et al. 1982, Adam et al. 1983). This correlation in energy with the σ_u shape resonance in the $3\sigma_g$ channel, together with strong angular distortion characteristic of high orbital momenta, is the basis of the surmise that the departure of N_2 $2\sigma_u$ photoionization from independent-electron model predictions is due to electronic continuum configuration mixing with the $3\sigma_g^{-1}\epsilon\sigma_u$ f-wave shape resonance. The results of a recent *ab initio* *K*-matrix study (Stephens and Dill 1985) showed directly that this mechanism is an important part of N_2 $2\sigma_u$ photoionization dynamics.

Shape-resonance-enhanced interchannel coupling has been known for many years in atomic photoionization (Starace 1979). For example, one-electron (Herman–Skillman and Hartree–Fock) rare-gas, s-subshell photoionization cross sections and angular distributions may be substantially modified by interchannel coupling with strong, shape-resonant amplitude in other photoionization channels (Starace 1979, Johnson and Cheng 1979). Shape-resonant enhancement, mediated by continuum–continuum coupling, has also been proposed recently to account for resonant activity seen in SF_6 photoionization channels that would not support shape resonances in the independent-electron approximation (see, e.g., Dehmer et al. 1982, and section 5.5).

As inferred from atomic interchannel photoionization studies, what Stephens and Dill included in their description is the probability amplitude of forming a quasibound excited complex composed predominantly of an electron excited out of the $3\sigma_g$ subshell into the $\epsilon\sigma_u$ continuum. Within this complex, the $\epsilon\sigma_u$ electron may collide with an electron in the $2\sigma_u$ subshell. Thereby a $2\sigma_u$ electron may be ejected by simultaneous de-excitation of the $\epsilon\sigma_u$ electron back into the $3\sigma_g$ subshell. The $2\sigma_u$ orbital is more compact than the outer valence levels, and for an electron ejected from the outermost $3\sigma_g$ orbital to experience close-collision with this inner-shell electron with significant probability, and with observable consequences, an amplification mechanism must exist. The mechanism here is the molecular shape resonance, in which electronic amplitude in the $3\sigma_g^{-1}\epsilon\sigma_u$ channel is quasibound by a potential barrier in the molecular field over a narrow range of electron kinetic energy. In this way, the $\epsilon\sigma_u$ electron maintains a large amplitude in the core region, and hence provides favorable conditions for electronic collision.

Various results for the photoelectron asymmetry parameter of the $2\sigma_u$ channel of N_2 are shown in figs. 31 and 32 to illustrate the effect of continuum–continuum coupling. The dashed curve is the single-channel multiple-scattering model (MSM) result (Wallace et al. 1979) indicating the predicted behavior in the independent-electron, fixed-*R*, local exchange approximation. The solid line

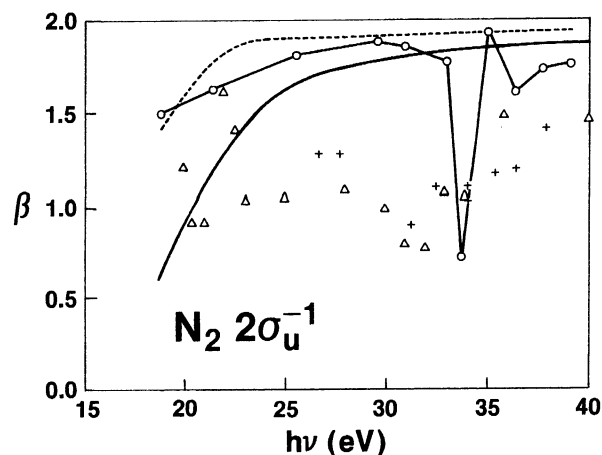


Fig. 31. Photoelectron asymmetry parameter for the $2\sigma_u$ level of N_2 : \circ , K -matrix results of Stephens and Dill (1985); —, Hartree-Fock results of Lucchese et al. (1982); ---, multiple-scattering model results of Wallace et al. (1979); Δ , experimental results of Marr et al. (1979); +, experimental results of Adam et al. (1983).

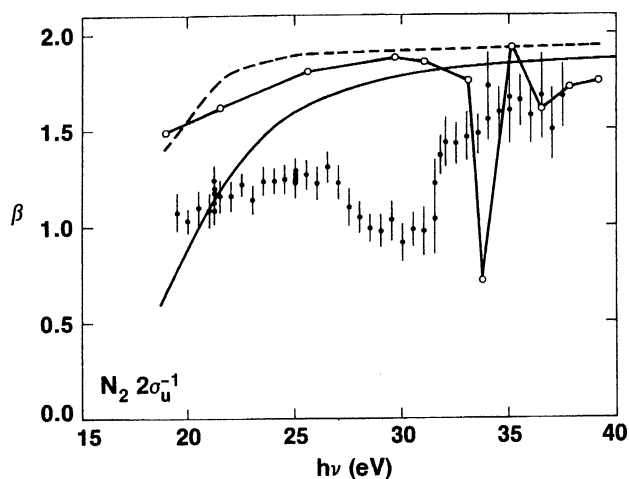


Fig. 32. Photoelectron asymmetry parameter for the $2\sigma_u$ level of N_2 : same conventions as fig. 31 plus data of Southworth et al. (1986), given by solid dots.

represents the Hartree-Fock result of Lucchese et al. (1982) which includes initial state correlation in addition to intrachannel coupling in the final state. This calculation improves both the initial state and the final state but still neglects coupling between alternative ionization channels. Early data on this channel taken independently by Marr et al. (1979) and by Adam et al. (1983) are shown in fig. 31. Although sparse, the data clearly shows a large systematic deviation from the one-electron calculations.

This deviation stimulated the K -matrix calculation of Stephens and Dill (1985). By adding electron–electron correlation in an MSM basis, they examined the effects of coupling between the σ_u shape resonance in the $3\sigma_g$ ionization channel and the nominally nonresonant $2\sigma_u$ channel. Their results are indicated by the open circles, connected by a solid line in figs. 31 and 32. These results show that coupling the two channels induces a dramatic dip in the β parameter at about 34 eV. This dip occurs at the photon energy of the σ_u shape resonance in the $3\sigma_g$ channel in the MSM model calculation used to generate the one-electron basis for the K -matrix calculation. The experimental energy of the shape resonance in the $3\sigma_g$ channel is, of course, near $h\nu = 30$ eV, as discussed above. (The MSM calculation could have been altered to reproduce this energy exactly, but this is usually not done as no new information is obtained and there is no point in exaggerating the accuracy of the method.)

At this point, it became apparent that better quality data was needed to interpret the significance of the pronounced dip in the K -matrix/MSM calculation. Hence, using second generation instrumentation, described in section 4, Southworth et al. (1986) reexamined the β for the $2\sigma_u$ channel of N_2 . The new data is shown as solid dots in fig. 32. This data shows the shape of the β curve much more clearly and allows us to draw several conclusions. First, the β curve exhibits a clear minimum at the photon energy of the σ_u shape resonance in the $3\sigma_g$ channel. Also, the width is close to the σ_u shape resonance width. These observations qualitatively confirm the continuum–continuum coupling mechanism evoked by Stephens and Dill. Second, the minimum is at lower energy and is broader than the calculation. The shift traces mainly to the location of the shape resonance in the independent-electron model calculation. The differences in shape, and to some extent the location, also arise from other approximations inherent in the prototype calculation, for example, neglect of vibrational motion. Third, the data converge to the HF results at energies above and below the shape resonance, indicating the return to essentially single-channel behavior in the absence of shape-resonance-enhanced interchannel coupling.

As in the other case studies emphasized here, this prototype study is but the tip of the iceberg in that this basic mechanism is expected to have widespread effects in molecular photoionization dynamics which can be explored in other circumstances now that the basic mechanism is understood.

5.4. Resonance effects in photoionization of the $1\pi_u$ level of C_2H_2

The fourth case study concerns the photoionization of the outermost $1\pi_u$ orbital of C_2H_2 in the region from the IP up to $h\nu \sim 25$ eV. This process has been under intense study, both experimentally (Kreile et al. 1981, Langhoff et al. 1981b, Unwin et al. 1981, Hayaishi et al. 1982, Keller et al. 1982, Parr et al. 1982a) and theoretically (Kreile et al. 1981, Langhoff et al. 1981b, Hayaishi et al. 1982, Keller et al. 1982, Machado et al. 1982, Levine and Soven 1983, Levine and Soven 1984, Lynch et al. 1984a), over the last few years. This keen interest results from three main interconnected questions which are posed by this spectrum: First,

C_2H_2 is isoelectronic with N_2 , which is rather well understood, so that the study of C_2H_2 represents a logical extension of previous work to a polyatomic molecule. In particular, how will the well-established π_g and σ_u shape resonance features influence the photoionization dynamics of this closely related molecule? Second, the total photoionization spectrum (Hayaishi et al. 1982, Berkowitz 1979, Botter et al. 1966, Collin and Delwiche 1967) of C_2H_2 displays a very prominent double hump structure with a deep minimum at $h\nu \sim 14$ eV. Strong non-Franck-Condon effects are also observed (Kreile et al. 1981, Langhoff et al. 1981b, Unwin et al. 1981, Keller et al. 1982, Parr et al. 1982a) in the vibrational branching ratios and v -dependent β s. The interpretation (Kreile et al. 1981, Langhoff et al. 1981b, Unwin et al. 1981, Hayaishi et al. 1982, Keller et al. 1982, Machado et al. 1982, Parr et al. 1982a, Levine and Soven 1983, 1984, Lynch et al. 1984a) of these structures has been a central topic of the recent work on C_2H_2 . Third, a key point in the photoionization dynamics of polyatomics is the existence of alternative vibrational modes. We discussed the shape-resonance-enhanced non-Franck-Condon effects in section 5.1 and the autoionization-induced non-Franck-Condon effects in section 5.2 for the case of N_2 . Having understood that case rather well, it is necessary to look for and understand the ramifications of resonances in other modes which arise in polyatomics. These issues represent increasing complexity relative to the previous case studies and are only partially answered here; however, this case was chosen to underscore the importance of extending our prototypical ideas to more complex molecules.

As mentioned above, the total photoionization spectrum (Hayaishi et al. 1982, Berkowitz 1979, Botter et al. 1966, Collin and Delwiche 1967) of C_2H_2 displays two prominent peaks in the $13 \text{ eV} \leq h\nu \leq 25 \text{ eV}$ region, one at $\sim 13.3 \text{ eV}$ (930 \AA) and another at 15.3 eV (810 \AA), with a dip centered at $\sim 14 \text{ eV}$. In order to examine the dynamics of this process in more detail, triply differential photoelectron measurements have been made on C_2H_2 in this region using synchrotron radiation (Keller et al. 1982, Parr et al. 1982a). We begin by introducing these data and emphasizing the effects of the two resonant features on vibration, including previously unobserved enhancement of weak bending modes below $h\nu \sim 16 \text{ eV}$ (Parr et al. 1982a).

The crux of the analysis of the data is an appreciation that the importance of alternative vibrational modes of the ion can vary drastically in different parts of the spectrum. In particular, predication of the analysis on the fact that the previously published HeI photoelectron spectrum (Baker and Turner 1968) of the $X^2\Pi_u$ band of C_2H_2^+ exhibits clearly only excitation of the C-C stretching mode would lead to an erroneous analysis of the spectra for $h\nu < 16 \text{ eV}$, where resonant excitation has been found (Parr et al. 1982a) to lead to substantial excitation of other modes, i.e., bending modes. In fact, this observation, documented below for C_2H_2^+ , is probably the rule rather than the exception for variable-wavelength studies of polyatomics, for which allowance must always be made for enhanced excitation of vibrational modes which have very small Franck-Condon factors and hence are often difficult to detect in photoelectron spectra at nonresonant wavelengths.

To illustrate this, we show angle-resolved photoelectron spectra of $\text{C}_2\text{H}_2^+ \text{X } ^2\Pi_u$ at $\lambda = 563.6 \text{ \AA}$ (22.0 eV) and at $\lambda = 885.6 \text{ \AA}$ (14.0 eV) in figs. 33 and 34, respectively. At $h\nu = 22 \text{ eV}$ (fig. 33) a single 0.222 eV vibrational spacing, corresponding to the C–C stretch mode, adequately describes the observed spectrum. Use of this single mode, together with a constant (instrumental) peak width of $\sim 120 \text{ meV}$ and a background level determined at the extremities of the data in fig. 33, results in an excellent least-squares fit and is in agreement with the He I photoelectron spectrum (Baker and Turner 1968). (In fig. 33 the solid line is the spectrum generated by the least-squares fit and the vertical solid bars indicate the position and relative strengths of the members of the C–C stretch progression.) Below $h\nu = 16 \text{ eV}$, however, this analysis procedure was found (Parr et al. 1982a) to be inadequate: The peak positions of the higher members of the progression appeared shifted, the valleys between the peaks appeared to fill in more than the resolution or background level warranted, and the quality-of-fit parameter degraded significantly. The key to this puzzle was supplied by a recent high-resolution, high-sensitivity He I photoelectron spectrum (Dehmer and Dehmer 1982) which indicated the location of previously unobserved bending modes of the ground state of C_2H_2^+ with intensities at the $\sim 1\%$ level. The observed vibrational spacings were 0.036 eV, 0.086 eV, and 0.172 eV, and are believed to correspond to a trans-bending mode and a cis-bending mode and its harmonic. The first of these is too close to the main C–C stretch progression to be separated with the

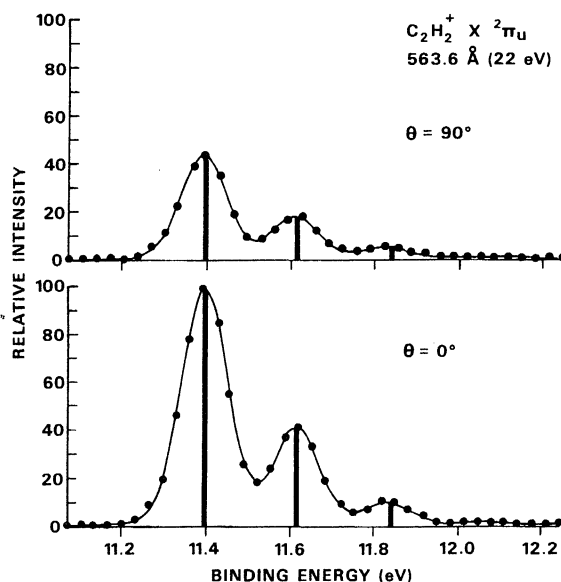


Fig. 33. Photoelectron spectra of $\text{C}_2\text{H}_2^+ \text{X } ^2\Pi_u$ at $h\nu = 22.0 \text{ eV}$ and at $\theta = 0^\circ$ and 90° . Both spectra are normalized so that the maximum counts in the $\theta = 0^\circ$ spectrum equals 100. The data points (\bullet) and nonlinear least-squares-fit curve (—) are indicated. The amplitudes and positions of the C–C stretch vibrational components yielded by the fit are represented by the vertical solid bars.

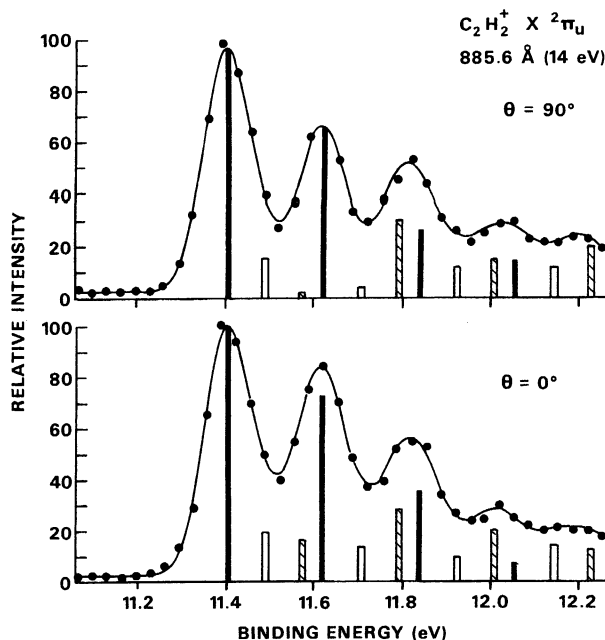


Fig. 34. Photoelectron spectra of $C_2H_2^+ X^2\Pi_u$ at $h\nu = 14$ eV and at $\theta = 0^\circ$ and 90° . Both spectra are normalized so that the maximum counts in the $\theta = 0^\circ$ spectrum equals 100. The data points (●) and nonlinear least-squares-fit curve (—) are indicated. The amplitudes and positions of the vibrational components yielded by the fit are as follows: solid bars: C–C stretch; clear bars: 0.086 eV bending mode; cross-hatched bar: 0.172 eV harmonic of bending mode.

resolution of the present experiment; however, when the 0.086 eV and 0.172 eV modes were added to the fitting procedure, the fit quickly converged with a quality-of-fit parameter equal to the high-energy ($h\nu > 16$ eV) fits. The result is illustrated in fig. 34 for $h\nu = 14.0$ eV, where the 0.222 eV, 0.086 eV, and 0.172 eV vibrational progressions are indicated by solid, clear, and hatched bars, respectively. Again, the vertical bars indicate the spectral position and relative intensities of the various vibrational components, and the solid line is the spectral shape of the band generated by the least-squares fit. In comparing figs. 33 and 34, note particularly the reduced peak-to-valley ratio and the shift of the experimental peaks away from the C–C stretch components in fig. 34. The cause for the changes in the spectral shape and peak positions is clearly attributable to the enhanced excitation of the bending modes in the low-energy portion of the excitation spectrum. In fact, transitions involving resonant excitation of bending vibrations become comparable to or even dominate higher members of the main progression at certain wavelengths. Another qualitative observation made clear by figs. 33 and 34 is that the lower-energy spectrum is more isotropic than the higher-energy spectrum, i.e., has a lower β value.

In figs. 35 and 36 we present the spectral variation of the vibrational branching ratios and v -dependent β 's for the dominant C–C stretch mode of $C_2H_2^+ X^2\Pi_u$ in

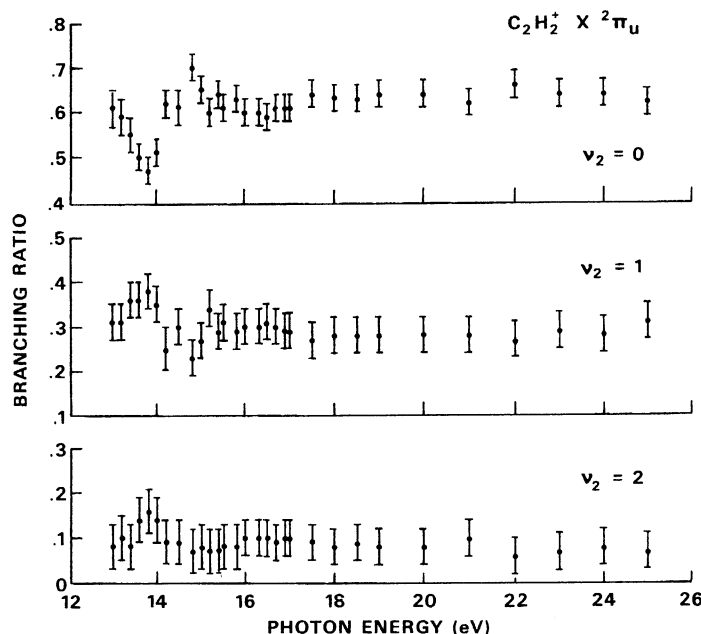


Fig. 35. Vibrational branching ratios for the $v_2 = 0, 1$, and 2 symmetric stretch components of $C_2H_2^+ X^2\Pi_u$.

the range $13 \text{ eV} \leq h\nu \leq 25 \text{ eV}$. Although fig. 34 demonstrates the importance of the bending modes for $h\nu < 16 \text{ eV}$, the branching ratios and β 's deduced from the least-squares fit were not of sufficient quality to clearly establish the spectral variation of these parameters in the $h\nu < 16 \text{ eV}$ region where they were excited with appreciable intensity. That is, they were usually of less statistical quality than the $v_2 = 2$ C-C stretch data in figs. 35 and 36. Also, they are excited almost exclusively by resonant excitation and tend to vary more sharply than the FC-allowed C-C stretch mode. Hence, they should be mapped on a finer energy mesh. Therefore, we confine further discussion of resonance effects to the stronger C-C stretch mode, whose analysis has nevertheless been improved by including the bending frequencies in the fit for $h\nu < 16 \text{ eV}$. We stress, therefore, that future higher resolution work remains to be done for $h\nu < 16 \text{ eV}$ to completely characterize the photoionization dynamics of this channel in C_2H_2 .

Focussing on the spectral behavior of the C-C stretch mode (referred to simply as $v_2 = 0, 1, 2$ from now on) in figs. 35 and 36, we can make the following general observations. First, in fig. 35, the vibrational branching ratios exhibit different profiles in the $h\nu < 16 \text{ eV}$ region and converge to constant values for $h\nu > 16 \text{ eV}$. Thus, they exhibit non-Franck-Condon behavior below $h\nu = 16 \text{ eV}$, and FC behavior above. For example, the $v_2 = 0$ curve exhibits a local dip at $h\nu \sim 13.8 \text{ eV}$, whereas the $v_2 = 1$ and 2 curves show an enhancement; and the $v_2 = 0$ is enhanced near $h\nu = 15 \text{ eV}$, at which energy the $v_2 = 1$ curve dips and the $v_2 = 2$ curve stays flat. Second, the spectral variation of the non-FC branching ratios in fig. 35 are

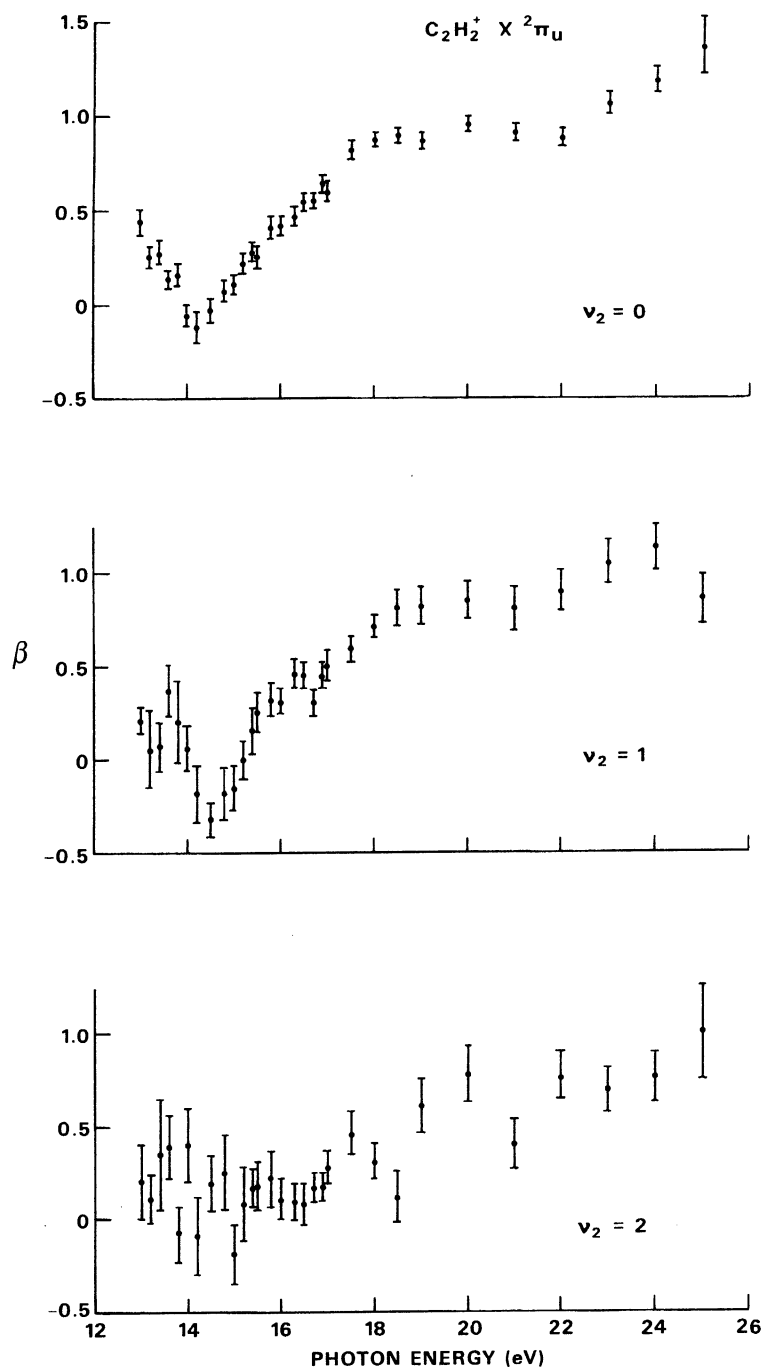


Fig. 36. Photoelectron asymmetry parameters for the $v_2 = 0, 1$, and 2 symmetric stretch components of $\text{C}_2\text{H}_2^+ \text{ X } ^2\pi_u$.

generally similar to the spectral variation of the “peak” intensities reported by Unwin et al. (1981); however, the present branching ratios are believed to be representative of a simple C–C stretching mode (with some admixture of the weak 0.036 eV bending mode) since we have separated it from the other vibrational modes which we have determined to be non-negligible in this spectral range. The $v_2 = 1$ and 2 data of Unwin et al. (1981) could be expected to be affected by this consideration. Above $h\nu \sim 16$ eV, where the excitation of bending modes and other manifestations of resonant excitation are no longer apparent, the branching ratios in fig. 35 agree well with those measured by Kreile et al. (1981) at the Ne I (16.67 eV and 16.85 eV), He I (21.22 eV), and Ne II (26.81 eV and 26.91 eV) resonance lines, and with branching ratios derived from FC factors (Dibeler and Walker 1973, McCulloh 1973) ($v_2 = 0$, 0.69; $v_2 = 1$, 0.21; $v_2 = 2$, 0.09). Third, in fig. 36, the β curves for $v_2 = 0$ and 1 show a distinct broad dip to below $\beta = 0$, centered at $h\nu \sim 14.25$ eV and $h\nu \sim 14.5$ eV, respectively, while the $v_2 = 2$ curve fluctuates near $\beta = 0$, although the statistical uncertainty prohibits a clear picture of the variation of $v_2 = 2$ for $h\nu < 16$ eV. Keep in mind that peaks with small FC factors like $v_2 \geq 2$ and the bending modes will tend to be populated mainly by resonant processes and, hence, may show much sharper variation within Rydberg series than do the FC-allowed channels. Fourth, all three β curves in fig. 36 rise at higher energy with grossly similar spectral shape, within error limits, to a value near $\beta \sim 1$. Note that photoionization of the $1\pi_u$ level of N_2 and the 1π level of CO, both isoelectronic with C_2H_2 , also result in a vibrationally-summed β which exhibits a general rise from $\beta = 0$ to $\beta \sim 1$ over the same kinetic energy range (Wallace et al. 1979, Holmes and Marr 1980). This rough correlation among similar orbitals in the three isoelectronic molecules for the nonresonant part of the spectrum seems reasonable. Fifth, comparison of the β values in fig. 36 with the resonance line work of Kreile et al. (1981) confirms the overall accuracy of the independent measurements: The agreement is excellent at all overlapping wavelengths, even at Ar II (13.30 eV and 13.48 eV), for which comparison is hazardous owing to differences in photon bandpass and the failure to take bending vibrations into account in the work by Kreile et al. Furthermore, measurements at the Ne II (26.8 eV and 26.9 eV) and He II (40.8 eV) resonance lines give (roughly v_2 -independent) β values of ~ 1.4 and ~ 1.6 , respectively, indicating that the trend observed above is continued to higher energy.

The main issue to be resolved en route to full elucidation of the dynamics reflected in this data is the nature of the resonant mechanism(s) responsible for the double hump structure below $h\nu \sim 16$ eV. This has been discussed extensively in the literature (Kreile et al. 1981, Langhoff et al. 1981b, Unwin et al. 1981, Hayaishi et al. 1982, Keller et al. 1982, Machado et al. 1982, Parr et al. 1982a, Levine and Soven 1983, 1984, Lynch et al. 1984a); and, at last, it is now possible to summarize a fairly clear picture of the mechanisms at play. First, there is virtual unanimity regarding the nature of the intense peak at 15.31 eV. Several different calculations place an intense $2\sigma_u \rightarrow 1\pi_g$ transition, converging to the $2\sigma_u^{-1}$ IP, very near this energy. Hence, the resonantly enhanced $1\pi_g$ appears well into the $1\pi_u$ continuum in C_2H_2 , partly because the $1\pi_u$ IP is lowered relative to

that in N_2 . Second, the calculation of Levine and Soven (1983, 1984) has incorporated intrachannel and interchannel interaction via a time-dependent local-density approximation (TDLDA) showing that the cross section in the vicinity of the $2\sigma_u \rightarrow 1\pi_g$ transition is accurately reproduced, thus confirming this interpretation. Third, that same calculation indicates that the lower energy peak owes half of its intensity to the $2\sigma_u \rightarrow 1\pi_g$ autoionization profile and the other half to a local maximum in the $1\pi_u \rightarrow \epsilon\pi_g$ continuum. This implies that, relative to the independent-particle approximation (IPA), inclusion of intrachannel interactions, within the RPA-type theory used, redistributes the nominally discrete $1\pi_u \rightarrow 1\pi_g$ oscillator strength to higher frequencies, some of which appears above the IP as part of the 13.3 eV peak. This is the first clear case in a molecular context of a mechanism known in atomic physics for many years (Starace 1979, Dehmer et al. 1971). Fourth, in a somewhat different framework, Lynch et al. (1984a) also argued that $1\pi_u \rightarrow 1\pi_g$ strength contributes to the low-energy feature. Some evidence also exists for a minor contribution from a $3\sigma_g \rightarrow 3\sigma_u$ autoionizing transition in the vicinity of the 13.3 eV peak.

The main contributions to the double hump structure would therefore seem to arise from both direct and indirect transitions involving the $1\pi_g$ state. This state is a resonantly enhanced bound state, in the independent-particle approximation, and is analogous to the $1\pi_g$ so prominent in the N_2 K-shell spectrum (see, e.g., section 2.2). To demonstrate that the interpretation summarized above is essentially correct, we show in fig. 37 the vibrationally unresolved β value computed using the TDLDA (Levine and Soven 1983) which is the only calculation on C_2H_2 incorporating the interactions due to electron correlation within and between IPA channels. The TDLDA results (solid line) agree semiquantitatively with the

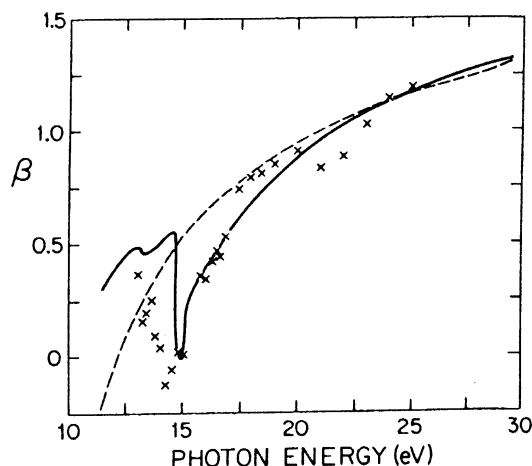


Fig. 37. Photoelectron asymmetry parameter for the $1\pi_u$ level of acetylene. Data from Parr et al. (1982a) have been averaged over vibrationally resolved levels using experimental branching ratios. Experimental uncertainty is typically $\pm 0.07 \beta$ units. Dashed curve, IPA calculation (Levine and Soven 1983); solid curve, TLDA calculation (Levine and Soven 1983).

vibrationally-averaged data (Parr et al. 1982a), clearly reflecting the prominent dip centered at $h\nu \sim 14\text{--}15\text{ eV}$, totally absent from the IPA calculation. The partial cross section is not shown here, but likewise shows semiquantitative agreement with the measured profile (Levine and Soven 1984). Other measurements are also consistent with these conclusions (Keller et al. 1982).

Hence, to summarize the results of this case study: (i) The prominent double peak has been successfully interpreted; (ii) the $1\pi_g$ state has a major impact, but is reflected differently than in N_2 , partly due to its spectral location relative to its own and other IPs (examination of the σ_u resonance is best carried out by examining the photoionization of the σ_g subshells); and (iii) bending vibrations are greatly enhanced in the resonance region, must be included in the analysis, but have not yet been characterized well. This is a notable challenge for future work.

5.5. Valence-shell photoionization of SF_6

The photoionization of SF_6 has been avidly studied over the past 10–15 years. One inducement has been its octahedral symmetry, which should render the study of its spectral properties more tractable than for other large polyatomics. A second, less trivial, motivation has been the central role played by SF_6 in the elucidation of shape-resonance effects in molecules. The four shape-resonant features (a_{1g} , t_{1u} , t_{2g} , and e_g) in the sulfur K-shell (LaVilla and Deslattes 1966, LaVilla 1972) and L-shell (Zimkina and Fomichev 1966, Zimkina and Vinogradov 1971, Blechschmidt et al. 1972, LaVilla 1972) spectra remain the most striking examples of potential barrier effects in molecular spectra, as noted in section 2.1. Third, SF_6 has important practical uses, most notably in gaseous electronics.

For these and other reasons, a large amount of information has been generated on SF_6 photoionization and related excitation processes: On the theoretical side, several groups have calculated the electronic structure (Gianturco et al. 1971, Connolly and Johnson 1971, von Niessen et al. 1975, Hay 1977, von Niessen et al. 1979) of SF_6 , and others have calculated partial photoionization cross sections (Gianturco et al. 1972, Sachenko et al. 1974, Levinson et al. 1979, Wallace 1980) and photoelectron angular distributions (Wallace 1980) for all the subshells of SF_6 . In addition, the elastic $e\text{--SF}_6$ scattering cross section (Dehmer et al. 1978, Benedict and Gyemant 1978) has been calculated indicating the role of the above-mentioned shape resonances and the close connection (Dehmer and Dill 1979a) between shape resonances in electron scattering and photoionization contexts. An even larger collection of experimental work includes: (i) X-ray absorption and emission cross sections from core levels (LaVilla and Deslattes 1966, Zimkina and Fomichev 1966, Zimkina and Vinogradov 1971, Blechschmidt et al. 1972, LaVilla 1972, Ågren et al. 1978), (ii) VUV absorption by valence levels (Nakamura et al. 1971, Blechschmidt et al. 1972, Sasanuma et al. 1978, Codling 1966, Lee et al. 1977), (iii) photoelectron spectra using X-rays (Gelius 1974) and VUV resonance lines (Gustafsson 1978, Gelius 1974, Potts et al. 1970, Sell and Kuppermann 1978), (iv) photoelectron angular distributions with He I

radiation (Sell and Kuppermann 1978), (v) partial photoionization cross sections (Gustafsson 1978, Dehmer et al. 1982, Ferrett et al. 1986) and photoelectron angular distributions (Dehmer et al. 1982, Ferrett et al. 1986) using synchrotron radiation, (vi) photoionization mass spectrometry and ionization yield measurements (Dibeler and Walker 1966, Sasanuma et al. 1979), and (vii) electron scattering measurements of total scattering (Kennerly et al. 1979) differential elastic scattering (Rohr 1979) and inelastic scattering in the low-energy (Simpson et al. 1966, Trajmar and Chutjian 1977), pseudo-optical limit (Hitchcock and Brion 1978a, Hitchcock et al. 1978, Hitchcock and van der Wiel 1979) and (e,2e) (Giardini-Guidoni et al. 1979) configurations.

Despite this great body of information, however, there remained major questions concerning the spectroscopy and dynamics of SF₆ photionization. The two issues of concern here are the ordering of the valence levels of SF₆ and the role of the t_{2g} shape resonance in valence-shell spectra. Concerning the ordering of valence levels, several ground-state configurations have been proposed on the basis of different types of evidence. This issue is complicated by the near degeneracy of two valence levels (which two is one of the central questions), resulting in the occurrence of six photoelectron peaks in the ionization potential (IP) range 16 eV ≤ IP ≤ 30 eV, where seven valence levels are known to lie. The study of shape resonance effects in valence-shell spectra depends very much on establishing the ground-state configurations as, *in the independent-electron approximation*, dipole selection rules govern which orbitals will make transitions to particular shape resonances. The significance of the qualification in italics will be discussed later.

In this case study, we discuss recent evidence (Dehmer et al. 1982) and review the previous literature in an attempt to resolve these problems. In particular, we discuss measurements (Dehmer et al. 1982) of partial photoionization cross sections, branching ratios, and photoelectron angular distributions for the valence levels of SF₆ in the photon range 16 eV ≤ hν ≤ 30 eV. The partial cross sections and branching ratios agree well with those measured earlier by Gustafsson (1978), where the two sets of data overlap. In addition, we compare this data with multiple-scattering calculations (Wallace 1980) of the same quantities. They are used here in a form chosen specifically for extracting the needed information from the data. Namely, they have been convoluted with the experimentally observed peak shapes and are plotted in alternative ways to illustrate the consequences of adopting various valence-level orderings. The discussion of these results suggests that the most plausible valence configuration is

$$5a_{1g}^2 4t_{1u}^6 1t_{2g}^6 3e_g^4 (1t_{2u}^6 + 5t_{1u}^6) 1t_{1g}^6 {}^1A_{1g},$$

although some small uncertainty still exists regarding the location of the 1t_{2u} level. We conclude by proposing further experimental and theoretical work to test these conclusions and to study the strong channel interaction effects implied by them.

There are seven occupied valence states of SF₆ with IP's less than 30 eV (Gelius 1974, Potts et al. 1970, Sell and Kuppermann 1978), all derived from the fluorine

2p and sulfur 3s, 3p, and 3d atomic orbitals. Their approximate ordering, starting with the least tightly bound, is $1t_{1g}^6$, $5t_{1u}^6$, $1t_{2u}^6$, $3e_g^4$, $1t_{2g}^6$, $4t_{1u}^6$, and $5a_{1g}^2$ combining to give a closed-shell ground state with $^1A_{1g}$ symmetry. The photoelectron spectrum (Gelius 1974, Potts et al. 1970, Sell and Kuppermann 1978) covering this range of IP's exhibits six peaks with vertical IPs of 15.7, 17.0, 18.6, 19.7, 22.5, and 26.8 eV. In the following, we will refer to these as peak 1 through peak 6, respectively, in order of increasing IP. Clearly, one of the peaks encompasses two IP's and the probable candidates are peak 2 and peak 3. This will be the main focus of the following discussion. Peak 6 is easily and unanimously assigned to the $5a_{1g}$ molecular orbital (MO) and is not discussed further here since its branching ratio is always <2% for $h\nu < 30$ eV (Gustafsson 1978), and it was not well characterized in the measurements discussed here.

The experimental results are presented in figs. 38–42 for peaks 1–5, respectively, along with corresponding theoretical results which will be described below. In each figure, the top frame contains the photoelectron asymmetry parameter β from the IP up to $h\nu = 29.2$ eV. The β values tend to gravitate around $\beta = 0$, and the resulting nearly isotropic distribution was easily measured with good precision. The average uncertainty was ± 0.03 with the largest being ± 0.1 . Including the uncertainty in the calibration procedure, we assign an overall accuracy of approximately ± 0.05 to the β values. Differences of up to 0.15 were noted relative to earlier measurements (Sell and Kuppermann 1978) of β at 584 Å; however, for all but peak 1, the β 's in figs. 38–42 lay in the range of β 's measured across the bands in the article by Sell and Kupperman (1978). In view of the likelihood of autoionization near 21.2 eV (Codling 1966), one need not be greatly concerned with the differences observed using the medium-resolution synchrotron radiation light source and the narrow-band resonance line.

The middle frames in figs. 38–42 give the branching ratios for peaks 1–5, relative to the sum of their intensities. Uncertainties in these quantities are typically ± 0.01 . Agreement with earlier measurements by Gustafsson (1978) is generally good, although local differences of 0.05 are observed. Differences in energy mesh, transmission function calibrations for low kinetic energies, and the β -dependence of the earlier measurements (Gustafsson 1978) probably contribute to this, although the differences do not significantly affect the following discussion.

The bottom frames in figs. 38–42 contain the partial cross sections for peaks 1–5, obtained by multiplying the measured branching ratios times the total ionization cross section (total photoabsorption cross section multiplied by the ionization efficiency) reported by Hitchcock and van der Wiel (1979). Again semiquantitative agreement was observed with the analogous analysis by Gustafsson (1978), who used total absorption data by Lee et al. (1977). The total absorption cross sections by Hitchcock and van der Wiel and Lee et al. are in good agreement throughout the range discussed here. The only significant issue is the assumption by Gustafsson (1978) that the ionization efficiency is unity throughout this range. The ionization efficiency measured by Hitchcock and van der Wiel was greater than 90% for $h\nu > 20$ eV, but fell off toward the ionization

threshold to a value of 25% at $h\nu = 16$ eV. This accounts for some, but by no means all, of the quantitative differences between the data sets. The observed semiquantitative agreement is considered satisfactory for this type of measurement at this time, and, although it would be desirable to remove the remaining minor discrepancies, they pose no significant problem vis-à-vis the issues discussed below. There, the occurrence of peaks in the partial cross sections represents the most significant aspects of the data; and, on this point, there is no qualitative disagreement.

The continuous curves in figs. 38–42 are theoretical results for each measured quantity. They have been presented (Dehmer et al. 1982) in the following manner to try to aid in resolving assignments in valence-shell photoionization of SF_6 by use of dynamical evidence. First, the partial cross section and photoelectron asymmetry parameter for each valence state of SF_6 was calculated (Wallace 1980) using the multiple-scattering model by now standard procedures (Dehmer and Dill 1979b). Second, three sets of theoretical curves were derived as described in table 1, each set corresponding to one of the possible valence configurations discussed later, each differing in the assignment of the $5t_{1u}$, $1t_{2u}$, and $3e_g$ initial states to peaks 2 and 3. Third, each set of dipole matrix elements and asymmetry parameters was combined with the corresponding experimental IP's, consistent with the assignments in that set, and was then folded with Gaussian line shapes with the halfwidths in the experimental spectrum (0.4, 0.6, 0.7, 0.7, and 0.4 eV for peaks 1–5, respectively). This avoided sudden jumps in the branching ratios at higher IP's and ensured that the comparison between experiment and theory was not confused by the intrinsic and instrumental widths of the photoelectron peaks.

To simplify the discussion of the complex body of data bearing on this subject, we will proceed by presenting a recommended valence-level structure, followed first by evidence supporting this conclusion and second by a discussion of various aspects of the assignment, including a tentative rationalization of seemingly contradictory evidence. Accordingly, we will consider the assignment of photoelectron peaks 1–5 to ionization from $1t_{1g}$, $5t_{1u} + 1t_{2u}$, $3e_g$, $1t_{2g}$, and $4t_{1u}$ MO's, respectively. This is also the ordering arrived at in earlier theoretical work by Connolly and Johnson (1971), Hay (1977), and von Niessen et al. (1975, 1979), and in experimental work by Gelius (1974).

General support for the above ordering is provided by the results of the two

Table 1
Trial assignments used to construct theoretical curves in figs.
38–42.

| Peak number | Solid curve | Dashed curve | Dashed-dotted curve |
|-------------|---------------------|------------------|---------------------|
| 1 | $1t_{1g}$ | $1t_{1g}$ | $1t_{1g}$ |
| 2 | $1t_{2u} + 5t_{1u}$ | $5t_{1u}$ | $1t_{2u}$ |
| 3 | $3e_g$ | $1t_{2u} + 3e_g$ | $5t_{1u} + 3e_g$ |
| 4 | $1t_{2g}$ | $1t_{2g}$ | $1t_{2g}$ |
| 5 | $4t_{1u}$ | $4t_{1u}$ | $4t_{1u}$ |

most sophisticated calculations of SF_6 electronic structure, namely, the many-body Green's-function calculations of von Niessen et al. (1975, 1979) and the generalized valence-bond calculation of Hay (1977). Both types of calculation yield the above sequence of MO's, and the ordering predicted by the calculations by von Niessen et al. was found (von Niessen et al. 1979) to be extremely stable with respect to large changes of basis functions and other conditions. In fact, in all calculations, only the relative ordering of the $5t_{1u}$ and the $1t_{2u}$, and the question of their quasidegeneracy varies.

Important experimental evidence is provided by X-ray emission, resulting from filling holes in the sulfur 1s and 2p subshells by dipole transitions from the valence shells. Sulfur K X-ray emission spectra reported by LaVilla (1972) locate the $3t_{1u}$, $4t_{1u}$, and $5t_{1u}$ valence levels and provide concrete confirmation of the $4t_{1u}$ and $5t_{1u}$ assignments given above. More recent, high-resolution X-ray emission spectra (Ågren et al. 1978) for the sulfur L-shell likewise locate the $5a_{1g}$, $1t_{2g}$, and $3e_g$ levels and provide concrete confirmation of the $3e_g$ and $1t_{2g}$ assignments given above. To summarize the X-ray emission evidence, the $5t_{1u}$, $3e_g$, $1t_{2g}$, and $4t_{1u}$ levels are associated with peaks 2, 3, 4, and 5, respectively.

This leaves the placement of the $1t_{1g}$ and $1t_{2u}$ orbitals. We conform to the assignment of the $1t_{1g}$ orbital to peak 1. There is little qualitative evidence for this (the t_{1g} does not have a dipole allowed component on the sulfur atom which would be active in the sulfur L emission spectrum); however, there is nearly universal agreement on this assignment. The placement of the $1t_{2u}$ orbital, on the other hand, is the most controversial assignment. We assign it to peak 2 mainly on the evidence of the X-ray photoelectron spectrum, as interpreted by Gelius (1974). At $h\nu = 1.25$ keV, the second peak in the photoelectron spectrum is approximately twice as large as the first, third, or fourth. As all of these are derived mainly from fluorine p orbitals, this suggests that the second peak consists of two overlapping bands. This is a simplified version of Gelius' more detailed analysis in terms of net atomic populations. This concludes the main arguments supporting the recommended assignment. Note that it relies heavily on X-ray data, which as we shall suggest later, is valuable in that it should be free from gross channel interaction effects that are believed to significantly modify valence-shell dynamics. Note also that this conclusion means that the slight splitting in peak 2 probably arises from the superposition of two peaks (although other causes could also distort the photoelectron peak) and that peak 3 is split at certain wavelengths and angles by the Jahn-Teller effect. See the work by Gustafsson (1978), Dehmer et al. (1982), Gelius (1974), Potts et al. (1970), and Sell and Kuppermann (1978) for discussions of the doublet structure in peaks 2 and 3.

The major difficulty with the above picture arises from work by Gustafsson (1978), who used partial cross section measurements, and earlier evidence (Dehmer 1972) that a shape resonance occurs at ~ 5 eV kinetic energy in the t_{2g} continuum, to conclude that peaks 2 and 3 corresponded to ionization from the $5t_{1u} + 3e_g$ and $1t_{2u}$ MO's, respectively, with the possible interchange of the two odd-parity MO's. This was later discussed in connection with multiple-scattering calculations with the same general conclusions (Levinson et al. 1979), although

the $5t_{1u}$ and $1t_{2u}$ were switched in that work. The reasoning was the following. Since a final-state shape resonance of t_{2g} symmetry is known to lie at ~ 5 eV kinetic energy, photoelectron peaks which are significantly enhanced approximately 5 eV above their respective IP's will be odd levels which couple to the t_{2g} resonance in a dipole transition. Peaks 2, 3, and 5 were observed to resonate between 5 and 6 eV above threshold, and therefore they would be assigned to the odd levels $5t_{1u}$, $1t_{2u}$, and $4t_{1u}$ with some ambiguity concerning the first two. Gustafsson used the X-ray photoelectron intensity arguments employed above to conclude that peak 2 contained two peaks and therefore the $3e_g$. It is now fairly clear from X-ray emission data that the $5t_{1u}$ and $3e_g$ levels are associated with peaks 2 and 3, respectively. However, the argument that peak 3 resonates at 5 eV kinetic energy, and therefore contains the $1t_{2u}$ peak is a serious contradiction to the assignment proposed earlier, particularly since the data in figs. 38–42 confirm the resonant behavior, and the existence of the t_{2g} shape resonance is well established.

Dehmer et al. (1982) tentatively resolve this dilemma by attributing the resonant activity of peak 3 to some form of continuum–continuum coupling whereby peak 3 shares in the huge resonant enhancement of peak 2 at $h\nu \sim 23$ –24 eV. The coupling could be direct Coulomb coupling between the nearly degenerate channels, since both have the same excited complex (ion plus photoelectron) symmetry, or possibly vibronic coupling. The latter may be enhanced (relative to typical direct molecular photoionization) since the electron is resonantly trapped, and hence delayed in its escape, and the SF_6^+ ion is known to be unstable relative to fragments of lower symmetry. The conjecture of continuum–continuum coupling is nebulous and would require more theoretical study to demonstrate its validity. However, it is supported by the following observations. First, strong channel interaction resulting in intensity borrowing in the vicinity of the strong resonant enhancement at $h\nu \sim 23$ eV in the total cross section would tend to occur near this photon energy. Indeed, peaks 2 and 3 reach a maximum at $h\nu \sim 23$ eV and are better aligned than on a kinetic energy scale. Second, peak 1, almost surely involving an even initial state, also peaks at $h\nu \sim 23$ eV when the sloping background is taken into account (see fig. 38). In fact, the local enhancement at $h\nu \sim 23$ eV in peak 1 is of the same magnitude (~ 15 Mb) as that in peak 3. The enhancement is more clearly displayed in fig. 38 than in Gustafsson's (1978) data, but both exhibit a clear rise at $h\nu \sim 22$ –23 eV, which is totally absent from the one-electron calculations. Third, the appearance of symmetry-forbidden transitions to shape resonant features has already been noted (Dehmer 1972) in inner-shell absorption spectra for SF_6 , e.g., the t_{1u} shape resonance aligns with the weak bump in the sulfur 2p absorption spectra, and the a_{1g} , t_{2g} , and e_g resonant features align with weak features in the sulfur 1s spectra, when the spectra's IP's are aligned. The coupling in the X-ray spectra is weak, only a few percent, whereas one would have to postulate coupling on the order of 20% in the valence shell; but the qualitative trend is reasonable owing to the quasidegeneracy in the valence spectra. Moreover, later work has documented the continuum–continuum coupling mechanism for the $2\sigma_u$ channel of N_2 , as described in the article by Stephens and Dill (1985) and section 5.3.

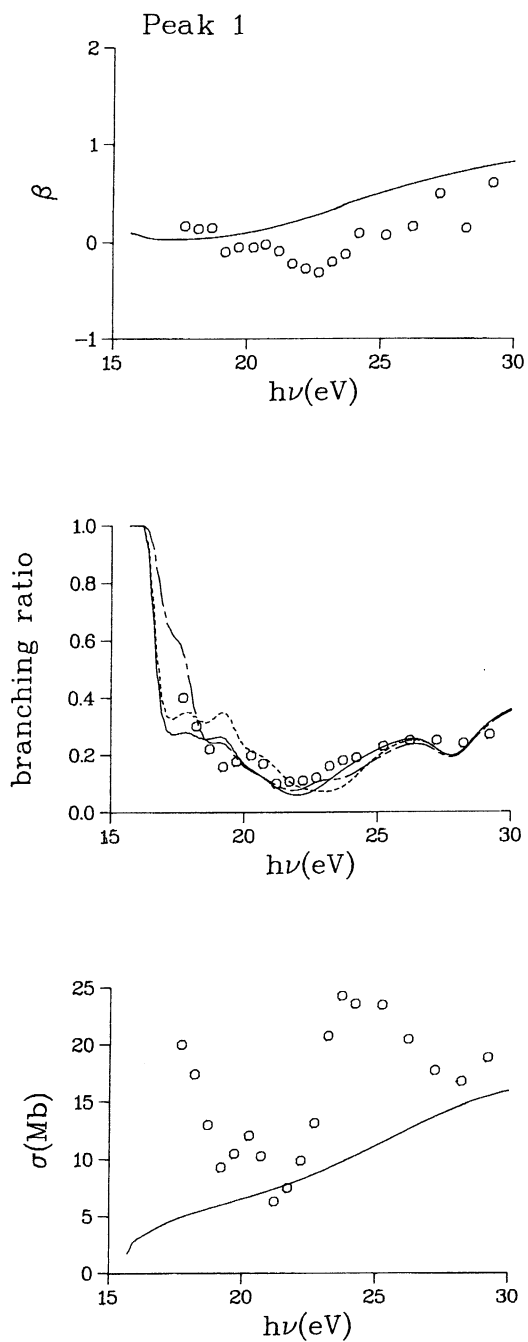


Fig. 38. Photoelectron asymmetry parameter, branching ratio, and partial cross section for peak 1 (IP = 15.7 eV) of the photoelectron spectrum of SF_6 . Open circles: data from Dehmer et al. (1982). Curves are theoretical calculations, as described in the text.

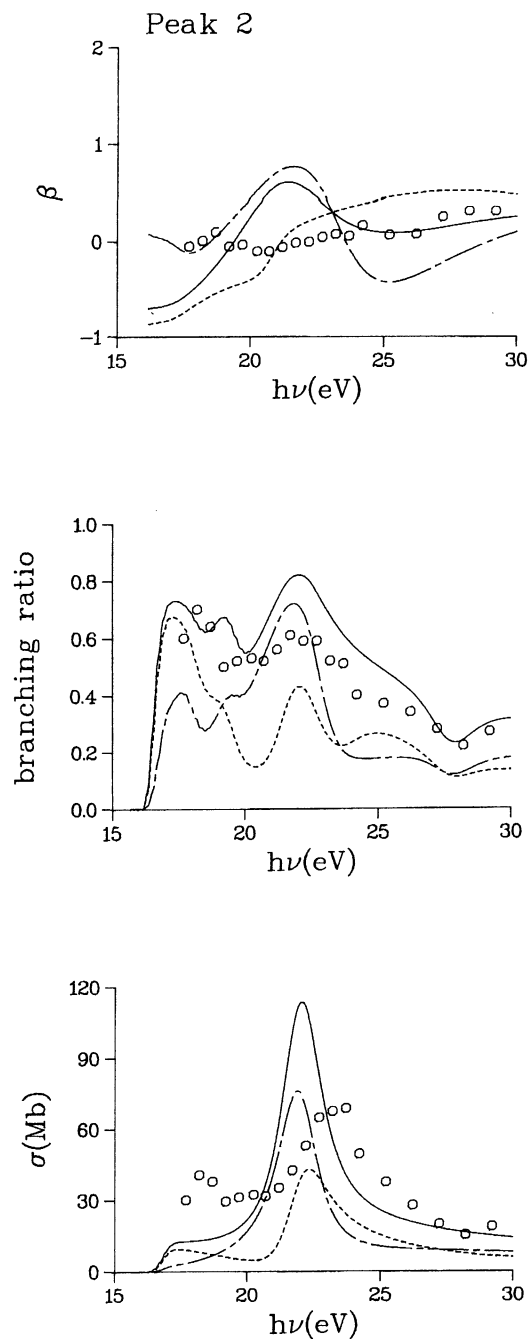


Fig. 39. Photoelectron asymmetry parameter, branching ratio, and partial cross section for peak 2 (IP = 17.0 eV) of the photoelectron spectrum of SF_6 . Open circles: data from Dehmer et al. (1982). Curves are theoretical calculations, as described in the text.

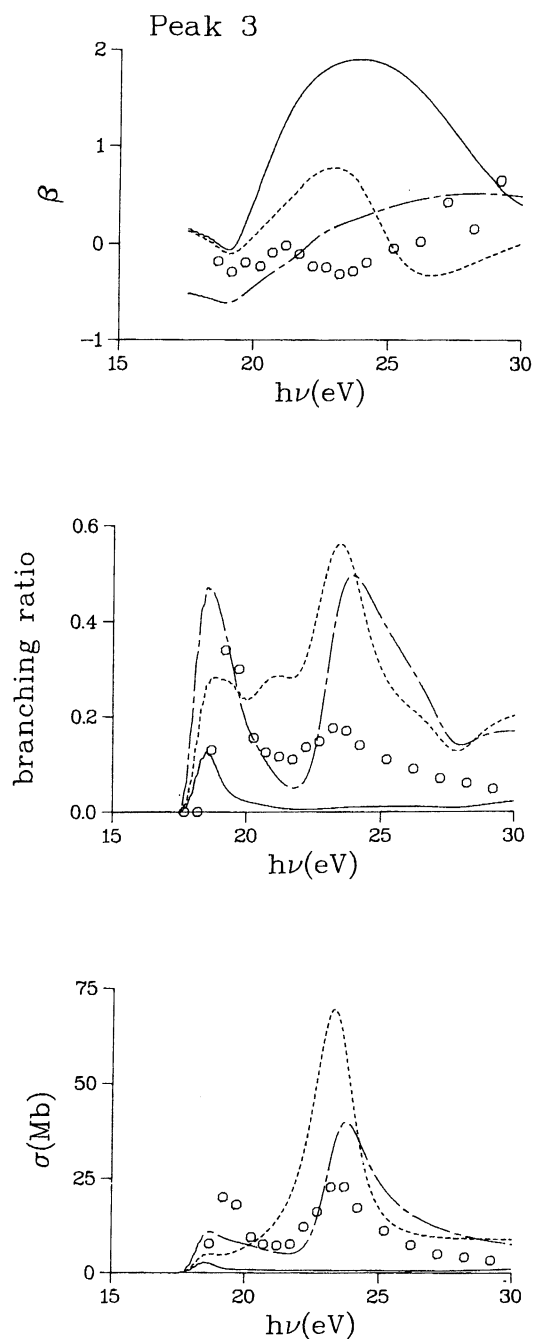


Fig. 40. Photoelectron asymmetry parameter, branching ratio, and partial cross section for peak 3 (IP = 18.6 eV) of the photoelectron spectrum of SF_6 . Open circles: data from Dehmer et al. (1982). Curves are theoretical calculations, as described in the text.

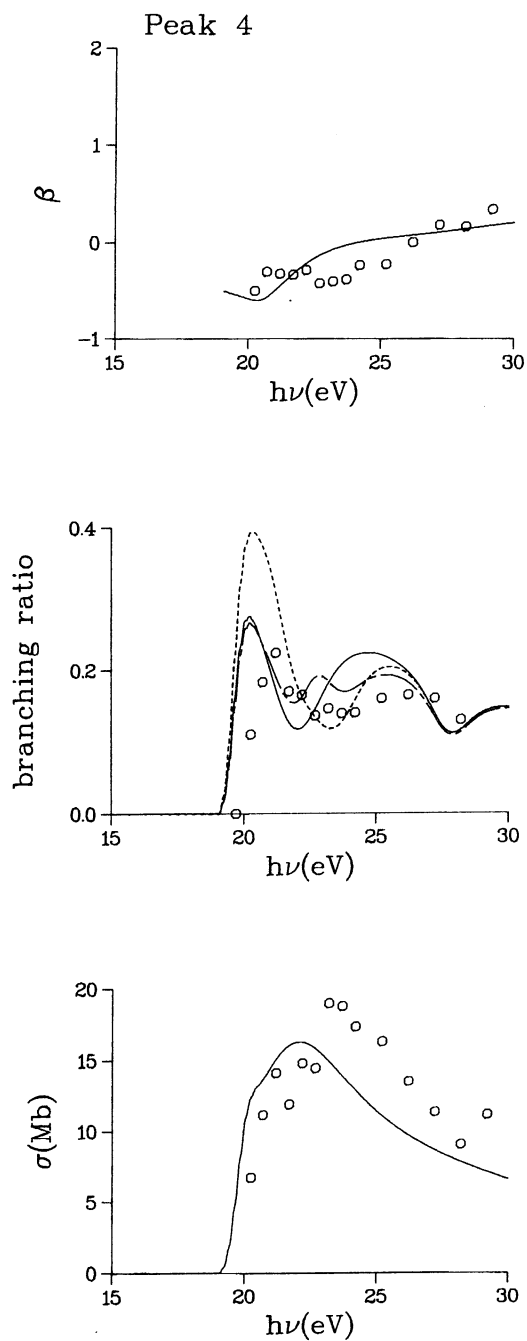


Fig. 41. Photoelectron asymmetry parameter, branching ratio, and partial cross section for peak 4 (IP = 19.7 eV) of the photoelectron spectrum of SF_6 . Open circles: data from Dehmer et al. (1982). Curves are theoretical calculations, as described in the text.

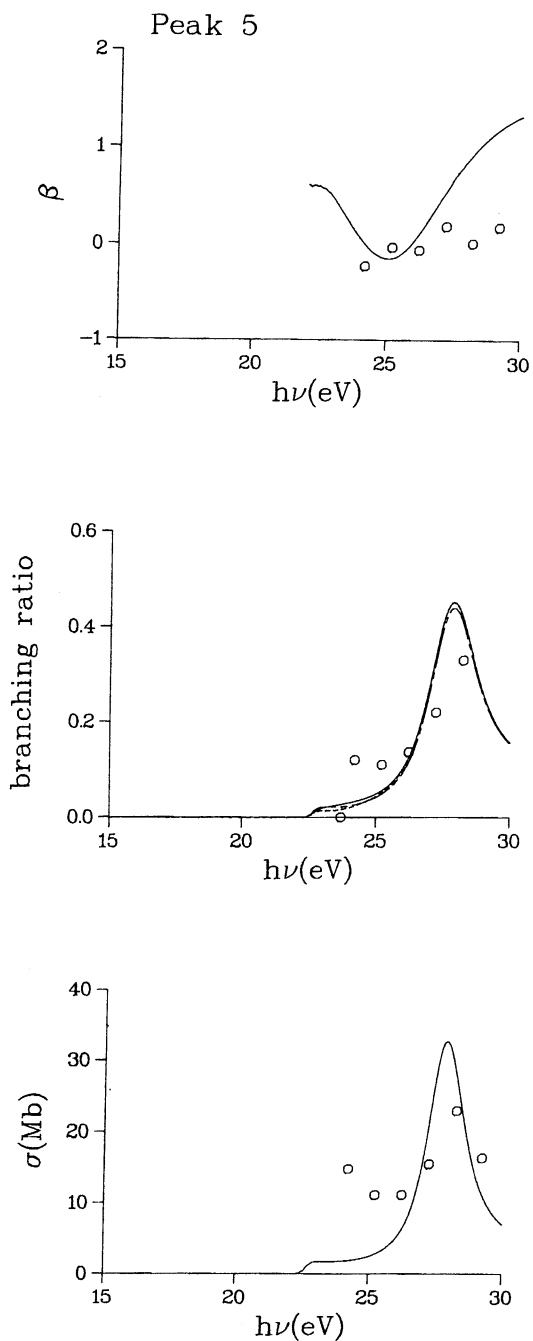


Fig. 42. Photoelectron asymmetry parameter, branching ratio, and partial cross section for peak 5 (IP = 22.5 eV) of the photoelectron spectrum of SF_6 . Open circles: data from Dehmer et al. (1982). Curves are theoretical calculations, as described in the text.

Another possible source for deviations from the independent-electron reasoning regarding the appearance of resonant enhancements in the partial cross sections, is autoionization structure, particularly that involving the shape-resonantly-enhanced antibonding $6a_{1g}$ and $6t_{1u}$ MO's, known to cause strong features below inner-shell thresholds. If one of these states occurred near $h\nu \sim 23$ eV, this could perturb the simplified shape-resonance picture. The two most likely candidates are the $5a_{1g} \rightarrow 6t_{1u}$ and the $4t_{1u} \rightarrow 6a_{1g}$ transitions. Taking the kinetic energy of the t_{2g} shape resonance as ~ 5.7 eV and the $6a_{1g}-t_{2g}$ and $6t_{1u}-t_{2g}$ spacings from X-ray absorption data, we arrive at transition energies of $h\nu \sim 17.2$ and 26.7 eV for the $5a_{1g} \rightarrow 6t_{1u}$ and the $4t_{1u} \rightarrow 6a_{1g}$ transitions, respectively. (Note that shape-resonant features shift by $\sim 1-4$ eV toward higher kinetic energy in going from inner-shell to valence-shell spectra due to different screening and other differences in relaxation effects. Therefore, we approximate relative energies from X-ray spectra, but normalize to the t_{2g} in the valence-shell spectra.) Neither matches the position of the main resonance peak at $h\nu \sim 23$ eV; however, we note in passing that the total ionization cross section has an unidentified peak at $h\nu \sim 17$ eV. This may be caused by the $5a_{1g} \rightarrow 6t_{1u}$, which in turn could account for the rises in the partial cross sections in figs. 38–40. A similar observation was made by Fock and Koch (1985). Hence, the $6a_{1g}$ and $6t_{1u}$ excited states do not appear to bear on the present discussion of the $h\nu \sim 23$ eV feature. Other weaker, nonresonantly enhanced autoionization states are known to lie in this region (Codling 1966) and may cause departures from a one-electron framework of interpretation. However, the observed structures are weak, relative to the magnitude of the resonant enhancements in peaks 1 and 3; and, therefore, the importance of autoionizing Rydberg states in this connection is tentatively discounted.

Against this background, we now examine the experimental and theoretical results presented in figs. 38–42. In assessing the agreement between experiment and theory, recall that, in most diatomic and triatomic cases studied, the independent-electron multiple-scattering model achieves qualitative to semiquantitative agreement with shape-resonant and nonresonant photoionization (Wallace 1980). The β 's are usually within 0.25 of a β unit and have the same general shape as the data. The partial cross sections exhibit most known shape resonances, although the theoretical resonance line shape tends to be too intense and narrow relative to the data and may be shifted by a few eV. Nuclear motion and electron correlation tend to smear out these sharp features. We might expect good agreement for SF_6 owing to the favorable close-packed geometry, which should minimize the impact of assumptions inherent in the multiple-scattering potential. However, anticipating our results, we find qualitative departures in the vicinity of the major resonance at $h\nu \sim 23$ eV and better agreement away from this main resonant peak, which tends to support the idea that the one-electron channels are exhibiting strong channel interaction enhanced near the t_{2g} shape resonance.

In fig. 38, the β computed for the $1t_{2g}$ channel agrees satisfactorily with the data. The measured branching ratio also agrees well with the calculations, regardless of how the assignments for peaks 2 and 3 are chosen. The base level of

the partial cross section also agrees well with the calculated curve, although significant enhancements exist at threshold and at $h\nu \sim 23\text{--}24\text{ eV}$, i.e., where large peaks occur in the total cross section, as noted above. We therefore conclude, in the context of the above discussion, that the dynamical information is consistent with the assignment of peak 1 to ionization of the $1t_{1g}$ valence orbital with significant coupling near the strong t_{2g} resonance in the $1t_{2u} + 5t_{1u}$ channel. Note that the branching ratio and partial cross section give rather different overall impressions about the agreement between experiment and theory. This arises since a small difference in the branching ratio can be amplified in the partial cross section by a large peak in the total ionization cross section. Moreover, differences in wavelength scale and bandwidth between the total-ionization and photoelectron measurements can produce artificial structure, although this is not believed to be a problem with the broad structures involved here.

In fig. 39, the comparisons with different assignments do not immediately suggest that the recommended solid curve ($5t_{1u} + 1t_{2u}$) agrees better with the data. However, the following points offer some support. First, beyond the resonance peak, $h\nu > 26\text{ eV}$, the data fall closest to the solid line. Second, this is also true at higher energies, e.g., $h\nu \sim 50\text{ eV}$, where peaks 2 and 3 have cross sections of $\sim 16\text{ Mb}$ and $\sim 6\text{ Mb}$, respectively (Gustafsson 1978) which is reasonably in agreement with the solid line which goes to 13 and 5.5 Mb for peaks 2 and 3, respectively (Levinson et al. 1979, Wallace 1980). Third, only the solid curve exceeds the experimental peak which, as stated above, is most often found in such comparisons. It should be mentioned that the $1t_{2u}$ is responsible for $\sim 2/3$ of the cross section in the peak, as indicated by the dash-dot curve so that its presence in the most intense channel (peak 2) is strongly suggested. Note also that the excess of theoretical cross section over experimental cross section roughly equals the magnitude of the resonant enhancement in peaks 1 and 3 at $h\nu \sim 23\text{ eV}$.

In fig. 40, the calculations all badly fail to account for major aspects of the data. The β , branching ratio, and partial cross section data depart qualitatively from the solid curves, particularly near $h\nu \sim 23\text{ eV}$. At the highest energy, however, they begin to converge with the solid curves, and at $h\nu \sim 50\text{ eV}$ the $3e_g$ cross section is $\sim 6\text{ Mb}$ (Gustafsson 1978), in good agreement with the calculated value of 5.5 Mb (Levinson et al. 1979, Wallace 1980). We therefore ascribe the enhanced cross section of peak 3 at $h\nu \sim 23\text{ eV}$ to intensity borrowing from the intense, nearly degenerate channel represented by peak 2. This assignment is made difficult by the fairly good agreement between the dash-dot curve and the cross section data and the β data in fig. 40; however, adoption of the dash-dot convention is in direct opposition to LaVilla's decisive argument based on X-ray emission data (LaVilla 1972).

In fig. 41, the overall agreement with the solid curve is very good, lending dynamical support to the assignment of peak 4 to ionization of the $1t_{2g}$ MO. In fig. 42, the appearance of the resonant enhancement at $\sim 5.5\text{ eV}$ kinetic energy indicates the action of the t_{2g} shape resonance in this channel and supports its assignment to $4t_{1u}$ ionization as suggested by Gustafsson (1978) and others.

To summarize, having examined diverse evidence concerning valence-shell

photoionization of SF₆, one is led to conclude that the valence configuration

$$5a_{1g}^2 4t_{1u}^6 1t_{2g}^6 3e_g^4 (1t_{2u}^6 + 5t_{1u}^6) 1t_{1g}^6 {}^1A_{1g}$$

is most consistent with the most definitive evidence. We note that apparent contradictions, such as the comparison of the data and the solid curve in fig. 40, challenge these conclusions. However, these contradictions are based on an independent-electron picture of valence-shell photoionization in SF₆. For reasons stated above, the evidence leads one to postulate (Dehmer et al. 1982) strong channel interaction in the vicinity of the very intense t_{2g} shape resonance in the 5t_{1u} + 1t_{2u} channel (peak 2) at $h\nu \sim 23$ eV. If this interpretation is correct, it reconfirms that shape-resonant features can be most easily identified in inner-shell spectra, whereas their role in valence-shell spectra can be significantly affected not only by the increased energy dependence of the dipole matrix element, but also by the possibility of strong channel interaction between the more closely spaced optical channels. This discussion should not be taken as conclusive on these issues as stressed by Dehmer et al. (1982). Clearly, more work tailored to this problem area needs to be carried out: Experimentally, it would be beneficial to extend triply differential measurements such as those reported here into the soft X-ray range, say up to $h\nu \sim 150$ eV, in order to avoid the strong channel interactions at lower energy. Gustafsson (1978) reported partial cross sections up to $h\nu \sim 50$ eV, which do, in fact, tend to support most of these conclusions, although they also raise additional interesting questions concerning the failure to clearly observe the strong e_g shape resonance at ~ 15 eV kinetic energy. Similar arguments to those discussed above may apply to this problem as well. In addition, high-energy, narrow shape resonances have been found (Swanson et al. 1980, 1981b, Lucchese et al. 1982) to be significantly smeared out by nuclear motion, which would be especially important for this resonance in SF₆. All these interesting aspects notwithstanding, it would be very useful to move into a region where such effects were absent in order to confirm important underlying assignments. On the theory side, it is imperative to begin examining channel interaction and vibrational effects in this and similar systems. Owing to the complexity of SF₆, this is probably only feasible at this time in connection with extensions (Stephens and Dill 1985) of the multiple scattering model, used here for independent-electron, fixed nuclei results. In any case, this case study should help stimulate some of this much needed advancement of present capabilities, since issues such as those raised here will surely be frequently encountered in the growing body of work in valence-shell photoionization of polyatomics using synchrotron radiation.

5.6. Valence-shell photoionization of BF₃

In this section, we present angle-resolved photoelectron data (J.L. Dehmer et al. 1984) for the valence shells of BF₃ to investigate valence-shell photoionization dynamics in this highly-symmetric polyatomic molecule. This case was chosen

because an e' shape resonance is firmly established (Fomichev 1967, Fomichev and Barinskii 1970, Hayes and Brown 1971, Dehmer 1972, Mazalov et al. 1974, Swanson et al. 1981a, Ishiguro et al. 1982) to occur at ~ 2.2 eV kinetic energy in the boron K-shell spectrum and because comprehensive independent-electron calculations (Swanson et al. 1981a) have been carried out for all the subshells of BF_3 using the multiple-scattering model. Furthermore, as the previous case study on SF_6 clarified the role of the t_{2g} resonance in valence-shell photoionization in SF_6 , the comparative study (J.L. Dehmer et al. 1984) of these two highly symmetric fluorides seemed promising. In fact, agreement between experiment and theory is very reasonable in many of the comparisons discussed below, indicating a realistic, first-order theoretical description (Swanson et al. 1981a). However, a predicted shape resonance feature in the branching ratio for the $4e'$ channel is absent, possibly due to some of the reasons touched upon in the last few sections. These results are discussed in the context of the analogous study on SF_6 and future measurements are suggested to clarify the role of the e' resonance in valence-shell spectra of BF_3 .

Figure 43 shows a typical set of data taken at a photon energy of $h\nu = 23$ eV. All three spectra are normalized so that the largest peak (third peak in the $\theta = 0^\circ$ spectrum) has a value of 100. In the top frame, the six peaks are labeled by the symmetry of the orbital being ionized, based on the well-established valence

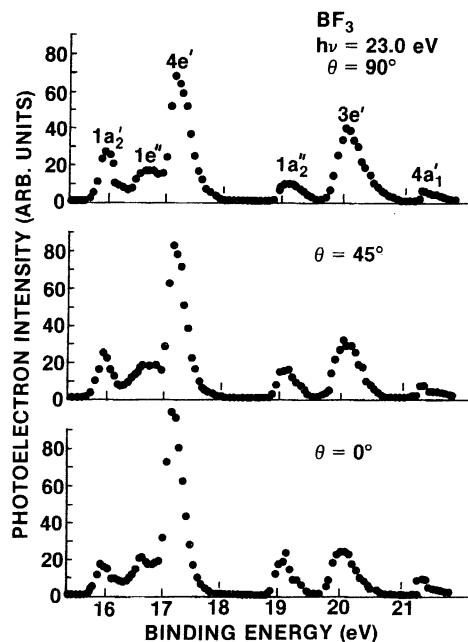


Fig. 43. Photoelectron spectra of BF_3 at $h\nu = 23$ eV and $\theta = 0^\circ$, 45° , and 90° . The normalization of the three spectra is internally consistent and set so that the maximum count rate (third peak of the $\theta = 0^\circ$ spectrum) is equal to 100.

configuration (Potts et al. 1970, Batten et al. 1978, Kimura et al. 1981, Åsbrink et al. 1981, Haller et al. 1983). By careful inspection of fig. 43, one can see that, at this wavelength, the β 's for peaks 1 and 5 are negative, the β for peak 2 is nearly isotropic, and the β 's for peaks 3 and 4 are positive.

At each angle of observation, the net counts in each photoelectron peak were summed, and the integrated counts were corrected for the transmission function of the electron spectrometer and a small $<4\%$ angular correction factor based on the aforementioned electron spectrometer angular calibration. The asymmetry parameter β was then determined for each peak, followed by the determination of the photoionization branching ratios from the measured intensities and β values. Note that in fig. 43, the $1e''$ and $4e'$ photoelectron bands (peaks 2 and 3) are not clearly resolved. In fact, recent theoretical work by Haller et al. (1983) indicates that a tail from the $1e''$ band runs under the $4e'$ band. As the actual shapes of the two bands are not known, the data is presented in two ways: In one approach, the partially resolved band has been deconvoluted simply by separating the two peaks at the point of minimum intensity. In the second approach, the sum of the two peaks is reported as a composite photoelectron band. This will be discussed below.

There are six occupied valence orbitals in BF_3 with ionization potentials in the energy range discussed in this case study. Starting with the outermost orbital, from the left in fig. 43, the symmetries and vertical IP's are as follows: $1a'_2$ (15.96 eV), $1e''$ (16.70 eV), $4e'$ (17.12 eV), $1a'_2$ (19.14 eV), $3e'$ (20.12 eV), and $4a'_1$ (21.4 eV). Here the symmetry assignments are taken from Haller et al. (1983) and agree with most previous assignments (Potts et al. 1970, Batten et al. 1978, Kimura et al. 1981, Åsbrink et al. 1981). The vertical IP's are an average of several independent measurements (Potts et al. 1970, Batten et al. 1978, Kimura et al. 1981, Åsbrink et al. 1981) all of which are in close agreement.

The results are presented in figs. 44–50 for each photoelectron peak and for a combination of the partially resolved $1e''$ and $4e'$ peaks (fig. 47). Included with the experimental data are results of recent theoretical calculations (Swanson et al. 1981a) employing the multiple-scattering model. The theoretical curves have been adjusted to correspond to the level ordering and the IP's listed in the last paragraph. Note that Swanson et al. (1981a) adopted the incorrect experimental ordering for the closely spaced $4e'$ and $1e''$ levels. The theoretical curves have not been folded with the finite instrumental resolution, but this does not affect the present comparison in any significant way. Each figure consists of three frames. The top frame presents the photoelectron asymmetry parameter, β , from the IP up to $h\nu = 30$ eV. The middle frame shows the photoelectron branching ratio for each channel. In the lower frame, the calculated partial cross section is displayed. Unfortunately, the total absorption cross section of BF_3 is not known in this wavelength range, so we are unable to convert the measured branching ratios to partial cross sections. A photoionization mass spectrometry measurement (Dibeler and Liston 1968) was made up to $h\nu \sim 20$ eV, but this wavelength range is too limited to be very helpful in the present discussion.

In the top frames of figs. 44–50, we see the degree to which the measured β 's

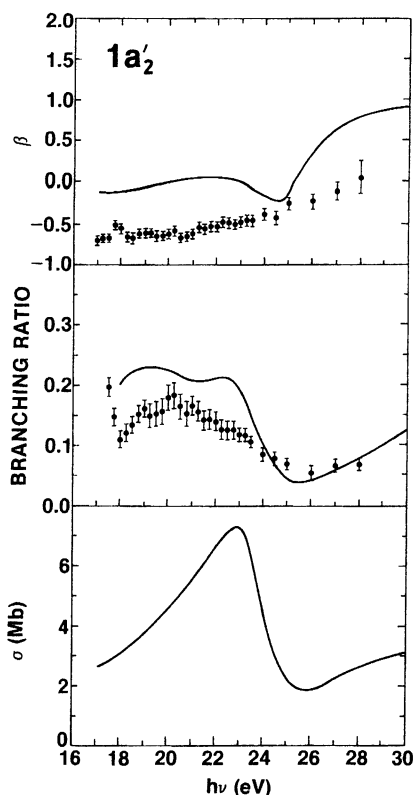


Fig. 44. Photoelectron asymmetry parameter, branching ratio, and partial cross section for photoionization of the $1a'_2$ orbital of BF_3 . Solid dots: data from J.L. Dehmer et al. (1984); solid curves: theoretical results from Swanson et al. (1981a).

agree with the predictions of the multiple scattering calculation. The results for the $1e''$, $4e'$, and $1a'_2$ orbitals (figs. 45–48) show excellent agreement between experiment and theory. For the $1a'_2$ (fig. 44) and $3e'$ (fig. 49) orbitals, the experiment and theory agree fairly well in shape, but the magnitudes are different by ~ 0.5 β units on the average, a difference not uncommon even in much simpler molecules. The poorest agreement is found for the $4a'_1$ orbital (fig. 50), which is also by far the weakest channel. On the whole, the agreement is satisfactory, in view of the standards in the field, and it indicates that the theoretical results realistically reflect the gross photoionization dynamics of BF_3 . In comparing the present results with those for SF_6 (section 5.5), it is interesting to note that the present β 's tend to be rather anisotropic (ranging from $\beta < -0.5$ to $\beta \sim 1.5$), whereas those for the valence orbitals of SF_6 tended to gravitate strongly toward the isotropic value $\beta = 0$. This is not surprising, but it does show that the very simple isotropic pattern for F 2p derived orbitals in SF_6 is not in any sense typical of highly coordinated fluorides.

The branching ratios are shown in the middle frames of figs. 44–50. For the $1a'_2$

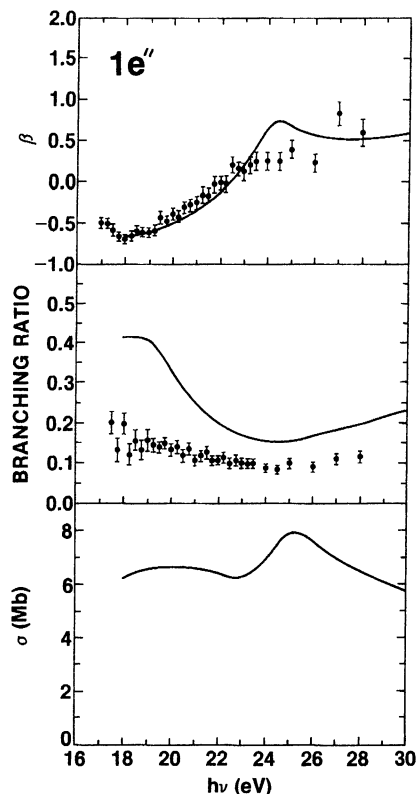


Fig. 45. Photoelectron asymmetry parameter, branching ratio, and partial cross section for photoionization of the $1e''$ orbital of BF_3 . Solid dots: data from J.L. Dehmer et al. (1984); solid curves: theoretical results from Swanson et al. (1981a).

(fig. 44) and $1a_2''$ (fig. 48) cases, good agreement between theory and experiment is observed, both in shape and magnitude. For the overlapping $1e''$ and $4e'$ orbitals, two discrepancies between theory and experiment emerge. Most obvious, the bump at $h\nu \sim 25$ eV in the calculated branching ratio for the $4e'$ orbital does not appear in the measured branching ratio. This will be discussed further below. The other discrepancy occurs on either side of this bump, where the measured branching ratios are lower than the theoretical curve for $1e''$ and higher than the theoretical curve for the $4e'$ orbital. The reason this is noteworthy is that this is consistent with the results of Haller et al. (1983) who predict that the $1e''$ photoelectron band runs under the $4e'$ band and that a sizable fraction of its intensity is thereby covered up by the $4e'$ band. Our method of separating the intensity of the overlapping bands would have the effect of erroneously shifting intensity from the $1e''$ peak to the $4e'$ peak. In fact, when the two are summed in fig. 47, the agreement away from the $h\nu \sim 25$ eV bump is remarkably good, adding some support to the prediction by Haller et al. (1983). Note that the separately determined β 's for these two channels should be much less sensitive to

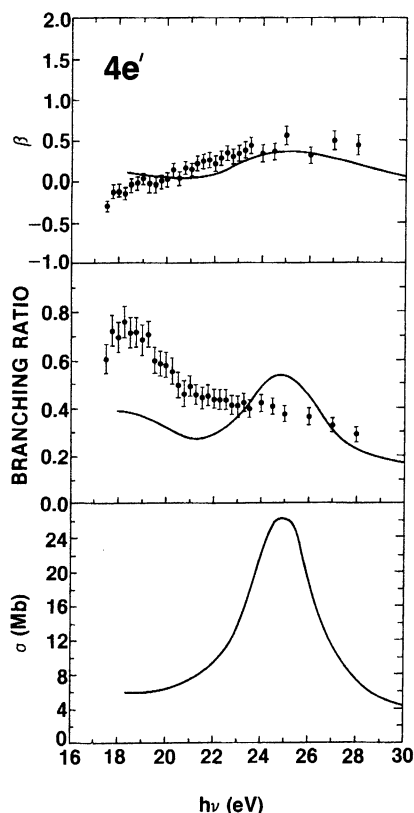


Fig. 46. Photoelectron asymmetry parameter, branching ratio, and partial cross section for photoionization of the $4e'$ orbital of BF_3 . Solid dots: data from J.L. Dehmer et al. (1984); solid curves: theoretical results from Swanson et al. (1981a).

this issue. The remaining two channels reflect rather good agreement between theory and experiment. The $3e'$ branching ratio, in fact, reflects a maximum, similar in magnitude to, but slightly shifted from that in the theoretical curve. The $4a'_1$ branching ratio agrees well in shape with the theoretical curve, both reflecting a sharp increase at high energy. The factor of two error in magnitude is not surprising in view of the very weak intensity in this channel just above its IP.

The bottom frames in figs. 44–50 contain the partial cross sections produced by the theoretical calculation (Swanson et al. 1981a). Comparison with experiment will require measurement of a total photoabsorption cross section, which, when multiplied by the present branching ratios, would yield experimental partial cross sections. Or, direct measurement by constant-ionic-state photoelectron spectroscopy would produce the needed experimental data. As neither is presently available, the theoretical curves are included for purposes of discussion, as partial cross sections and branching ratios present rather different views of the photoionization process. We anticipate ourselves by noting that the most definitive evidence

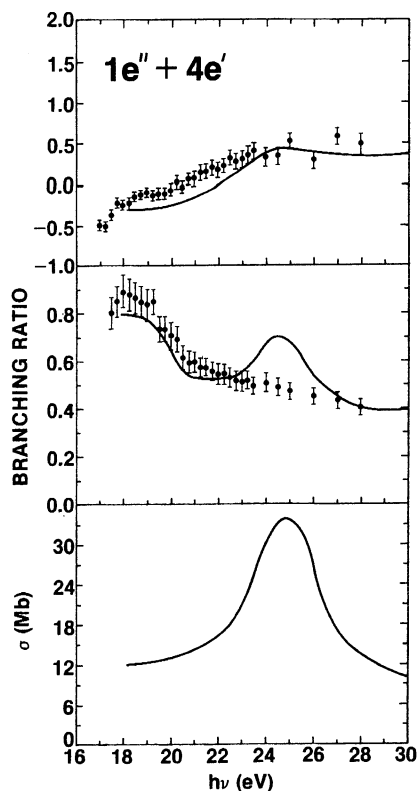


Fig. 47. Photoelectron asymmetry parameter, branching ratio, and partial cross section for photoionization of the $1e''$ and $4e'$ orbitals of BF_3 . Solid dots: data from J.L. Dehmer et al. (1984); solid curves: theoretical results from Swanson et al. (1981a).

for the e' shape resonance in valence-shell photoionization is likely to result from measurement of the $4e'$ partial cross section.

The boron K-shell X-ray absorption spectrum (Fomichev 1967, Fomichev and Barinskii 1970, Hayes and Brown 1971, Dehmer 1972, Mazalov et al. 1974, Robin 1975, Swanson et al. 1981a, Ishiguro et al. 1982) displays two prominent features – an intense peak ~ 7 eV below the IP, and a broad (FWHM ~ 4 eV), intense peak centered at ~ 2.2 eV above the IP. Recent multiple-scattering calculations (Swanson et al. 1981a) show that these features can be understood at the independent-electron level and that they correspond to transitions to a $2a_2''$ bound state and an e' shape resonance, respectively, in accordance with other interpretations (Fomichev 1967, Fomichev and Barinskii 1970, Hayes and Brown 1971, Dehmer 1972, Mazalov et al. 1974, Ishiguro et al. 1982). Since the e' shape resonance is a final-state feature, it should also be accessed in symmetry-allowed transitions from the valence shells. One of the primary motivations of this work was to investigate the role of the e' resonance in valence-shell photoionization dynamics of BF_3 . Indeed, calculations (Swanson et al. 1981a) show that five of the

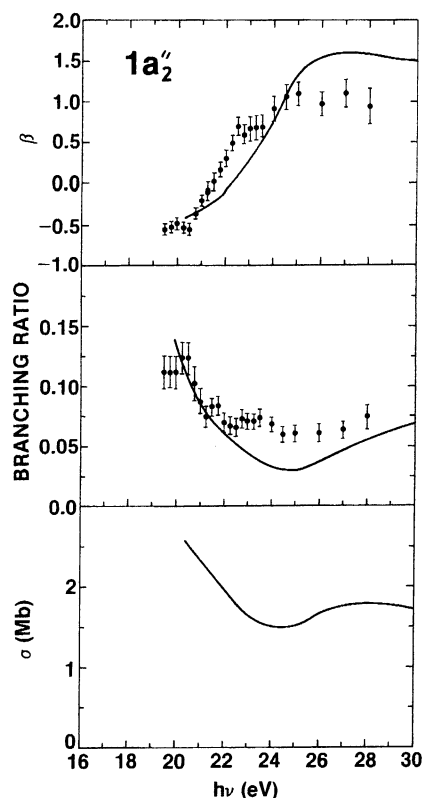


Fig. 48. Photoelectron asymmetry parameter, branching ratio, and partial cross section for photoionization of the $1a''$ orbital of BF_3 . Solid dots: data from J.L. Dehmer et al. (1984); solid curves: theoretical results from Swanson et al. (1981a).

six valence orbitals of BF_3 (all but the $1a''$) are connected to the e' continuum by dipole selection rules and, further, that the e' is predicted to have clearly visible effects. As so often happens, however, the valence-shell properties do not follow the independent-electron predictions as clearly as do the inner-shell properties. Nevertheless, in this case, rather good, though indirect, evidence for the e' shape resonance is given by the β 's, and the $3e'$ and $4a_1'$ branching ratios show direct evidence near the upper limit of the energy range. However, a predicted peak in the $4e'$ branching ratio is missing in the data, indicating the presence of interactions which are not adequately incorporated in the calculation.

Accordingly, it is important to have an independent way of estimating the location of the e' shape resonance in the valence-shell continua, so as to establish the presence or absence of such effects. Fortunately, this can be fairly reliably done based on the position of the e' shape resonance in the inner-shell spectra, plus a kinetic energy shift associated with differences in screening between a localized hole and a valence-shell hole. Examining well-characterized cases in N_2 , CO , and SF_6 , it is found that shape resonances experience a shift to higher kinetic

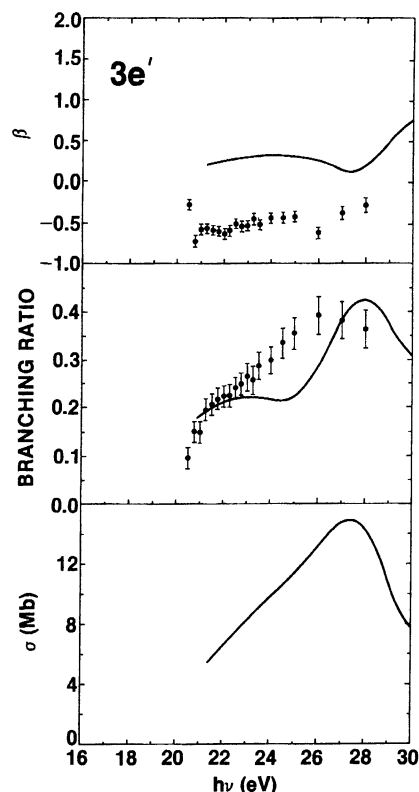


Fig. 49. Photoelectron asymmetry parameter, branching ratio, and partial cross section for photoionization of the $3e'$ orbital of BF_3 . Solid dots: data from J.L. Dehmer et al. (1981a); solid curves: theoretical results from Swanson et al. (1981a).

energies when going from an inner-shell spectrum to a valence-shell spectrum. These shifts cluster around ~ 3 eV and always fall in the range 1–4 eV. Therefore, the e' shape resonance, which is centered at 2.2 eV kinetic energy in the boron K-shell spectrum, should fall in the 3–6 eV kinetic energy range in the valence-shell spectra. As the calculation quoted here placed the resonance at ~ 8 eV kinetic energy, the true resonance position should fall to the low-energy side of the predicted position. This means that the photon energy range studied in this work should suffice to investigate the role of the e' shape resonance in the six channels studied, though the resonance position in the $3e'$ and $4a'_1$ channels falls near the high-energy limit of the data reported here.

For completeness, we mention other states that will influence the valence-shell photoionization of BF_3 in this energy range. Multiple scattering model calculations (Swanson et al. 1981a) also predict a shape resonance in the a'_1 continuum, approximately 1–2 eV below the e' shape resonance. The a'_1 resonance derives from the trapping of p-waves on the fluorine sites, as does the e' resonance, but it is not dipole-allowed in boron K-shell photoexcitation and, hence, does not arise

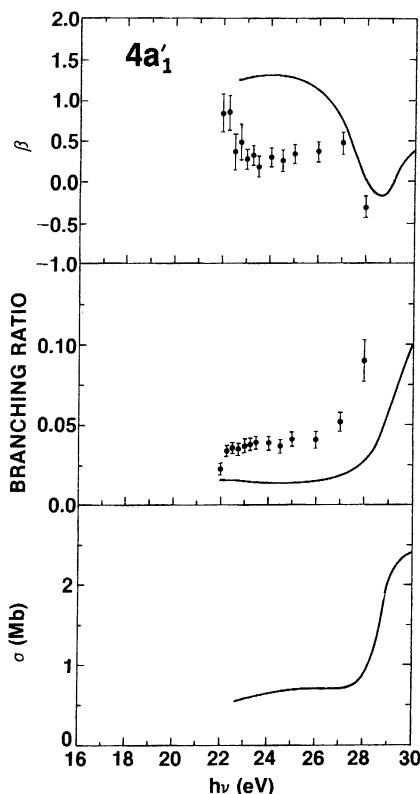


Fig. 50. Photoelectron asymmetry parameter, branching ratio, and partial cross section for photoionization of the $4a_1'$ orbital of BF_3 . Solid dots: from J.L. Dehmer et al. (1984); solid curves: theoretical results from Swanson et al. (1981a).

in earlier discussions involving inner-shell processes. Among the valence shells, the a_1' continuum is dipole-allowed from the $4e'$, $1a_2''$, and $3e'$ initial states. According to the theoretical results (Swanson et al. 1981a), the a_1' resonance is masked by a much more intense e' resonance in the $4e'$ channel and is suppressed by a coincident zero in the dipole matrix element in the $1a_2''$ channel. However, in the $3e'$ channel, it is equal in strength and shifted slightly from the e' shape resonance. Therefore, the net resonant feature in the $3e'$ channel must be considered a composite resonance with significant contributions from shape resonances in both the e' and a_1' continua. However, as the e' resonance is sharper, it still determines the peak position of the combined resonance feature in the $3e'$ partial cross section. For this reason, we will continue to refer to the e' resonance in what follows, although the likely contribution from the a_1' resonance should be recognized.

Another possible class of states to consider is autoionizing states converging to all but the lowest IP. Although we do not detect any narrow structure in the data that would indicate autoionizing structure, channel interaction with the Rydberg

states converging to the $1e''$ through $4a_1'$ thresholds may contribute to the failure to see features predicted from independent-electron calculations. Of particular interest is the possibility that transitions to the $2a_2''$ state (essentially a boron $2p_z$ orbital), so prominent in the boron K-shell spectra (Fomichev 1967, Fomichev and Barinskii 1970, Hayes and Brown 1971, Dehmer 1972, Mazalov et al. 1974, Robin 1975, Swanson et al. 1981a, Ishiguro et al. 1982), might affect the present data. In the K-shell spectra, this peak is ~ 7 eV below the IP. If we assume a 2–3 eV shift for the valence-shell spectra, this state should not affect the present range, except possibly in the $4a_1'$ channel where it would fall at $h\nu \sim 17$ eV, to a first approximation. However, as known (Levine and Soven 1983, 1984) from examples in both atoms and molecules, intrashell or intravalence transitions can undergo significant splitting and redistribution of oscillator strength to higher energies, relative to an independent-electron picture. Although these possibilities must be recognized in considering the experimental results, we have no particular reason to believe that they play an important role in this case.

We now examine the data in figs. 44–50 for the effects of the e' shape resonance. In doing so, we examine separately the β 's, branching ratios, and partial cross sections, as each reflects the photoionization dynamics in a different way. The β 's differ from the other two in that they contain information on the relative phases of the continuum wavefunctions. However, as seen in an earlier study (Dehmer et al. 1982) of valence-shell photoionization of SF_6 (section 5.5), the branching ratios and partial cross sections also differ greatly in the way they display photoionization features. In the upper frames of figs. 44–50, the gross shapes of the measured curves agree reasonably well with theory, and the agreement is excellent, in shape and magnitude, for the $1e''$, $4e'$, and $1a_2''$ channels. The e' shape resonance plays significant roles for all but the $1a_2''$ channel, so that one is tempted to consider this indirect evidence that the role of the e' shape resonance in this spectral range is observed and reasonably accounted for by the calculations. Turning to the branching ratios, we note fair to good agreement between experiment and theory for all except the $4e'$ channel. In particular, the broad maximum at $h\nu \sim 26$ eV in the $3e'$ branching ratio and the rising branching ratio at high photon energy for $4a_1'$ represent direct evidence for the e' shape resonance in those channels. Using the $3e'$ branching ratio data, one can place the resonance position at $h\nu \sim 26$ eV, corresponding to a kinetic energy of ~ 6 eV, in accordance with expectations. The surprising aspect of these results is the absence of an e' -induced peak at $h\nu \sim 25$ eV in the $4e'$ branching ratio. This will be discussed further below. The partial cross sections in the bottom frames are presently available from theory only. They show that the e' shape resonance will emerge much more clearly when presented in this form. In particular, the peak at $h\nu \sim 25$ eV in the $4e'$ partial cross section is predicted to have a much greater contrast ratio than the same feature in the branching ratio. Similarly, the e' resonance will be displayed more clearly in the partial cross section than in the branching ratio for the $1e''$ and the $1a_2''$ channels as well. For the $3e'$ and $4a_1'$ channels, both parameters display the resonance equally clearly, and, in fact, these are the two cases in which the e' shape resonance can be observed in the

present branching ratio data. Recall that in the $3e'$ channel, the a'_1 shape resonance also contributes to the resonant feature at $h\nu \sim 26$ eV, as discussed earlier.

The failure to observe in valence-shell properties a final-state resonance that is well established in inner-shell spectra is not at all unprecedented. In SF_6 , an e_g shape resonance causes an intense peak ~ 15 eV above the sulfur $L_{2,3}$ IP, but is absent from valence-shell partial cross sections where its presence is predicted by theory (Levinson et al. 1979, Wallace 1980). An even more subtle example is the $4\sigma_g$ ionization channel of CO_2 which was predicted (Grimm et al. 1980, Swanson et al. 1980, Padial et al. 1981a, Swanson et al. 1981b, Lucchese and McKoy 1982a,b) to access a strong σ_u shape resonance at ~ 20 eV kinetic energy. Nothing resembling the predicted resonance feature was observed in early partial cross section measurements (Brion and Tan 1978, Gustafsson et al. 1978a); however, a predicted dip in the β curve (Grimm et al. 1980, Swanson et al. 1981b, Lucchese and McKoy 1982a,b) at the resonance energy was subsequently observed experimentally (Carlson et al. 1981a), giving evidence that the "missing" resonance existed. More recently, the resonance has been observed (Roy et al. 1984) in the partial cross section, only shifted several eV and smeared out relative to predictions. Thus, its manifestation in the partial cross section has been drastically reduced and shifted by some as yet uncharacterized interaction(s). So we add to this list the $4e'$ channel in BF_3 which has a β curve consistent with theory but fails to show the branching ratio feature resulting from the presence of the e' shape resonance.

Without further evidence, we can only speculate as to possible causes for the missing e' feature: First, it is well-known that multiple-scattering model calculations produce shape resonance profiles that are too narrow and too intense. Hence, effects such as intrachannel coupling (Levine and Soven 1983, 1984) and/or averaging over vibrational motion (Swanson et al. 1981b) will tend to smear out and diminish a shape resonant feature. Nevertheless, the feature may still be observable in the partial cross section, even if it is absent from the branching ratio. This is certainly possible in the present case since, if the total photoabsorption cross section peaks near $h\nu \sim 25$ eV, a flat branching ratio will produce a peak in the partial cross section. Second, interchannel coupling (either discrete-continuum or continuum-continuum) with other underlying valence channels can significantly alter the predictions based on an independent-electron theory. For instance, continuum-continuum coupling is known to have dramatic effects in $2\sigma_u$ photoionization in N_2 (Stephens and Dill 1985), and is believed to strongly influence valence-shell photoionization in SF_6 (Dehmer et al. 1982). Such channel interaction can be expected to be stronger among valence channels with their closely spaced IP's. The good agreement found for the β results tend to argue against this possibility. Note that in the N_2 case, the $2\sigma_u$ β is strongly affected (Stephens and Dill 1985), and in SF_6 , the β results (Dehmer et al. 1982) showed very poor agreement between experiment and theory for the affected channels. Third, vibronic coupling has been shown (Haller et al. 1983) to play a very important role in photoelectron spectra of BF_3 . This and other vibrational

effects are excluded from the calculations (Swanson et al. 1981a) quoted here. We do not know how to assess the importance of such effects at this time. Other possibilities clearly exist, but these examples serve to indicate the types of mechanisms which may be causing the reduction of certain shape resonance effects in valence-shell spectra. Taken together, the examples quoted in CO_2 , BF_3 , and SF_6 pose a major challenge to our understanding of shape resonance phenomena.

We conclude by suggesting future work to help clarify the role of the e' shape resonance in BF_3 photoionization processes. Clearly it is very important to measure the partial photoionization cross sections for the valence shells to complete the comparisons begun in figs. 44–50. This would require the total photoabsorption cross section in order to convert the present branching ratios to partial cross sections, or that a constant-ionic-state photoelectron measurement be made on the valence shells of BF_3 . New measurements at higher energy would also be very valuable, both to complete the study of the e' features at the high-energy limit of the present data, and to investigate the role of the e' resonance in the inner-valence $3a'_1$ and $2e'$ orbitals whose IP's are predicted to fall near $h\nu \sim 40\text{--}43$ eV.

6. Survey of related work

Molecular photoionization dynamics is a rich, multifaceted subject, requiring an eclectic approach to gain the greatest insight from the many complementary sources of information. In the main body of this chapter we have focussed on the use of triply differential photoelectron spectroscopy to probe the dynamics of two central resonant mechanisms – autoionization and shape resonances. We have further stressed the use of synchrotron radiation in six case studies to illustrate important topics of current interest. What we have failed so far to do is convey the diversity and extent of information from other techniques and for other physical circumstances. In this section we will now try to create a much broader perspective by noting very briefly various types of work which complement in an essential way what we have covered in detail. Even at this superficial level, we stress that this survey is not at all comprehensive, but, rather, is intended to give a general impression of the richness of the field.

(i) As indicated in the Introduction and in the shape resonance bibliography (see Appendix), the study of shape resonances has been very vigorous and productive over the last decade or so. Using a variety of probes (synchrotron radiation, electron energy loss spectroscopy, X-ray sources, electron spectroscopy, mass spectroscopy, fluorescence spectroscopy, etc.) shape resonances in well over fifty molecules have been studied. These include simple diatomics (N_2 , O_2 , CO , NO), triatomics (e.g., CO_2 , CS_2 , OCS , N_2O , HCN) and more highly-coordinated molecules and local molecular environments (e.g., SF_6 , SO_4^{2-} , SF_5CF_3 , SF_2O_2 , SF_2O , BF_3 , SiF_4 , SiCl_4 , SiF_6^{2-} , SiO_2 , NF_3 , CF_4 , CCl_4 , C_2H_2 ,

C_2N_2). There has also been extensive study of shape resonances in adsorbed molecules (Gustafsson et al. 1978b, Gustafsson 1980b, 1983, Stöhr and Jaeger 1982, Stöhr et al. 1983, 1984, Koestner et al. 1984) and molecular solids (Blehschmidt et al. 1972, Lau et al. 1982, Fock 1983, Fock et al. 1984, Fock and Koch 1984, 1985) which exploit the localized nature of shape resonances to probe the condensed state. Several important themes are developed in the literature on shape resonances which space did not permit covering here. These include electron optics of molecular fields (Dehmer and Dill 1979b), hole localization (Dill et al. 1978, 1979a) and relaxation effects (Lynch and McKoy 1984), Auger angular distribution anisotropies (Dill et al. 1980, Lindle et al. 1984, Truesdale et al. 1984), triply differential studies of deep inner-shell photoionization (Ferrett et al. 1986), chemical effects on shape resonances (many examples in the bibliography), as well as others highlighted below in other contexts. A somewhat related theme has involved the study of so-called "Cooper zeros" in molecular photoionization (Carlson et al. 1982b, 1983a,c, 1984a,c). These minima in the ionization cross section are well known in atomic physics (Fano and Cooper 1968, Starace 1979, Johnson and Cheng 1979, Kennedy and Manson 1972) and result from a cancellation in the dipole matrix element due to the passage of a final state node through the valence-shell part of the initial-state wavefunction. In several examples, e.g., valence p-shell photoionization in Ar, Kr, and Xe (Johnson and Cheng 1979, Kennedy and Manson 1972), the node of interest immediately follows the resonantly penetrating antinode which causes the shape resonance in those channels. In the molecular cases studied (Carlson et al. 1982b, 1983a,c, 1984a,c) so far, photoionization of halogen compounds have been treated and analyzed with respect to this closely related rare gas behavior.

(ii) As stated earlier, the literature on autoionization is extensive; however, detailed *ab initio* theoretical work was largely limited to prototypical work on H_2 until a few years ago. More recently, major progress has been made in larger molecules, e.g., N_2 (Lefebvre-Brion and Giusti-Suzor 1983, Raoult et al. 1983, Giusti-Suzor and Lefebvre-Brion 1984), O_2 (Morin et al. 1982a), NO (Collins and Schneider 1984, Giusti-Suzor 1982, Giusti-Suzor and Jungen 1984, Jungen 1984a), HI (Lefebvre-Brion et al. 1985), and C_2H_2 (Levine and Soven 1983, 1984). To date, various authors have treated rotational (Jungen and Dill 1980, Raoult et al. 1980), vibrational (Jungen and Dill 1980, Raoult et al. 1980, Raoult and Jungen 1981), electronic (Levine and Soven 1983, 1984, Collins and Schneider 1984, Raoult et al. 1983, Giusti-Suzor and Lefebvre-Brion 1984, Raseev 1985), spin-orbit (Lefebvre-Brion et al. 1985), and indirect autoionization mechanisms (or "complex resonances") (Giusti-Suzor and Lefebvre-Brion 1984), and the competition with predissociation has now been incorporated (Giusti-Suzor and Jungen 1984, Jungen 1984b, Mies 1984, Mies and Julienne 1984) in an MQDT treatment. On the experimental side, detailed triply differential photoelectron studies are now ripe for expansion with a few preliminary studies already complete, e.g., N_2 (Parr et al. 1981, West et al. 1981), CO (Ederer et al. 1981), CO_2 (Parr et al. 1982b, Hubin-Franskin et al. 1984), O_2 (Morin et al. 1980, Tabché-Fouhailé et al. 1981, Morin et al. 1982a,b, Codling et al. 1981), N_2O (Carlson et al. 1983b,

Truesdale et al. 1983b), C_2H_2 (Unwin et al. 1981, Keller et al. 1982, Parr et al. 1982a).

(iii) The interaction between shape resonances and autoionizing resonances in valence-shell spectra has been a most challenging problem. In the case of O_2 , an analogous σ_u shape resonance to that discussed in connection with N_2 is expected to occur in the valence-shell spectra, but its identification in the photoionization spectrum has been complicated by the existence of extensive autoionization structure in the region of interest. Recent work (Morin et al. 1980, Tabché-Fouhailé et al. 1981, Morin et al. 1982a,b) using variable wavelength photoelectron measurements and an MQDT analysis of the principal autoionizing Rydberg series have sorted out this puzzle, with the result that the σ_u shape resonance was established to be approximately where expected, but was not at all clearly identifiable without the extensive analysis used in this case. Similar, but less well-analyzed examples occur in CO (see, e.g., Stockbauer et al. 1979, Stephens et al. 1981) and NO (see, e.g., Brion and Tan 1981, Delaney et al. 1982b, Southworth et al. 1982a, Wallace et al. 1982, Smith et al. 1983, Collins and Schneider 1984). Resolution of the joint shape resonance/autoionization dynamics in these and other cases is a current challenge.

(iv) A class of phenomena which appears to be very common in inner-valence-shell spectra is the breakdown of the single-particle model brought on by extensive vibronic coupling among the high density of states in the inner-valence region (Krummacher et al. 1980, 1983, Bagus and Viinikka 1977, Cederbaum and Domcke 1977, Schirmer et al. 1977, Cederbaum et al. 1977, 1978, 1980, Wendin 1981, Schirmer and Walter 1983). This breakdown manifests itself as a high density of satellites in the photoelectron spectrum (consisting of admixtures of single-hole states, two-hole one-particle states and certain higher-order combinations), to the extent that the main photoelectron line associated with a single inner-valence hole can even be difficult to recognize. This has been observed experimentally (Krummacher 1980, 1983) and treated successfully (Bagus and Viinikka 1977, Cederbaum and Domcke 1977, Schirmer et al. 1977, Cederbaum et al. 1977, 1978, 1980, Wendin 1981, Schirmer and Walter 1983), e.g., in the case of the " $2\sigma_g$ " spectrum of N_2 by many-body Green's function techniques, and may be expected to be an important dynamical effect in the photoionization of molecular levels having IP's in the $h\nu \sim 30$ to 50 eV range.

(v) Multiphoton ionization is a recently developed technique which has great potential for expanding our understanding of photoionization dynamics in totally new directions. When used in conjunction with photoelectron detection, such as that described in section 4, vibrational intensities and photoelectron angular distributions can be measured for small molecules (see, e.g., Miller and Compton 1981a,b, Kimman et al. 1982, Miller et al. 1982, Miller and Compton 1982, Glowia et al. 1982, Achiba et al. 1982, White et al. 1982, Pratt et al. 1983a,b,c, Achiba et al. 1983, Anderson et al. 1984, Pratt et al. 1984a,b,c, White et al. 1984, Sato et al. 1984, Wilson et al. 1984, Müller-Dethlefs et al. 1984, Kimman 1984) which are windows onto the dynamics of the multiphoton process, just as they are in the single photon case. In addition, when the multiphoton process proceeds via

resonances with excited neutral states, such as the excited valence states of N_2 in fig. 19, very high resolution ($\Delta\lambda < 0.05 \text{ cm}^{-1}$) spectroscopy and dynamics of these excited molecular states can be examined. Although the laser sources used in multiphoton ionization are technically quite different from those used in the VUV and soft X-ray work emphasized in the body of this chapter, there is a strong scientific relationship which ties them together.

(vi) Another recently developed technique is polarization of fluorescence (Poliakoff et al. 1981, 1982, Guest et al. 1983, Greene and Zare 1983, Guest et al. 1984) from molecular ions formed by photoionization. This approach accesses information on the orientation of the molecular ion and the relative strengths of degenerate photoelectron channels in the photoionization process. To give a concrete example, photoionization of N_2 to form the $B^2\Sigma_u^+$ state of N_2^+ (fig. 19) leads to the rightmost photoelectron band in fig. 20. This band consists of electrons in degenerate $\varepsilon\sigma_g$ and $\varepsilon\pi_g$ ionization channels which cannot be separated by straight electron spectroscopy or by β measurements. Nevertheless, by observation of the polarization of the B–X fluorescence, information on the branching ratio for these degenerate photoelectron channels can be obtained (Poliakoff et al. 1981, Guest et al. 1983). This provides a unique test of dynamical information which exists but usually remains implicit in theoretical calculations. Another apparently dissimilar technique to examine relative strengths of degenerate photoionization channels is the measurement of angular distributions of photoions from dissociative photoionization (Dehmer and Dill 1978). The common link between these techniques is that they do not detect (and, hence integrate over the angular distribution of) the photoelectrons, thus eliminating the interference effects between the degenerate channels and isolating their relative strengths in the observed parameters.

(vii) An important extension of the triply differential studies discussed above is the extension to measuring the spin polarization of the photoelectrons. Spin polarization measurements access additional dynamical information described in detail elsewhere (Heinzmann 1980, Johnson et al. 1980). Full quadruply differential measurements have already been performed on atoms (Heinzmann 1980) and spin polarization studies have begun on molecules (Heinzmann et al. 1980, 1981, Cherepkov 1981a,b, Schäfers et al. 1983, Schönhense et al. 1984).

(viii) A variety of dissociative phenomena occur either in competition with or subsequent to molecular photoionization, and are an important part of the broader picture. For example, MQDT has been applied (Giusti-Suzor and Jungen 1984, Jungen 1984b, Mies 1984, Mies and Julienne 1984) to the competition between predissociation and autoionization in photoexcitation of H_2 and NO , representing the extension of MQDT analysis to dissociation channels and serving as a prototype for an extensive class of processes always present to some degree in molecular photoexcitation spectra. Another subject with a rich literature (see, e.g., Batten et al. 1978, Danby and Eland 1972, Brehm et al. 1973, Stockbauer 1973, Werner et al. 1974, Stockbauer and Inghram 1975, Peatman 1976, Mintz and Baer 1976, Batten et al. 1976, Stockbauer and Inghram 1976, Stockbauer 1977, Guyon et al. 1978, Peatman et al. 1978, Baer et al. 1979, Baer 1979,

Stockbauer 1980, Guyon et al. 1983) is fragmentation of molecular ions formed by photoionization. Usually studied by photoelectron-photoion coincidence techniques, this subfield focuses on the decay of excited molecular ions into alternative dissociation channels. In most work, a particular molecular ion state is selected by tuning the excitation energy so that a zero energy electron is produced, indicating that an ion state at an excitation energy equal to the photon energy is formed. Events producing zero electrons can be detected very efficiently either by an electrostatic zero-energy trap (Danby and Eland 1972, Brehm et al. 1973, Stockbauer 1973, Wernet et al. 1974, Stockbauer and Inghram 1975, Peatman 1976, Mintz and Baer 1976, Batten et al. 1976, Stockbauer and Inghram 1976, Stockbauer 1977, Guyon et al. 1978, Peatman et al. 1978, Baer et al. 1979, Baer 1979, Stockbauer 1980, Guyon et al. 1983) or by electron attachment to an electron scavenger (Chutjian and Ajello 1977, Ajello et al. 1980, Chutjian and Ajello 1980). In either case, measurement of the resulting fragment ions will indicate the fragmentation pattern of the parent ion. Alternatively, measurement of threshold electrons as a function of excitation energy (see, e.g., Kimura et al. 1981, Danby and Eland 1972, Brehm et al. 1973, Stockbauer 1973, Werner et al. 1974, Stockbauer and Inghram 1975, Peatman 1976, Mintz and Baer 1976, Batten et al. 1976, Stockbauer and Inghram 1976, Stockbauer 1977, Guyon et al. 1978, Peatman et al. 1978, Baer et al. 1979, Baer 1979, Stockbauer 1980, Guyon et al. 1983) map the spectroscopy of highly excited autoionizing states which decay to excited states of the ion by ejection of a thermal electron. This produces a source of information on the spectroscopy of highly vibrationally excited molecular ions which are otherwise difficult to observe; however, the detailed dynamics of these processes is often complicated and difficult to analyze.

7. Prospects for future progress

Discussing the future directions of a research field is an extremely limited exercise since it is inherently steeped in existing ideas and experience. Invariably, new ideas, insights, and/or techniques come along and redirect the field into unforeseen directions. Nevertheless, it is still useful to discuss prospects for future work if it is done briefly and not taken too seriously. We will do so here in terms of three themes: developing our prototypical concepts, new probes, and new systems.

Our present knowledge of shape and autoionizing resonances is still in the prototype stage of development. In the case of shape resonances, we have established deep insight for a broad range of phenomena in N_2 , but attempts to extend this understanding to even closely related cases, e.g., CO, C_2H_2 , O_2 , NO, HCN, C_2N_2 , has been met with new challenges, in many cases requiring extensive revision of our initial expectations. Moreover, serious study has only just begun on other important facets of shape resonant behavior: vibrational effects in polyatomic molecules, continuum-continuum coupling, interaction with autoionizing states, triply differential photoelectron studies of deep inner-shell spectra, and so on. In addition, the inventory of known shape resonances, though

seemingly extensive, is only the tip of the iceberg and the depth of understanding in most cases is superficial. Exploration of shape resonances should remain vigorous, should explore new types of molecular environments, and should aim to establish the special dynamics in each case. A high order of challenge lies in the unification of different useful points of view and in understanding the fundamental similarities among different physical environments, excitation mechanisms, and observation channels.

The progress toward understanding autoionization phenomena is extremely impressive, yet it also is still in the development stage. Ultimate sophistication and insight has been achieved only for H_2 , and attempts to extend this progress to other diatomics has made impressive progress, but has been arduous and has produced less complete results. Extension of theoretical work to larger molecules and a broader range of detection channels will be a high-priority and fruitful direction of work for many years to come. On the experimental side, only the most preliminary measurements have been carried out *within* autoionizing resonances at the triply differential level. Enhanced synchrotron light capabilities and more sophisticated instrumentation just coming on line will have a major impact on this fundamental type of measurement. Let us hope we will soon see a definitive experimental test of the MQDT predictions discussed in section 3.2.

Another widespread phenomena in need of further study is the breakdown of single particle behavior in inner-valence spectra. Prototype work succeeded in establishing the phenomena qualitatively; however, many theoretical predictions remain untested, and higher resolution is required to test the theoretical predictions in any detail.

These exemplars show clearly that expansion, refinement, and unification of molecular photoionization dynamics will provide a stimulating theme in the coming years.

New probes of molecular photoionization dynamics will invariably draw intense interest and stimulate new growth. At the time of this writing, several new approaches are in development and in preliminary use, but are not discussed in the literature to any significant extent. These include photoionization of laser excited molecular states (the atomic analog is much better established); photoionization of molecules oriented in a molecular beam (Kaesdorf et al. 1985); and the study of double ionization by measurement of both outgoing electrons in coincidence, either in the fast electron/slow electron case or in the Wannier limit of equal, low velocities. These are very exciting, new directions which will undoubtedly exhibit new dynamics. Their exploitation will benefit from new technology, e.g., undulators and free-electron lasers, and will stimulate new ideas and theoretical initiatives.

Nearly all work stressed in this chapter has dealt with standard molecular targets, partly owing to ease of handling and strong signal levels. With recent progress in synchrotron sources and the development of automated, more sensitive spectrometers, extension of these studies to more exotic species is ripe. It should now be straightforward to bring the broad spectral range and time structure of synchrotron radiation to bear on such species as clusters, free radicals, metastable states, and high-temperature molecules. There is strong

interest in these species for both basic and applied reasons, and exploration of new species with a new experimental capability would seem to be a very enticing subject for future work.

In closing, we emphasize that, although this chapter is not at all comprehensive, we hope it does succeed in indicating the present richness of the field of molecular photoionization dynamics and the potential for significant progress in the future.

Appendix. A bibliography on shape resonances in molecular photoionization through early 1985

| Reference | Molecule |
|------------------------------|---|
| <i>1966</i> | |
| LaVilla and Deslattes | SF ₆ |
| Zimkina and Fomichev | SF ₆ |
| <i>1967</i> | |
| Fomichev | BF ₃ |
| <i>1969</i> | |
| Nakamura et al. | N ₂ |
| <i>1970</i> | |
| Fomichev and Barinskii | BF ₃ , BCl ₃ |
| Nefedov | SF ₆ , Cr(CO) ₆ |
| <i>1971</i> | |
| Hayes and Brown | BF ₃ |
| Nakamura et al. | N ₂ , O ₂ , CO, SF ₆ |
| Zimkina and Vinogradov | review article |
| <i>1972</i> | |
| Blechschmidt et al. | SF ₆ |
| Cadioli et al. | BF ₃ |
| Dehmer | SF ₆ , BF ₃ , CS ₂ , SO ₂ , SO ₄ ²⁻ , SiCl ₄ , SiO ₂ , SiF ₄ , SiF ₆ ²⁻ , CF ₃ SF ₅ , SF ₂ O, SF ₂ O ₂ |
| El-Sherbini and van der Wiel | N ₂ , CO |
| Fano | review article |
| Gianturco et al. | SF ₆ |
| LaVilla | SF ₆ |
| van der Wiel and El-Sherbini | N ₂ , CO |
| Wight et al. (1972/73) | N ₂ , CO |
| <i>1973</i> | |
| Barinskii and Kulikova | SF ₆ , BF ₃ |
| LaVilla | fluoromethanes |

| Reference | Molecule |
|-------------------------|--|
| <i>1974</i> | |
| Dehmer | review article |
| Mazalov et al. | BF ₃ |
| Morioka et al. | NO |
| Sachenko et al. | SF ₆ |
| Tam and Brion | HCN |
| Vinogradov et al. | N ₂ |
| Wight and Brion (1974a) | CO ₂ , N ₂ O |
| Wight and Brion (1974b) | NO, O ₂ |
| Wight and Brion (1974c) | CF ₄ |
| Wight and Brion (1974d) | CS ₂ , COS |
| Wight and Brion (1974e) | (CH ₃) ₂ CO |
| <i>1975</i> | |
| Dehmer and Dill | N ₂ |
| LaVilla | O ₂ , CO ₂ |
| Robin | CH ₄ , B ₂ H ₆ , BF ₃ , N ₂ , HCl, H ₂ S, PH ₃ , SiH ₄ , SiF ₄ |
| <i>1976</i> | |
| Davenport (1976a) | N ₂ , CO |
| Davenport (1976b) | N ₂ , CO, CO ₂ , H ₂ |
| Dehmer and Dill (1976a) | N ₂ |
| Dehmer and Dill (1976b) | review article |
| Dill et al. | N ₂ , CO |
| Eberhardt et al. | C ₂ H ₂ |
| Hamnett et al. | CO, N ₂ |
| Samson and Gardner | CO |
| Tronc et al. | CO, CH ₄ |
| Wight et al. | N ₂ , CO |
| <i>1977</i> | |
| Davenport | H ₂ , N ₂ , CO |
| Hitchcock and Brion | C ₂ H ₂ , C ₂ H ₄ , C ₂ H ₆ , C ₆ H ₆ |
| Kay et al. | N ₂ , CO |
| King et al. | N ₂ |
| Kondratenko et al. | N ₂ , CO |
| Langhoff | N ₂ , H ₂ CO |
| Langhoff et al. | H ₂ CO |
| Plummer et al. | N ₂ , CO |
| Rescigno and Langhoff | N ₂ |
| Samson et al. (1977a) | O ₂ |
| Samson et al. (1977b) | N ₂ |
| Schwarz et al. | NO ₂ |

| Reference | Molecule |
|-----------------------------|--|
| <i>1978</i> | |
| Bianconi et al. | N ₂ , N ₂ O |
| Brion and Tan | N ₂ O, CO ₂ |
| Brown et al. | fluoromethanes |
| Dill et al. | N ₂ , CO |
| Gustafsson | SF ₆ |
| Gustafsson et al. (1978a) | CO ₂ |
| Hitchcock and Brion (1978a) | SF ₆ |
| Hitchcock and Brion (1978b) | chloromethanes |
| Hitchcock et al. | SF ₆ |
| Iwata et al. | N ₂ , CO, C ₂ H ₂ |
| Langhoff et al. | H ₂ CO |
| McCoy et al. | O ₂ |
| Padial et al. | CO |
| Rescigno et al. | N ₂ |
| Sasanuma et al. | SF ₆ |
| <i>1979</i> | |
| Barrus et al. | O ₂ , CO, CO ₂ , N ₂ O |
| Brion and Tan | N ₂ O, CO ₂ |
| Brion et al. | O ₂ |
| Dehmer and Dill (1979a) | review article |
| Dehmer and Dill (1979b) | review article |
| Dehmer et al. | N ₂ |
| Dill et al. | N ₂ , CO |
| Hitchcock and Brion (1979a) | HCN |
| Hitchcock and Brion (1979b) | HCN, C ₂ N ₂ |
| Hitchcock and van der Wiel | SF ₆ |
| Langhoff | review article |
| Langhoff et al. | O ₂ |
| Levinson et al. | SF ₆ |
| Marr et al. | N ₂ , CO |
| Stockbauer et al. | CO |
| Tronc et al. | CO, CH ₄ , CF ₄ , CO ₂ , COS, C ₂ H ₂ , C ₂ H ₄ |
| Wallace et al. | N ₂ , CO |
| <i>1980</i> | |
| Carlson et al. | N ₂ |
| Cole et al. | CO |
| Dehmer and Dill | review article |
| Dill et al. | N ₂ , CO |
| Friedrich et al. | SiF ₄ |
| Gerwer et al. | O ₂ |

| Reference | Molecule |
|-----------------------------|--|
| <i>1980 (cont'd)</i> | |
| Grimm | CO, CO ₂ , COS |
| Grimm et al. | N ₂ , CO, CO ₂ , COS, CS ₂ |
| Gustafsson | O ₂ |
| Hitchcock and Brion (1980a) | CO ₂ , N ₂ , O ₂ |
| Hitchcock and Brion (1980b) | H ₂ CO, CH ₃ CHO, (CH ₃) ₂ CO |
| Holmes and Marr | N ₂ , O ₂ , CO |
| Krummacher et al. | N ₂ |
| Langhoff et al. | review article |
| Morin et al. | O ₂ |
| Orel et al. | F ₂ |
| Raseev et al. | N ₂ |
| Ritchie and Tambe | CO |
| Swanson et al. | CO ₂ |
| Tronc et al. | N ₂ , NO, N ₂ O |
| van der Wiel | review article |
| Wallace | N ₂ , CO, NO, O ₂ , SF ₆ |
| West et al. | N ₂ |
| <i>1981</i> | |
| Brion and Tan | NO |
| Carlson et al. (1981a) | CO ₂ |
| Carlson et al. (1981b) | COS, CS ₂ |
| Carnovale et al. | CS ₂ |
| Grimm et al. | CO ₂ |
| Gustafsson and Levinson | NO |
| Hermann and Langhoff | H ₂ , N ₂ |
| Hitchcock and Brion | HF, F ₂ |
| Kreile et al. | C ₂ H ₂ |
| Langhoff et al. (1981a) | N ₂ CO |
| Langhoff et al. (1981b) | C ₂ H ₂ |
| Loomba et al. | N ₂ |
| Lucchese and McKoy (1981a) | CO ₂ |
| Lucchese and McKoy (1981b) | N ₂ |
| Ninomiya et al. | HCl, Cl ₂ |
| Padial et al. (1981a) | CO ₂ |
| Padial et al. (1981b) | O ₃ |
| Raseev et al. | O ₂ |
| Stephens et al. | CO |
| Swanson et al. (1981a) | BF ₃ |
| Swanson et al. (1981b) | CO ₂ |
| Tabché-Fouhailé et al. | O ₂ |
| Thiel | H ₂ , N ₂ , O ₂ , CO, CO ₂ |

| Reference | Molecule |
|----------------------------|--|
| <i>1981 (cont'd)</i> | |
| Unwin et al. | C ₂ H ₂ |
| White et al. | COS |
| Williams and Langhoff | N ₂ , CO |
| <i>1982</i> | |
| Carlson et al. | CS ₂ , COS |
| Dehmer et al. | SF ₆ |
| Delaney et al. (1982a) | O ₂ |
| Delaney et al. (1982b) | NO |
| Dittman et al. | O ₂ |
| Hayaishi et al. | C ₂ H ₂ |
| Hitchcock et al. | F ₂ |
| Ishiguro et al. | BF ₃ , BCl, BBr ₃ |
| Keller et al. | C ₂ H ₂ |
| Kreile et al. | HCN, C ₂ H ₂ |
| Lucchese and McKoy (1982a) | CO ₂ |
| Lucchese and McKoy (1982b) | CO ₂ |
| Lucchese et al. | N ₂ |
| Machado et al. | C ₂ H ₂ |
| Morin et al. (1982a) | O ₂ |
| Morin et al. (1982b) | O ₂ |
| Parr et al. | C ₂ H ₂ |
| Shaw et al. | N ₂ |
| Southworth et al. | NO |
| Thiel | CO ₂ , N ₂ |
| Wallace et al. | NO |
| <i>1983</i> | |
| Carlson et al. | N ₂ O |
| Dittman et al. | CO ₂ |
| Eberhardt et al. (1983a) | CO, (CH ₃) ₂ CO |
| Eberhardt et al. (1983b) | N ₂ |
| Grimm | C ₂ H ₄ |
| Grimm and Carlson | N ₂ |
| Holland et al. | C ₂ N ₂ |
| Keller et al. (1983a) | chloromethanes |
| Keller et al. (1983b) | SiF ₄ , Si(CH ₃) ₄ |
| Kreile et al. | C ₂ N ₂ |
| Krummacher et al. | CO |
| Levine and Soven | C ₂ H ₂ |
| Lucchese and McKoy | CO |
| McKoy et al. | N ₂ , CO, CO ₂ , C ₂ H ₂ |
| Morin | O ₂ , NO, N ₂ |

| Reference | Molecule |
|---------------------------|--|
| <i>1983 (cont'd)</i> | |
| Nenner | CO, O ₂ , N ₂ O |
| Schwarz et al. | BF ₃ , CF ₄ , KBF ₄ , NaBF ₄ , NH ₄ BF ₄ |
| Smith et al. | NO |
| Thiel | N ₂ , CO ₂ |
| Truesdale et al. | CO |
| <i>1984</i> | |
| Ågren and Arneberg | CO |
| Brion and Thomson (1984a) | data compilation – HF, HCl, HBr, O ₂ , NO, CO, N ₂ , H ₂ O, NH ₃ , CH ₄ , CO ₂ , COS, CS ₂ , N ₂ O |
| Brion and Thomson (1984b) | data compilation – H ₂ , CO, N ₂ , O ₂ , NO, HF, HCl, HBr, H ₂ O, NH ₃ , CH ₄ , N ₂ O, CO ₂ , COS, CS ₂ , SF ₆ |
| Carlson et al. | CF ₄ |
| Collins and Schneider | H ₂ , N ₂ , NO, CO ₂ |
| Dehmer | review article |
| Dehmer et al. | BF ₃ |
| Grimm et al. | C ₃ H ₄ |
| Hermann et al. | CO, H ₂ CO |
| Hitchcock et al. | 1-butene, cis-2-butene, trans-2-butene, trans-1,3-butene, perfluoro-2-butene, review of other molecules with C–C bonds |
| Holland et al. | HCN |
| Kanamori et al. | BF ₃ |
| Keller et al. (1984a) | 12 unsaturated organic molecules |
| Keller et al. (1984b) | H ₂ CO, CH ₃ OH |
| Kreile et al. | N ₂ , CO, C ₂ H ₂ , HCN, CO ₂ , N ₂ O, C ₂ N ₂ , C ₄ H ₂ , NC ₃ H |
| Langhoff | review article |
| Leal et al. | N ₂ |
| Levine and Soven | N ₂ , C ₂ H ₂ |
| Lindle et al. | N ₂ , NO |
| Lynch and McKoy | N ₂ |
| Lynch et al. (1984a) | C ₂ H ₂ |
| Lynch et al. (1984b) | review article |
| McKoy et al. | review article |
| Piancastelli et al. | CCl ₄ , SiCl ₄ , GeCl ₄ |
| Roy et al. | CO ₂ |
| Schneider and Collins | review article |

| Reference | Molecule |
|-------------------------|---|
| <i>1984 (cont'd)</i> | |
| Sette et al. | C ₂ H ₂ , C ₂ H ₄ , C ₆ H ₆ , CH ₃ HCO, (CH ₃) ₂ CO, C ₂ H ₆ , HCN, C ₂ N ₂ , CH ₃ NH ₂ , N ₂ , CO, H ₂ CO, CH ₃ HCO, (CH ₃) ₂ CO, BF ₃ , CH ₃ OCH ₃ , CH ₃ OH, NO, CF ₄ , CHF ₃ , CH ₂ F ₂ , CH ₃ F, O ₂ , NF ₃ |
| Shaw et al. | CO |
| Sodhi | NF ₃ , Si(CH ₃) ₃ , PH ₃ , P(CH ₃) ₃ , PF ₃ , PCl ₃ , PF ₅ , OPF ₃ , OPCl ₃ , methylamines, NH ₃ , CH ₂ =C=CH ₂ , t-1,3-butadiene, allene |
| Sodhi and Brion | SF ₆ , CO, N ₂ |
| Sodhi et al. | NF ₃ |
| Tossell and Davenport | CX ₄ , SiX ₄ (X = H, F, Cl) |
| Truesdale et al. | CO, CO ₂ , CF ₄ , OCS |
| <i>1985</i> | |
| Dehmer et al. | review article |
| Ferrett et al. (1986) | SF ₆ |
| Kosman and Wallace | N ₂ |
| Sodhi and Brion (1985a) | methylamines, NH ₃ |
| Sodhi and Brion (1985b) | t-1,3-butadiene, allene |
| Sodhi and Brion (1985c) | PH ₃ , P(CH ₃) ₃ , PCl ₃ , PF ₃ |
| Sodhi and Brion (1985d) | PF ₅ , OPF ₃ , OPCl ₃ |
| Sodhi et al. | (CH ₃) ₄ Si |
| Stephens and Dill | N ₂ |
| Tossell | C ₂ H ₂ |

References

- Åberg, T., and J.L. Dehmer, 1973, *J. Phys. C* **6**, 1450.
 Achiba, Y., K. Sato, K. Shobatake and K. Kimura, 1982, *J. Chem. Phys.* **77**, 2709.
 Achiba, Y., K. Sato, K. Shobatake and K. Kumara, 1983, *J. Chem. Phys.* **78**, 5474.
 Adam, M.Y., P. Morin, P. Lablanquie and I. Nenner, 1983, *Int. Workshop on Atomic and Molecular Photoionization* (Fritz-Haber-Institut der Max-Planck-Gesellschaft, Berlin).
 Ågren, H., and R. Arneberg, 1984, *Phys. Scr.* **30**, 55.
 Ågren, H., J. Nodgren, L. Selander, C. Nordling and K. Siegbahn, 1978, *Phys. Scr.* **18**, 499.
 Ajello, J.M., A. Chutjian and R. Winchell, 1980, *J. Electron Spectrosc.* **19**, 197.
 Anderson, S.L., G.D. Kubiak and R.N. Zare, 1984, *Chem. Phys. Lett.* **105**, 22.
 Åsbrink, L., A. Svensson, W. von Niessen and G. Bieri, 1981, *J. Electron Spectrosc.* **24**, 293.
 Atabek, O., D. Dill and Ch. Jungen, 1974, *Phys. Rev. Lett.* **33**, 123.
 Azaroff, L.V., 1963, *Rev. Mod. Phys.* **35**, 1012.
 Baer, T., 1979, in: *Gas Phase Ion Chemistry*, ed. M.T. Bowers (Academic Press, New York) ch. 5.

- Baer, T., P.M. Guyon, I. Nenner, A. Tabché-Fouhailé, R. Botter, L.F.A. Ferreira and T.R. Govers, 1979, *J. Chem. Phys.* **70**, 1585.
- Bagus, P.S., and H.F. Schaefer, 1972, *J. Chem. Phys.* **56**, 224.
- Bagus, P.S., and E.K. Viinikka, 1977, *Phys. Rev. A* **15**, 1486.
- Bahr, J.L., A.J. Blake, J.H. Carver, J.L. Gardner and V. Kumar, 1971a, *J. Quant. Spectrosc. & Radiat. Transfer* **11**, 1839.
- Bahr, J.L., A.J. Blake, J.H. Carver, J.L. Gardner and V. Kumar, 1971b, *J. Quant. Spectrosc. & Radiat. Transfer* **11**, 1853.
- Baker, C., and D.W. Turner, 1968, *Proc. R. Soc. London Ser. A* **308**, 19.
- Bardsley, J.N., and F. Mandl, 1968, *Rep. Prog. Phys.* **31**, 472.
- Barinskii, R.L., and I.M. Kulikova, 1973, *Zh. Strukt. Khim.* **14**, 372 [*J. Struct. Chem.* **14**, 335].
- Barrus, D.M., R.L. Blake, A.J. Burek, K.C. Chambers and A.L. Pregonzer, 1979, *Phys. Rev. A* **20**, 1045.
- Batten, C.F., J.A. Taylor and G.G. Meisels, 1976, *J. Chem. Phys.* **65**, 3316.
- Batten, C.F., J.A. Taylor, B.P. Tsai and G.G. Meisels, 1978, *J. Chem. Phys.* **69**, 2547.
- Benedict, M.G., and I. Gyemant, 1978, *Int. J. Quantum Chem.* **13**, 597.
- Berkowitz, J., 1979, *Photoabsorption, Photoionization and Photoelectron Spectroscopy* (Academic Press, New York).
- Berkowitz, J., and W.A. Chupka, 1969, *J. Chem. Phys.* **51**, 2341.
- Berkowitz, J., and J.H.D. Eland, 1977, *J. Chem. Phys.* **67**, 2740.
- Berry, R.S., and S.E. Nielsen, 1970a, *Phys. Rev. A* **1**, 383.
- Berry, R.S., and S.E. Nielsen, 1970b, *Phys. Rev. A* **1**, 395.
- Bianconi, A., H. Peterson, F.C. Brown and R.Z. Bachrach, 1978, *Phys. Rev. A* **17**, 1907.
- Birtwistle, D.T., and A. Herzenberg, 1971, *J. Phys. B* **4**, 53.
- Blake, A.J., J.L. Bahr, J.H. Carver and V. Kumar, 1970, *Philos. Trans. Roy. Soc. London A* **268**, 159.
- Blechschmidt, D., R. Haensel, E.-E. Koch, U. Nielsen and T. Sagawa, 1972, *Chem. Phys. Lett.* **14**, 33.
- Botter, R., V.H. Dibeler, J.A. Walker and H.M. Rosenstock, 1966, *J. Chem. Phys.* **44**, 1271.
- Brehm, B., J.H.D. Eland, R. Frey and A. Kustler, 1973, *Int. J. Mass. Spectrom. & Ion Phys.* **12**, 197.
- Brion, C.E., and K.H. Tan, 1978, *Chem. Phys.* **34**, 141.
- Brion, C.E., and K.H. Tan, 1979, *J. Electron Spectrosc.* **15**, 241.
- Brion, C.E., and K.H. Tan, 1981, *J. Electron Spectrosc.* **23**, 1.
- Brion, C.E., and J.P. Thomson, 1984a, *J. Electron Spectrosc.* **33**, 287.
- Brion, C.E., and J.P. Thomson, 1984b, *J. Electron Spectrosc.* **33**, 301.
- Brion, C.E., K.H. Tan, M.J. van der Wiel and Ph.E. van der Leeuw, 1979, *J. Electron Spectrosc.* **17**, 101.
- Brown, F.C., R.Z. Bachrach and A. Bianconi, 1978, *Chem. Phys. Lett.* **54**, 425.
- Cadioli, B., U. Pincelli, E. Tosatti, U. Fano and J.L. Dehmer, 1972, *Chem. Phys. Lett.* **17**, 15.
- Caprace, G., J. Delwiche, P. Natalis and J.E. Collin, 1976, *Chem. Phys.* **13**, 43.
- Carlson, T.A., 1971, *Chem. Phys. Lett.* **9**, 23.
- Carlson, T.A., and A.E. Jonas, 1971, *J. Chem. Phys.* **55**, 4913.
- Carlson, T.A., and G.E. McGuire, 1972, *J. Electron Spectrosc.* **1**, 209.
- Carlson, T.A., G.E. McGuire, A.E. Jonas, K.L. Cheng, C.P. Anderson, C.C. Lu and B.P. Pullen, 1972, in: *Electron Spectroscopy*, ed. D.A. Shirley (North-Holland, Amsterdam) p. 207.
- Carlson, T.A., M.O. Krause, D. Mehaffy, J.W. Taylor, F.A. Grimm and J.D. Allen, 1980, *J. Chem. Phys.* **73**, 6056.
- Carlson, T.A., M.O. Krause, F.A. Grimm, J.D. Allen, D. Mehaffy, P.R. Keller and J.W. Taylor, 1981a, *Phys. Rev. A* **23**, 3316.
- Carlson, T.A., M.O. Krause, F.A. Grimm, J.D. Allen, D. Mehaffy, P.R. Keller and J.W. Taylor, 1981b, *J. Chem. Phys.* **75**, 3288.
- Carlson, T.A., M.O. Krause and F.A. Grimm, 1982a, *J. Chem. Phys.* **77**, 1701.
- Carlson, T.A., M.O. Krause, F.A. Grimm, P. Keller and J.W. Taylor, 1982b, *J. Chem. Phys.* **77**, 5340.

- Carlson, T.A., M.O. Krause, F.A. Grimm and T.A. Whitley, 1983a, *J. Chem. Phys.* **78**, 638.
- Carlson, T.A., P.R. Keller, J.W. Taylor, T. Whitley and F.A. Grimm, 1983b, *J. Chem. Phys.* **79**, 97.
- Carlson, T.A., M.O. Krause, A. Fahlman, P.R. Keller, J.W. Taylor, T. Whitley and F.A. Grimm, 1983c, *J. Chem. Phys.* **79**, 2157.
- Carlson, T.A., A. Fahlman, M.O. Krause, P.R. Keller, J.W. Taylor, T. Whitley and F.A. Grimm, 1984a, *J. Chem. Phys.* **80**, 3521.
- Carlson, T.A., A. Fahlman, W.A. Svensson, M.O. Krause, T.A. Whitley, F.A. Grimm, M.N. Piancastelli and J.W. Taylor, 1984b, *J. Chem. Phys.* **81**, 3828.
- Carlson, T.A., A. Fahlman, M.O. Krause, T.A. Whitley and F.A. Grimm, 1984c, *J. Chem. Phys.* **81**, 5389.
- Carnovale, F., M.G. White and C.E. Brion, 1981, *J. Electron Spectrosc.* **24**, 63.
- Carr, R.G., T.K. Sham and W.E. Eberhardt, 1985, *Chem. Phys. Lett.* **113**, 63.
- Cederbaum, L.S., and W. Domcke, 1977, *Adv. Chem. Phys.* **36**, 205.
- Cederbaum, L.S., J. Schirmer, W. Domcke and W. von Niessen, 1977, *J. Phys. B* **10**, L549.
- Cederbaum, L.S., J. Schirmer, W. Domcke and W. von Niessen, 1978, *J. Electron Spectrosc.* **16**, 59.
- Cederbaum, L.S., W. Domcke, J. Schirmer and W. von Niessen, 1980, *Phys. Scr.* **21**, 481.
- Chandra, N., and A. Temkin, 1976, *Phys. Rev. A* **13**, 188.
- Chase, D.M., 1956, *Phys. Rev.* **104**, 838.
- Cherepkov, N.A., 1981a, *J. Phys. B* **14**, 2165.
- Cherepkov, N.A., 1981b, *J. Phys. B* **14**, L73.
- Child, M.S., 1974, *Molecular Collision Theory* (Academic Press, New York) p. 51.
- Chupka, W.A., and J. Berkowitz, 1969, *J. Chem. Phys.* **51**, 4244.
- Chutjian, A., and J.M. Ajello, 1977, *J. Chem. Phys.* **66**, 4544.
- Chutjian, A., and J.M. Ajello, 1980, *Chem. Phys. Lett.* **72**, 504.
- Codling, K., 1966, *J. Chem. Phys.* **44**, 4401.
- Codling, K., A.C. Parr, D.L. Ederer, R. Stockbauer, J.B. West, B.E. Cole and J.L. Dehmer, 1981, *J. Phys. B* **14**, 657.
- Cole, B.E., D.L. Ederer, R. Stockbauer, K. Codling, A.C. Parr, J.B. West, E.D. Poliakoff and J.L. Dehmer, 1980, *J. Chem. Phys.* **72**, 6308.
- Collin, J.E., and J. Delwiche, 1967, *Can. J. Chem.* **45**, 1883.
- Collin, J.E., and P.J. Natalis, 1969, *Int. J. Mass Spectrom. & Ion Phys.* **2**, 231.
- Collin, J.E., J. Delwiche and P. Natalis, 1972, in: *Electron Spectroscopy*, ed. D.A. Shirley (North-Holland, Amsterdam) p. 401.
- Collins, L.A., and B.I. Schneider, 1984, *Phys. Rev. A* **29**, 1695.
- Connolly, J.W.D., and K.H. Johnson, 1971, *Chem. Phys. Lett.* **10**, 616.
- Danby, C.J., and J.H.D. Eland, 1972, *Int. J. Mass. Spectrom. & Ion Phys.* **8**, 153.
- Davenport, J.W., 1976a, *Phys. Rev. Lett.* **36**, 945.
- Davenport, J.W., 1976b, Ph.D. Thesis (Univ. of Pennsylvania).
- Davenport, J.W., 1977, *Int. J. Quantum Chem. Quantum Chem. Symp.* **11**, 89.
- Davenport, J.W., W. Ho and J.R. Schrieffer, 1978, *Phys. Rev. B* **17**, 3115.
- Dehmer, J.L., 1972, *J. Chem. Phys.* **56**, 4496.
- Dehmer, J.L., 1974, *Phys. Fenn.* **9S**, 60.
- Dehmer, J.L., 1984, in: *Resonances in Electron-Molecule Scattering, van der Waals Complexes and Reactive Chemical Dynamics*, ACS Symposium Series, No. 263, ed. D.G. Truhlar (American Chemical Society, Washington, DC) ch. 8, p. 139.
- Dehmer, J.L., and D. Dill, 1975, *Phys. Rev. Lett.* **35**, 213.
- Dehmer, J.L., and D. Dill, 1976a, *J. Chem. Phys.* **65**, 5327.
- Dehmer, J.L., and D. Dill, 1976b, in: *Proc. 2nd Int. Conf. on Inner-Shell Ionization Phenomena*, eds W. Mehlhorn and R. Brenn (Fakultät für Physik, Universität Freiburg) p. 221.
- Dehmer, J.L., and D. Dill, 1978, *Phys. Rev. A* **18**, 164.
- Dehmer, J.L., and D. Dill, 1979a, in: *Symp. on Electron-Molecule Collisions*, eds I. Shimamura and M. Matsuzawa (Univ. of Tokyo Press, Tokyo) p. 95.
- Dehmer, J.L., and D. Dill, 1979b, in: *Electron-Molecule and Photon-Molecule Collisions*, eds T. Rescigno, V. McKoy and B. Schneider (Plenum, New York) p. 225.

- Dehmer, J.L., and D. Dill, 1980, in: *Electronic and Atomic Collisions*, eds N. Oda and K. Takayanagi (North-Holland, Amsterdam) p. 195.
- Dehmer, J.L., A.F. Starace, U. Fano, J. Sugar and J.W. Cooper, 1971, *Phys. Rev. Lett.* **26**, 1521.
- Dehmer, J.L., W.A. Chupka, J. Berkowitz and W.T. Jivery, 1975, *Phys. Rev. A* **12**, 1966.
- Dehmer, J.L., J. Siegel and D. Dill, 1978, *J. Chem. Phys.* **69**, 5205.
- Dehmer, J.L., D. Dill and S. Wallace, 1979, *Phys. Rev. Lett.* **43**, 1005.
- Dehmer, J.L., J. Siegel, J. Welch and D. Dill, 1980, *Phys. Rev. A* **21**, 101.
- Dehmer, J.L., A.C. Parr, S. Wallace and D. Dill, 1982, *Phys. Rev. A* **26**, 3283.
- Dehmer, J.L., A.C. Parr, S.H. Southworth and D.M.P. Holland, 1984, *Phys. Rev. A* **30**, 1783.
- Dehmer, J.L., D. Dill and A.C. Parr, 1985, in: *Photophysics and Photochemistry in the Vacuum Ultraviolet*, eds S. McGlynn, G. Findley and R. Huebner (Reidel, Dordrecht) p. 341.
- Dehmer, P.M., and W.A. Chupka, 1975, *J. Chem. Phys.* **62**, 4525.
- Dehmer, P.M., and W.A. Chupka, 1976, *J. Chem. Phys.* **65**, 2243.
- Dehmer, P.M., and J.L. Dehmer, 1982, *J. Electron Spectrosc.* **28**, 145.
- Dehmer, P.M., P.J. Miller and W.A. Chupka, 1984, *J. Chem. Phys.* **80**, 1030.
- Delaney, J.J., I.H. Hillier and V.R. Saunders, 1982a, *J. Phys. B* **15**, L37.
- Delaney, J.J., I.H. Hillier and V.R. Saunders, 1982b, *J. Phys. B* **15**, 1477.
- Derenbach, H., R. Malutzki and V. Schmidt, 1983, *Nucl. Instrum. Methods* **208**, 845.
- Dibeler, V.H., and S.K. Liston, 1968, *Inorg. Chem.* **7**, 1742.
- Dibeler, V.H., and J.A. Walker, 1966, *J. Chem. Phys.* **44**, 4405.
- Dibeler, V.H., and J.A. Walker, 1967, *J. Opt. Soc. Am.* **57**, 1007.
- Dibeler, V.H., and J.A. Walker, 1973, *Int. J. Mass Spectrom. & Ion Phys.* **11**, 49.
- Dill, D., 1972, *Phys. Rev. A* **6**, 160.
- Dill, D., and J.L. Dehmer, 1974, *J. Chem. Phys.* **61**, 692.
- Dill, D., and Ch. Jungen, 1980, *J. Phys. Chem.* **84**, 2116.
- Dill, D., J. Siegel and J.L. Dehmer, 1976, *J. Chem. Phys.* **65**, 3158.
- Dill, D., S. Wallace, J. Siegel and J.L. Dehmer, 1978, *Phys. Rev. Lett.* **41**, 1230.
- Dill, D., S. Wallace, J. Siegel and J.L. Dehmer, 1979a, *Phys. Rev. Lett.* **42**, 411(E).
- Dill, D., J. Welch, J.L. Dehmer and J. Siegel, 1979b, *Phys. Rev. Lett.* **43**, 1236.
- Dill, D., R. Swanson, S. Wallace and J.L. Dehmer, 1980, *Phys. Rev. Lett.* **45**, 1393.
- Dittman, P.M., D. Dill and J.L. Dehmer, 1982, *J. Chem. Phys.* **76**, 5703.
- Dittman, P.M., D. Dill and J.L. Dehmer, 1983, *Chem. Phys.* **78**, 405.
- Doolittle, P.H., and R.I. Schoen, 1965, *Phys. Rev. Lett.* **14**, 348.
- Duzy, C., and R.S. Berry, 1976, *J. Chem. Phys.* **64**, 2431.
- Eberhardt, W., R.P. Haelbich, M. Iwan, E.-E. Koch and C. Kunz, 1976, *Chem. Phys. Lett.* **40**, 180.
- Eberhardt, W., T.K. Sham, R. Carr, S. Krummacher, M. Strongin, S.L. Wergand and D. Wesner, 1983a, *Phys. Rev. Lett.* **50**, 1038.
- Eberhardt, W., J. Stöhr, J. Feldhaus, E.W. Plummer and F. Sette, 1983b, *Phys. Rev. Lett.* **51**, 2370.
- Ederer, D.L., B.E. Cole and J.B. West, 1980, *Nucl. Instrum. Methods* **172**, 185.
- Ederer, D.L., A.C. Parr, B.E. Cole, R. Stockbauer, J.L. Dehmer, J.B. West and K. Codling, 1981, *Proc. R. Soc. London Ser. A* **378**, 423.
- El-Sherbini, Th.M., and M.J. van der Wiel, 1972, *Physica* **59**, 433.
- Eland, J.H.D., 1980, *J. Chem. Phys.* **72**, 6015.
- Fano, U., 1935, *Nuovo Cimento* **12**, 156.
- Fano, U., 1961, *Phys. Rev.* **124**, 1866.
- Fano, U., 1970, *Phys. Rev. A* **2**, 353.
- Fano, U., 1972, *Comments At. & Mol. Phys.* **3**, 75.
- Fano, U., 1975, *J. Opt. Soc. Am.* **65**, 979.
- Fano, U., 1983, *Rep. Prog. Phys.* **46**, 97 and references cited therein.
- Fano, U., and J.W. Cooper, 1968, *Rev. Mod. Phys.* **40**, 441.
- Ferrett, T.A., D.W. Lindle, P.A. Heimann, H.G. Kerkhoff, V.E. Becker and D.A. Shirley, 1986, *Phys. Rev. A* **34**, 1916.
- Fock, J.-H., 1983, Ph.D. Thesis (University of Hamburg).
- Fock, J.-H., and E.-E. Koch, 1984, *Chem. Phys. Lett.* **105**, 38.

- Fock, J.-H., and E.-E. Koch, 1985, *Chem. Phys.* **96**, 125.
- Fock, J.-H., H.-J. Lau and E.-E. Koch, 1984, *Chem. Phys.* **83**, 377.
- Fomichev, V.A., 1967, *Fiz. Tverd. Tela* **9**, 3167 [1968, *Sov. Phys.-Solid State* **9**, 2496].
- Fomichev, V.A., and R.L. Barinskii, 1970, *Zh. Strukt. Khim.* **11**, 875 [*J. Struct. Chem.* **11**, 810].
- Friedrich, H., B. Pittel, P. Rabe, W.H.E. Schwarz and B. Sonntag, 1980, *J. Phys. B* **13**, 25.
- Gardner, J.L., and J.A.R. Samson, 1973, *J. Electron Spectrosc.* **2**, 153.
- Gardner, J.L., and J.A.R. Samson, 1974a, *J. Chem. Phys.* **60**, 3711.
- Gardner, J.L., and J.A.R. Samson, 1974b, *Chem. Phys. Lett.* **26**, 240.
- Gardner, J.L., and J.A.R. Samson, 1978, *J. Electron Spectrosc.* **13**, 7.
- Gelius, U., 1974, *J. Electron Spectrosc.* **5**, 985.
- Gerwer, A., C. Asaro, B.V. McKoy and P.W. Langhoff, 1980, *J. Chem. Phys.* **72**, 713.
- Gianturco, F.A., C. Guidotti, U. Lamanna and R. Moccia, 1971, *Chem. Phys. Lett.* **10**, 269.
- Gianturco, F.A., C. Guidotti and U. Lamanna, 1972, *J. Chem. Phys.* **57**, 840.
- Giardini-Guidoni, A., R. Fantoni, R. Tiribelli, D. Vinciguerra, R. Camilloni and G. Stefani, 1979, *J. Chem. Phys.* **71**, 3182.
- Giusti-Suzor, A., 1982, in: *Physics of Electronic and Atomic Collisions*, ed. S. Datz (North-Holland, Amsterdam) p. 381.
- Giusti-Suzor, A., and U. Fano, 1984a, *J. Phys. B* **17**, 215.
- Giusti-Suzor, A., and U. Fano, 1984b, *J. Phys. B* **17**, 4267.
- Giusti-Suzor, A., and Ch. Jungen, 1984, *J. Chem. Phys.* **80**, 986.
- Giusti-Suzor, A., and H. Lefebvre-Brion, 1980, *Chem. Phys. Lett.* **76**, 132.
- Giusti-Suzor, A., and H. Lefebvre-Brion, 1984, *Phys. Rev. A* **30**, 3057.
- Glowia, J.H., S.J. Riley, S.D. Colson, J.C. Miller and R.N. Compton, 1982, *J. Chem. Phys.* **77**, 68.
- Greene, C.H., and R.N. Zare, 1983, *J. Chem. Phys.* **78**, 6741.
- Grimm, F.A., 1980, *Chem. Phys.* **53**, 71.
- Grimm, F.A., 1983, *Chem. Phys.* **81**, 315.
- Grimm, F.A., and T.A. Carlson, 1983, *Chem. Phys.* **80**, 389.
- Grimm, F.A., T.A. Carlson, W.B. Dress, P. Agron, J.O. Thomson and J.W. Davenport, 1980, *J. Chem. Phys.* **72**, 3041.
- Grimm, F.A., J.D. Allen, T.A. Carlson, M.O. Krause, D. Mehaffy, P.R. Keller and J.W. Taylor, 1981, *J. Chem. Phys.* **75**, 92.
- Grimm, F.A., T.A. Whitley, P.R. Keller and J.W. Taylor, 1984, *J. Electron Spectrosc.* **33**, 361.
- Guest, J.A., K.A. Jackson and R.N. Zare, 1983, *Phys. Rev. A* **28**, 2217.
- Guest, J.A., M.A. O'Halloran and R.N. Zare, 1984, *J. Chem. Phys.* **81**, 2689.
- Gurtler, P., V. Saile and E.-E. Koch, 1977, *Chem. Phys. Lett.* **48**, 245.
- Gustafsson, T., 1978, *Phys. Rev. A* **18**, 1481.
- Gustafsson, T., 1980a, *Chem. Phys. Lett.* **75**, 505.
- Gustafsson, T., 1980b, *Surf. Sci.* **94**, 593.
- Gustafsson, T., 1983, in: *Atomic Physics 8*, eds I. Lindgren, A. Rosen and S. Svanberg (Plenum, New York) p. 355.
- Gustafsson, T., and H.J. Levinson, 1981, *Chem. Phys. Lett.* **78**, 28.
- Gustafsson, T., E.W. Plummer, D.E. Eastman and W. Gudat, 1978a, *Phys. Rev. A* **17**, 175.
- Gustafsson, T., E.W. Plummer, E.W. Liebsch, 1978b, in: *Photoemission and the Electronic Properties of Surfaces*, eds B. Feuerbacher, B. Fitton and R.F. Willis (Wiley, New York).
- Guyon, P.-M., T. Baer, L.F.A. Ferreira, I. Nenner, A. Tabché-Fouhailé, R. Botter and T.R. Govers, 1978, *J. Phys. B* **11**, L141.
- Guyon, P.-M., T. Baer and I. Nenner, 1983, *J. Chem. Phys.* **78**, 3665.
- Haller, E., H. Köppel, L.S. Cederbaum, W. von Niessen and G. Bieri, 1983, *J. Chem. Phys.* **78**, 1359.
- Hamnett, A., W. Stoll and C.E. Brion, 1976, *J. Electron Spectrosc.* **8**, 367.
- Hancock, W.H., and J.A.R. Samson, 1976, *J. Electron Spectrosc.* **9**, 211.
- Hara, S., 1985, *J. Phys. B* **18**, 3759.
- Hara, S., and S. Ogata, 1985, *J. Phys. B* **18**, L59.
- Harting, E., and F.H. Read, 1976, *Electrostatic Lenses* (North-Holland, Amsterdam).

- Hay, P.J., 1977, *J. Am. Chem. Soc.* **99**, 1003.
- Hayaishi, T., S. Iwata, M. Sasanuma, E. Ishiguro, Y. Morioka, Y. Iida and M. Nakamura, 1982, *J. Phys. B* **15**, 79.
- Hayes, W., and F.C. Brown, 1971, *J. Phys. B* **4**, L85.
- Heinzmann, U., 1980, *Appl. Opt.* **19**, 4087.
- Heinzmann, U., F. Schäfers and B.A. Hess, 1980, *Chem. Phys. Lett.* **69**, 284.
- Heinzmann, U., B. Osterheld, F. Schäfers and G. Schönhense, 1981, *J. Phys. B* **14**, L79.
- Hermann, M.R., and P.W. Langhoff, 1981, *Chem. Phys. Lett.* **82**, 242.
- Hermann, M.R., G.H.F. Dierksen, B.W. Fatyga and P.W. Langhoff, 1984, *Int. J. Quantum Chem.* **18**, 719.
- Herzberg, G., and Ch. Jungen, 1972, *J. Mol. Spectrosc.* **41**, 425.
- Herzenberg, A., and F. Mandl, 1962, *Proc. R. Soc. London Ser. A* **270**, 48.
- Hitchcock, A.P., 1982, *J. Electron. Spectrosc.* **25**, 245.
- Hitchcock, A.P., and C.E. Brion, 1977, *J. Electron Spectrosc.* **10**, 317.
- Hitchcock, A.P., and C.E. Brion, 1978a, *Chem. Phys.* **33**, 55.
- Hitchcock, A.P., and C.E. Brion, 1978b, *J. Electron Spectrosc.* **14**, 417.
- Hitchcock, A.P., and C.E. Brion, 1979a, *J. Electron Spectrosc.* **15**, 201.
- Hitchcock, A.P., and C.E. Brion, 1979b, *Chem. Phys.* **37**, 319.
- Hitchcock, A.P., and C.E. Brion, 1980a, *J. Electron Spectrosc.* **18**, 1.
- Hitchcock, A.P., and C.E. Brion, 1980b, *J. Electron Spectrosc.* **19**, 231.
- Hitchcock, A.P., and C.E. Brion, 1981, *J. Phys. B* **13**, 4399.
- Hitchcock, A.P., and M.J. van der Wiel, 1979, *J. Phys. B* **12**, 2153.
- Hitchcock, A.P., C.E. Brion and M.J. van der Wiel, 1978, *J. Phys. B* **11**, 3245.
- Hitchcock, A.P., C.E. Brion, G.R.J. Williams and P.W. Langhoff, 1982, *Chem. Phys.* **66**, 435.
- Hitchcock, A.P., S. Beaulieu, T. Steel, J. Stöhr and F. Sette, 1984, *J. Chem. Phys.* **80**, 3927.
- Holland, D.M.P., A.C. Parr, D.L. Ederer, J.L. Dehmer and J.B. West, 1982, *Nucl. Instr. Methods* **195**, 331.
- Holland, D.M.P., A.C. Parr, D.L. Ederer, J.B. West and J.L. Dehmer, 1983, *Int. J. Mass. Spectrom. & Ion Phys.* **52**, 195.
- Holland, D.M.P., A.C. Parr and J.L. Dehmer, 1984, *J. Phys. B* **17**, 1343.
- Holmes, R.M., and G.V. Marr, 1980, *J. Phys. B* **13**, 945.
- Hopfield, J.J., 1930a, *Phys. Rev.* **35**, 1133.
- Hopfield, J.J., 1930b, *Phys. Rev.* **36**, 789.
- Horton, V.G., E.T. Arakawa, R.N. Hamin and M.W. Williams, 1969, *Appl. Opt.* **8**, 667.
- Hubin-Franskin, M.-J., J. Delwiche, P. Morin, M.Y. Adam, I. Nenner and P. Roy, 1984, *J. Chem. Phys.* **81**, 4246.
- Ishiguro, E., S. Iwata, Y. Suzuki, A. Mikuni and T. Sasaki, 1982, *J. Phys. B* **15**, 1841.
- Itikawa, Y., H. Takagi, H. Nakamura and H. Sato, 1983, *Phys. Rev. A* **27**, 1319.
- Iwata, S., N. Kosugi and O. Nomura, 1978, *J. Appl. Phys. Jpn.* **17**(Suppl. 17-2), 109.
- Johnson, W.R., and K.T. Cheng, 1979, *Phys. Rev. A* **20**, 978.
- Johnson, W.R., K.T. Cheng, K.-N. Huang and M. LeDourneuf, 1980, *Phys. Rev. A* **22**, 989.
- Jungen, Ch., 1980, *J. Chim. Phys.* **77**, 27.
- Jungen, Ch., 1984a, *Ann. Israel Phys. Soc.* **6**, 491.
- Jungen, Ch., 1984b, *Phys. Rev. Lett.* **53**, 2394.
- Jungen, Ch., and O. Atabek, 1977, *J. Chem. Phys.* **66**, 5584.
- Jungen, Ch., and D. Dill, 1980, *J. Chem. Phys.* **73**, 3338.
- Jungen, Ch., and M. Raoult, 1981, *Faraday Disc. Chem. Soc.* **71**, 253.
- Kaestdorf, S., G. Schönhense and U. Heinzmann, 1985, *Phys. Rev. Lett.* **54**, 885.
- Kanamori, H., S. Iwata, A. Mikuni and T. Sasaki, 1984, *J. Phys. B* **17**, 3887.
- Katsumata, S., Y. Achiba and K. Kimura, 1979, *J. Electron Spectrosc.* **17**, 229.
- Kay, R.B., Ph.E. van der Leeuw and M.J. van der Wiel, 1977, *J. Phys. B* **10**, 2513.
- Keller, P.R., D. Mehaffy, J.W. Taylor, F.A. Grimm and T.A. Carlson, 1982, *J. Electron Spectrosc.* **27**, 223.

- Keller, P.R., J.W. Taylor, T.A. Carlson and F.A. Grimm, 1983a, *Chem. Phys.* **79**, 269.
- Keller, P.R., J.W. Taylor, F.A. Grimm, P. Senn, T.A. Carlson and M.O. Krause, 1983b, *Chem. Phys.* **74**, 247.
- Keller, P.R., J.W. Taylor, T.A. Carlson and F.A. Grimm, 1984a, *J. Electron Spectrosc.* **33**, 333.
- Keller, P.R., J.W. Taylor, F.A. Grimm and T.A. Carlson, 1984b, *Chem. Phys.* **90**, 147.
- Kennedy, D.J., and S.T. Manson, 1972, *Phys. Rev. A* **5**, 227.
- Kennerly, R.E., 1980, *Phys. Rev. A* **21**, 1876.
- Kennerly, R.E., R.A. Bonham and M. McMillan, 1979, *J. Chem. Phys.* **70**, 2039.
- Kibel, M.H., F.J. Leng and G.L. Nyberg, 1979, *J. Electron Spectrosc.* **15**, 281.
- Kimman, J., 1984, Ph.D. Thesis (FOM-Institute for Atomic and Molecular Physics, Amsterdam).
- Kimman, J., P. Kruit and M.J. van der Wiel, 1982, *Chem. Phys. Lett.* **88**, 576.
- Kimura, K., S. Katsumata, Y. Achiba, T. Yamazaki and S. Iwata, 1981, *Handbook of HeI Photoelectron Spectra of Fundamental Organic Molecules* (Japan Scientific Societies Press, Tokyo and Halsted Press, New York).
- Kincaid, B.M., and P. Eisenberger, 1975, *Phys. Rev. Lett.* **34**, 1361.
- King, G.C., F.H. Read and M. Tronc, 1977, *Chem. Phys. Lett.* **52**, 50.
- Kleimenov, V.I., Yu.V. Chizhov and F.I. Vilesov, 1972, *Opt. Spektrosk.* **32**, 702 [*Opt. Spectrosc.* **32**, 371].
- Koch, E.-E., ed., 1983, *Handbook on Synchrotron Radiation*, Vol. 1 (North-Holland, Amsterdam).
- Koch, E.-E., and B.F. Sonntag, 1979, in: *Synchrotron Radiation: Techniques and Applications*, ed. C. Kunz (Springer, Berlin) p. 269.
- Koestner, R.J., J. Stöhr, J.L. Gland and J.A. Horsley, 1984, *Chem. Phys. Lett.* **105**, 332.
- Kondratenko, A.V., L.N. Mazalov, F.Kh. Gel'mukhanov, V.I. Avdeev and E.A. Saprykhina, 1977, *Zh. Strukt. Khim.* **18**, 546 [*J. Struct. Chem.* **18**, 437].
- Kosman, W.M., and S. Wallace, 1985, *J. Chem. Phys.* **82**, 1385.
- Krause, M.O., T.A. Carlson and P.R. Woodruff, 1981, *Phys. Rev. A* **24**, 1374.
- Krauss, M., and F.H. Mies, 1970, *Phys. Rev. A* **1**, 1592.
- Kreile, J., and A. Schweig, 1980, *J. Electron Spectrosc.* **20**, 191.
- Kreile, J., A. Schweig and W. Thiel, 1981, *Chem. Phys. Lett.* **79**, 547.
- Kreile, J., A. Schweig and W. Thiel, 1982, *Chem. Phys. Lett.* **87**, 473.
- Kreile, J., A. Schweig and W. Thiel, 1983, *Chem. Phys. Lett.* **100**, 351.
- Kreile, J., A. Schweig and W. Thiel, 1984, *Chem. Phys. Lett.* **108**, 259.
- Kronig, R. de L., 1931, *Z. Phys.* **70**, 317.
- Kronig, R. de L., 1932, *Z. Phys.* **75**, 191.
- Krummacker, S., V. Schmidt and F. Willeumier, 1980, *J. Phys. B* **13**, 3993.
- Krummacker, S., V. Schmidt, F.J. Willeumier, J.M. Bizau and D.L. Ederer, 1983, *J. Phys. B* **16**, 1733.
- Kumar, V., and E. Krishnakumar, 1981, *J. Electron Spectrosc.* **22**, 109.
- Kumar, V., and E. Krishnakumar, 1983, *J. Chem. Phys.* **78**, 46.
- Kunz, C., ed., 1979, *Synchrotron Radiation: Techniques and Applications* (Springer, Berlin).
- Lane, N.F., 1980, *Rev. Mod. Phys.* **52**, 29.
- Langhoff, P.W., 1977, *Int. J. Quantum Chem. Quantum Chem. Symp.* **11**, 301.
- Langhoff, P.W., 1979, in: *Electron-Molecule and Photon-Molecule Collisions*, eds T.N. Rescigno, V. McKoy and B. Schneider (Plenum, New York) p. 183.
- Langhoff, P.W., 1984, in: *Resonances in Electron-Molecule Scattering, van der Waals Complexes and Reactive Chemical Dynamics*, ACS Symposium Series, No. 263, ed. D.G. Truhlar (American Chemical Society, Washington, DC) ch. 7, p. 113.
- Langhoff, P.W., S.R. Langhoff and C.T. Corcoran, 1977, *J. Chem. Phys.* **67**, 1722.
- Langhoff, P.W., A. Orel, T.N. Rescigno and B.V. McKoy, 1978, *J. Chem. Phys.* **69**, 4689.
- Langhoff, P.W., A. Gerwer, C. Asaro and B.V. McKoy, 1979, *Int. J. Quantum Chem. Quantum Chem. Symp.* **13**, 645.
- Langhoff, P.W., T.N. Rescigno, N. Padial, G. Csanak and B.V. McKoy, 1980, *J. Chim. Phys.* **77**, 590.
- Langhoff, P.W., S.R. Langhoff, T.N. Rescigno, J. Schirmer, L.S. Cederbaum, W. Domcke and W. von Niessen, 1981a, *Chem. Phys.* **58**, 71.

- Langhoff, P.W., B.V. McKoy, R. Unwin and A.M. Bradshaw, 1981b, *Chem. Phys. Lett.* **83**, 270.
- Lau, H.-J., J.-H. Fock and E.-E. Koch, 1982, *Chem. Phys. Lett.* **89**, 281.
- LaVilla, R.E., 1972, *J. Chem. Phys.* **57**, 899.
- LaVilla, R.E., 1973, *J. Chem. Phys.* **58**, 3841.
- LaVilla, R.E., 1975, *J. Chem. Phys.* **63**, 2733.
- LaVilla, R.E., and R.D. Deslattes, 1966, *J. Chem. Phys.* **44**, 4399.
- Leal, E.P., L.E. Machado and L. Mu-Tao, 1984, *J. Phys. B* **17**, L569.
- Lee, L.C., E. Phillips and D.L. Judge, 1977, *J. Chem. Phys.* **67**, 1237.
- Lee, P.A., P.H. Citrin, P. Eisenberger and B.M. Kincaid, 1981, *Rev. Mod. Phys.* **53**, 769.
- Lefebvre-Brion, H., and A. Giusti-Suzor, 1983, in: *Electron-Atom and Electron-Molecule Collisions*, ed. J. Hinze (Plenum, New York) p. 215.
- Lefebvre-Brion, H., A. Giusti-Suzor and G. Raseev, 1985, *J. Chem. Phys.* **83**, 1557.
- Levine, Z.H., and P. Soven, 1983, *Phys. Rev. Lett.* **50**, 2074.
- Levine, Z.H., and P. Soven, 1984, *Phys. Rev. A* **29**, 625.
- Levinson, H., T. Gustafsson and P. Soven, 1979, *Phys. Rev. A* **19**, 1089.
- Lindle, D.W., C.M. Truesdale, P.H. Kobrin, T.A. Ferrett, P.A. Heimann, U. Becker, H.G. Kerkhoff and D.A. Shirley, 1984, *J. Chem. Phys.* **81**, 5375.
- Loomba, D., S. Wallace, D. Dill and J.L. Dehmer, 1981, *J. Chem. Phys.* **75**, 4546.
- Lozes, R.L., O. Goscinski, U.I. Wahlgren, 1979, *Chem. Phys. Lett.* **63**, 77.
- Lucchese, R.R., and V. McKoy, 1981a, *J. Phys. Chem.* **85**, 2166.
- Lucchese, R.R., and V. McKoy, 1981b, *J. Phys. B* **14**, L629.
- Lucchese, R.R., and V. McKoy, 1981c, *Phys. Rev. A* **24**, 770.
- Lucchese, R.R., and V. McKoy, 1982a, *Phys. Rev. A* **26**, 1406.
- Lucchese, R.R., and V. McKoy, 1982b, *Phys. Rev. A* **26**, 1992.
- Lucchese, R.R., and V. McKoy, 1983, *Phys. Rev. A* **28**, 1382.
- Lucchese, R.R., D.K. Watson and V. McKoy, 1980, *Phys. Rev. A* **22**, 421.
- Lucchese, R.R., G. Raseev and V. McKoy, 1982, *Phys. Rev. A* **25**, 2572.
- Lynch, D.L., and V. McKoy, 1984, *Phys. Rev. A* **30**, 1561.
- Lynch, D.L., M.-T. Lee, R.R. Lucchese and V. McKoy, 1984a, *J. Chem. Phys.* **80**, 1907.
- Lynch, D.L., V. McKoy and R.R. Lucchese, 1984b, 208.
- Machado, L.E., E.P. Leal, G. Csanak, B.V. McKoy and P.W. Langhoff, 1982, *J. Electron Spectrosc.* **25**, 1.
- Marr, G.V., and J.B. West, 1976, *At. Data & Nucl. Data Tables* **18**, 497.
- Marr, G.V., and P.R. Woodruff, 1976, *J. Phys. B* **9**, L377.
- Marr, G.V., J.M. Morton, R.M. Holmes and D.G. McCoy, 1979, *J. Phys. B* **12**, 43.
- Mazalov, L.N., F.Kh. Gel'muskhonov and V.M. Chermoshentsev, 1974, *Zh. Strukt. Khim.* **15**, 1099 [J. Struct. Chem. **15**, 975].
- McCoy, D.G., J.M. Morton and G.V. Marr, 1978, *J. Phys. B* **11**, L547.
- McCulloh, K.E., 1973, *J. Chem. Phys.* **59**, 4250.
- McKoy, V., D. Lynch and R.R. Lucchese, 1983, *Int. J. Quantum Chem. Symp.* **17**, 89.
- McKoy, V., T.A. Carlson and R.R. Lucchese, 1984, *J. Phys. Chem.* **88**, 3188.
- Mies, F.H., 1984, *J. Chem. Phys.* **80**, 2514.
- Mies, F.H., and P.S. Julienne, 1984, *J. Chem. Phys.* **80**, 2526.
- Miller, J.C., and R.N. Compton, 1981a, *J. Chem. Phys.* **75**, 22.
- Miller, J.C., and R.N. Compton, 1981b, *J. Chem. Phys.* **75**, 2020.
- Miller, J.C., and R.N. Compton, 1982, *Chem. Phys. Lett.* **93**, 453.
- Miller, J.C., R.N. Compton, T.E. Carney and T. Baer, 1982, *J. Chem. Phys.* **76**, 5648.
- Mintz, D.M., and T. Baer, 1976, *J. Chem. Phys.* **65**, 2407.
- Mintz, D.M., and A. Kuppermann, 1978, *J. Chem. Phys.* **69**, 3953.
- Morgenstern, R., A. Niehaus and M.W. Ruf, 1971, in: *Electronic and Atomic Collisions*, eds L. Branscomb, H. Ehrhardt, R. Geballe, F.J. de Heer, N.V. Fedorenko, J. Kistemaker, M. Barat, E.E. Nikitin and A.C.H. Smith (North-Holland, Amsterdam) p. 167.
- Morin, P., 1983, Ph.D. Thesis (Université de Paris-Sud).
- Morin, P., I. Nenner, P.-M. Guyon, O. Dutuit and K. Ito, 1980, *J. Chim. Phys.* **77**, 605.

- Morin, P., I. Nenner, M.Y. Adam, M.-J. Hubin-Franskin, J. Delwiche, H. Lefebvre-Brion and A. Giusti-Suzor, 1982a, *Chem. Phys. Lett.* **92**, 609.
- Morin, P., I. Nenner, P.-M. Guyon, L.F.A. Ferreira and K. Ito, 1982b, *Chem. Phys. Lett.* **92**, 103.
- Morin, P., M.Y. Adam, I. Nenner, J. Delwiche, M.-J. Hubin-Franskin and P. Lablanquie, 1983, *Nucl. Instrum. Methods* **208**, 761.
- Morin, P., I. Nenner, M.Y. Adam, P. Lablanquie, J. Delwiche and M.-J. Hubin-Franskin, 1987, to be published.
- Morioka, Y., M. Nakamura, E. Ishiguro and M. Sasanuma, 1974, *J. Chem. Phys.* **61**, 1426.
- Müller-Dethlefs, K., M. Sander and E.W. Schlag, 1984, *Chem. Phys. Lett.* **112**, 291.
- Nakamura, M., M. Sasanuma, S. Sato, M. Watanabe, H. Yamashita, Y. Iguchi, A. Ejiri, S. Nakai, S. Yamaguchi, T. Sagawa, Y. Nakai and T. Oshio, 1969, *Phys. Rev.* **178**, 80.
- Nakamura, M., Y. Morioka, T. Hayaishi, E. Ishiguro and M. Sasanuma, 1971, in: *Conference Digest, Third Int. Conf. on Vacuum Ultraviolet Radiation Physics*, ed. Y. Nakai (Physical Society of Japan, Tokyo) p. 1pA1-6.
- Natalis, P., J. Delwiche, J.E. Collin, G. Caprace and M.-T. Praet, 1977, *Chem. Phys. Lett.* **49**, 177.
- Nefedov, V.I., 1970, *Zh. Strukt. Khim.* **11**, 292 [*J. Struct. Chem.* **11**, 272].
- Nenner, I., 1983, *Laser Chem.* **3**, 339.
- Nenner, I., and A. Beswick, 1987, ch. 6, this volume.
- Newton, R.G., 1966, *Scattering Theory of Waves and Particles* (McGraw-Hill, New York) p. 457.
- Niehaus, A., and M.W. Ruf, 1972, *Z. Phys.* **252**, 84.
- Ninomiya, K., E. Ishiguro, S. Iwata, A. Mikuni and T. Sasaki, 1981, *J. Phys. B* **14**, 1777.
- Ogawa, M., and Y. Tanaka, 1962, *Can. J. Phys.* **40**, 1593.
- Ono, Y., E.A. Osuch and C.Y. Ng, 1982, *J. Chem. Phys.* **76**, 3905.
- Orel, A.E., T.N. Rescigno, B.V. McKoy and P.W. Langhoff, 1980, *J. Chem. Phys.* **72**, 1265.
- Padiál, N., G. Csanak, B.V. McKoy and P.W. Langhoff, 1978, *J. Chem. Phys.* **69**, 2992.
- Padiál, N., G. Csanak, B.V. McKoy and P.W. Langhoff, 1981a, *Phys. Rev. A* **23**, 218.
- Padiál, N., G. Csanak and P.W. Langhoff, 1981b, *J. Chem. Phys.* **74**, 4581.
- Parr, A.C., R. Stockbauer, B.E. Cole, D.L. Ederer, J.L. Dehmer and J.B. West, 1980, *Nucl. Instrum. Methods* **172**, 357.
- Parr, A.C., D.L. Ederer, B.E. Cole, J.B. West, R. Stockbauer, K. Codling and J.L. Dehmer, 1981, *Phys. Rev. Lett.* **46**, 22.
- Parr, A.C., D.L. Ederer, J.B. West, D.M.P. Holland and J.L. Dehmer, 1982a, *J. Chem. Phys.* **76**, 4349.
- Parr, A.C., D. Ederer, J.L. Dehmer and D.M.P. Holland, 1982b, *J. Chem. Phys.* **77**, 111.
- Parr, A.C., S.H. Southworth, J.L. Dehmer and D.M.P. Holland, 1983, *Nucl. Instrum. Methods* **208**, 767.
- Parr, A.C., S.H. Southworth, J.L. Dehmer and D.M.P. Holland, 1984, *Nucl. Instrum. Methods* **222**, 221.
- Pavlovic, Z., M.J.W. Boness, A. Herzenberg and G.J. Schulz, 1972, *Phys. Rev. A* **6**, 676.
- Peatman, W.B., 1976, *J. Chem. Phys.* **64**, 4368.
- Peatman, W.B., B. Gotchev, P. Gürtler, E.-E. Koch and V. Saile, 1978, *J. Chem. Phys.* **69**, 2089.
- Piancastelli, M.N., P.R. Keller, J.W. Taylor, F.A. Grimm, T.A. Carlson, M.O. Krause and D. Lichtenberger, 1984, *J. Electron Spectrosc.* **34**, 205.
- Plummer, E.W., T. Gustafsson, W. Gudat and D.E. Eastman, 1977, *Phys. Rev. A* **15**, 2339.
- Poliakoff, E.D., J.L. Dehmer, D. Dill, A.C. Parr, K.H. Jackson and R.N. Zare, 1981, *Phys. Rev. Lett.* **46**, 907.
- Poliakoff, E.D., J.L. Dehmer, A.C. Parr and G.E. Leroi, 1982, *J. Chem. Phys.* **77**, 5243.
- Potts, A.W., H.J. Lempka, D.G. Streets and W.C. Price, 1970, *Philos. Trans. R. Soc. London A* **268**, 59.
- Pratt, S.T., E.D. Poliakoff, P.M. Dehmer and J.L. Dehmer, 1983a, *J. Chem. Phys.* **78**, 65.
- Pratt, S.T., P.M. Dehmer and J.L. Dehmer, 1983b, *J. Chem. Phys.* **78**, 4315.
- Pratt, S.T., P.M. Dehmer and J.L. Dehmer, 1983c, *J. Chem. Phys.* **79**, 3234.
- Pratt, S.T., P.M. Dehmer and J.L. Dehmer, 1984a, *Chem. Phys. Lett.* **105**, 28.
- Pratt, S.T., P.M. Dehmer and J.L. Dehmer, 1984b, *J. Chem. Phys.* **80**, 1706.

- Pratt, S.T., P.M. Dehmer and J.L. Dehmer, 1984c, *J. Chem. Phys.* **81**, 3444.
- Price, W.C., 1968, *J. Mol. Spectrosc.* **4**, 221.
- Pulm, H., B. Marquardt, H.-J. Freund, R. Engelhardt, K. Seki, U. Karlsson, E.-E. Koch and W. von Niessen, 1985, *Chem. Phys.* **92**, 457.
- Raoult, M., and Ch. Jungen, 1981, *J. Chem. Phys.* **74**, 3388.
- Raoult, M., Ch. Jungen and D. Dill, 1980, *J. Chim. Phys.* **77**, 599.
- Raoult, M., H. Le Rouzo, G. Raseev and H. Lefebvre-Brion, 1983, *J. Phys. B* **16**, 4601.
- Raseev, G., 1985, *J. Phys. B* **18**, 423.
- Raseev, G., and H. Le Rouzo, 1983, *Phys. Rev. A* **27**, 268.
- Raseev, G., H. Le Rouzo and H. Lefebvre-Brion, 1980, *J. Chem. Phys.* **72**, 5701.
- Raseev, G., H. Lefebvre-Brion, H. Le Rouzo and A.L. Roche, 1981, *J. Chem. Phys.* **74**, 6686.
- Rescigno, T.N., and P.W. Langhoff, 1977, *Chem. Phys. Lett.* **51**, 65.
- Rescigno, T.N., C.F. Bender, B.V. McKoy and P.W. Langhoff, 1978, *J. Chem. Phys.* **68**, 970.
- Richards, J.A., and F.P. Larkins, 1984, *J. Phys. B* **17**, 1015.
- Richards, J.A., and F.P. Larkins, 1986, *J. Phys. B* **19**, 1945.
- Ritchie, B., and B.R. Tambe, 1980, *J. Phys. B* **13**, L225.
- Robin, M.B., 1975, *Chem. Phys. Lett.* **31**, 140.
- Rohr, K., 1979, *J. Phys. B* **12**, L185.
- Roy, P., I. Nenner, M.Y. Adam, J. Delwiche, M.-J. Hubin-Franskin, P. Lablanquie and D. Roy, 1984, *Chem. Phys. Lett.* **109**, 607.
- Rumble, J.R., D.G. Truhlar and M.A. Morrison, 1981, *J. Phys. B* **14**, L301.
- Sachenko, V.P., V.E. Polozhentsev, A.P. Kovtun, Yu.F. Migal, R.V. Vedrinski and V.V. Kolesnikov, 1974, *Phys. Lett. A* **48**, 169.
- Samson, J.A.R., and J.L. Gardner, 1976, *J. Electron Spectrosc.* **8**, 35.
- Samson, J.A.R., and A.F. Starace, 1975, *J. Phys. B* **8**, 1806.
- Samson, J.A.R., J.L. Gardner and G.N. Haddad, 1977a, *J. Electron Spectrosc.* **12**, 281.
- Samson, J.A.R., G.N. Haddad and J.L. Gardner, 1977b, *J. Phys. B* **10**, 1749.
- Sasanuma, M., E. Ishiguro, H. Masuko, Y. Morioka and M. Nakamura, 1978, *J. Phys. B* **11**, 3655.
- Sasanuma, M., E. Ishiguro, T. Hayaisha, H. Masuko, Y. Morioka, T. Nakajima and M. Nakamura, 1979, *J. Phys. B* **12**, 4057.
- Sato, K., Y. Achiba and K. Kimura, 1984, *J. Chem. Phys.* **81**, 57.
- Schäfers, F., M.A. Baig and U. Heinzmann, 1983, *J. Phys. B* **16**, L1.
- Schirmer, J., and O. Walter, 1983, *Chem. Phys.* **78**, 201.
- Schirmer, J., L.S. Cederbaum, W. Domcke and W. von Niessen, 1977, *Chem. Phys.* **26**, 149.
- Schneider, B.I., and L.A. Collins, 1984, in: *Resonances in Electron-Molecule Scattering*, van der Waals Complexes and Reactive Chemical Dynamics, ACS Symposium Series, No. 263, ed. D.G. Truhlar (American Chemical Society, Washington, DC) ch. 5, p. 65.
- Schneider, B.I., M. LeDourneuf and Vo Ky Lan, 1979, *Phys. Rev. Lett.* **43**, 1926.
- Schönhense, G., V. Dzidzonou, S. Kaesdorf and U. Heinzmann, 1984, *Phys. Rev. Lett.* **52**, 811.
- Schulz, G.J., 1973, *Rev. Mod. Phys.* **45**, 422.
- Schulz, G.J., 1976, in: *Principles of Laser Plasmas*, ed. G. Bekefi (Wiley, New York) p. 33.
- Schwarz, W.H.E., T.C. Chang and J.P. Connerade, 1977, *Chem. Phys. Lett.* **49**, 207.
- Schwarz, W.H.E., L. Mensching, K.H. Hallmeier and R. Szargan, 1983, *Chem. Phys.* **82**, 57.
- Sell, J.A., and A. Kuppermann, 1978, *Chem. Phys.* **33**, 379.
- Sell, J.A., A. Kuppermann and D.M. Mintz, 1979, *J. Electron Spectrosc.* **16**, 127.
- Sette, F., J. Stöhr and A.P. Hitchcock, 1984, *J. Chem. Phys.* **81**, 4906.
- Shaw, D.A., G.C. King, F.H. Read and D. Cvejanovic, 1982, *J. Phys. B* **15**, 1785.
- Shaw, D.A., G.C. King, D. Cvejanovic and F.H. Read, 1984, *J. Phys. B* **17**, 2091.
- Shimamura, I., and K. Takayanagi, eds, 1984, *Electron-Molecule Collisions* (Plenum, New York).
- Simpson, J., C. Kuyatt and S. Mielczarek, 1966, *J. Chem. Phys.* **44**, 4403.
- Smith, M.E., R.R. Lucchese and V. McKoy, 1983, *J. Chem. Phys.* **79**, 1360.
- Sodhi, R.N.S., 1984, Ph.D. Thesis (Department of Chemistry, Univ. British Columbia).
- Sodhi, R.N.S., and C.E. Brion, 1984, *J. Electron Spectrosc.* **34**, 363.
- Sodhi, R.N.S., and C.E. Brion, 1985a, *J. Electron Spectrosc.* **36**, 187.

- Sodhi, R.N.S., and C.E. Brion, 1985b, *J. Electron Spectrosc.* **37**, 1.
Sodhi, R.N.S., and C.E. Brion, 1985c, *J. Electron Spectrosc.* **37**, 97.
Sodhi, R.N.S., and C.E. Brion, 1985d, *J. Electron Spectrosc.* **37**, 125.
Sodhi, R.N.S., C.E. Brion and R.G. Cavell, 1984, *J. Electron Spectrosc.* **34**, 373.
Sodhi, R.N.S., S. Daviel, C.E. Brion and G.G.B. de Souza, 1985, *J. Electron Spectrosc.* **35**, 45.
Southworth, S., W.D. Brewer, C.M. Truesdale, P.H. Kobrin, D.W. Lindle and D.A. Shirley, 1982b, *J. Electron Spectrosc.* **26**, 43.
Southworth, S.H., C.M. Truesdale, P.H. Kobrin, D.W. Lindle, W.D. Brewer and D.A. Shirley, 1982a, *J. Chem. Phys.* **76**, 143.
Southworth, S.H., A.C. Parr, J.E. Hardis and J.L. Dehmer, 1986, *Phys. Rev. A* **33**, 1020.
Starace, A.F., 1979, in: *Handbuch der Physik*, Vol. 31, ed. W. Mehlhorn (Springer, Berlin) p. 1.
Stephens, J.A., and D. Dill, 1983, in: *Abstracts of Papers, Proc. of the XIII Int. Conf. on the Physics of Electronics and Atomic Collisions*, eds J. Eichler, W. Fritsch, I.V. Hertel, N. Stolterfoht and U. Wille (ICPEAC e.V., Berlin) p. 34.
Stephens, J.A., and D. Dill, 1985, *Phys. Rev. A* **31**, 1968.
Stephens, J.A., D. Dill and J.L. Dehmer, 1981, *J. Phys. B* **14**, 3911.
Stockbauer, R., 1973, *J. Chem. Phys.* **58**, 3800.
Stockbauer, R., 1977, *Int. J. Mass Spectrom. & Ion Phys.* **25**, 89.
Stockbauer, R., 1980, *Adv. Mass Spectrom.* **8**, 79.
Stockbauer, R., and M.G. Inghram, 1975, *J. Chem. Phys.* **62**, 4862.
Stockbauer, R., and M.G. Inghram, 1976, *J. Chem. Phys.* **65**, 4081.
Stockbauer, R., B.E. Cole, D.L. Ederer, J.B. West, A.C. Parr and J.L. Dehmer, 1979, *Phys. Rev. Lett.* **43**, 757.
Stöhr, J., and R. Jaeger, 1982, *Phys. Rev. B* **26**, 4111.
Stöhr, J., J.L. Gland, W. Eberhardt, D. Outka, R.J. Madix, F. Sette, R.J. Koestner and U. Doebler, 1983, *Phys. Rev. Lett.* **51**, 2414.
Stöhr, J., F. Sette and A.L. Johnson, 1984, *Phys. Rev. Lett.* **53**, 1684.
Swanson, J.R., D. Dill and J.L. Dehmer, 1980, *J. Phys. B* **13**, L231.
Swanson, J.R., D. Dill and J.L. Dehmer, 1981a, *J. Chem. Phys.* **75**, 619.
Swanson, J.R., D. Dill and J.L. Dehmer, 1981b, *J. Phys. B* **14**, L207.
Tabché-Fouhailé, A., I. Nenner, P.-M. Guyon and J. Delwiche, 1981, *J. Chem. Phys.* **75**, 1129.
Tam, W.-C., and C.E. Brion, 1974, *J. Electron Spectrosc.* **3**, 281.
Tanaka, K., and I. Tanaka, 1973, *J. Chem. Phys.* **59**, 5042.
Teo, B.K., and D.C. Joy, eds, 1981, *EXAFS Spectroscopy, Techniques and Applications* (Plenum, New York).
Thiel, W., 1981, *Chem. Phys.* **57**, 227.
Thiel, W., 1982, *Chem. Phys. Lett.* **87**, 249.
Thiel, W., 1983, *J. Electron Spectrosc.* **31**, 151.
Tossell, J.A., 1985, *J. Phys. B* **18**, 387.
Tossell, J.A., and J.W. Davenport, 1984, *J. Chem. Phys.* **80**, 813.
Trajmar, S., and A. Chutjian, 1977, *J. Phys. B* **10**, 2943.
Tronc, M., G.C. King, R.C. Bradford and F.H. Read, 1976, *J. Phys. B* **9**, L555.
Tronc, M., G.C. King and F.H. Read, 1979, *J. Phys. B* **12**, 137.
Tronc, M., G.C. King and F.H. Read, 1980, *J. Phys. B* **13**, 999.
Truesdale, C.M., S.H. Southworth, P.H. Kobrin, U. Becker, D.W. Lindle, H.G. Kerkhoff and D.A. Shirley, 1983a, *Phys. Rev. Lett.* **50**, 1265.
Truesdale, C.M., S.H. Southworth, P.H. Kobrin, D.W. Lindle and D.A. Shirley, 1983b, *J. Chem. Phys.* **78**, 7117.
Truesdale, C.M., D.W. Lindle, P.H. Kobrin, U.E. Becker, H.G. Kerkhoff, P.A. Heimann, T.A. Ferrett and D.A. Shirley, 1984, *J. Chem. Phys.* **80**, 2319.
Truhlar, D.G., S. Trajmar and W. Williams, 1972, *J. Chem. Phys.* **57**, 3250.
Unwin, R., I. Khan, N.V. Richardson, A.M. Bradshaw, L.S. Cederbaum and W. Domcke, 1981, *Chem. Phys. Lett.* **77**, 242.

- van der Wiel, M.J., 1980, in: *Electronic and Atomic Collisions*, eds N. Oda and K. Takayanagi (North-Holland, Amsterdam) p. 209.
- van der Wiel, M.J., and Th.M. El-Sherbini, 1972, *Physica* **59**, 453.
- Vinogradov, A.S., B. Shlarbaum and T.M. Zimkina, 1974, *Opt. Spektrosk.* **36**, 658 [*Opt. Spectrosc.* **36**, 383].
- von Niessen, W., L.S. Cederbaum, G.H.F. Diercksen and G. Hohlneicher, 1975, *Chem. Phys.* **11**, 399.
- von Niessen, W., P. Kraemer and G.H.F. Diercksen, 1979, *Chem. Phys. Lett.* **63**, 65.
- Wallace, S., 1980, Ph.D. Thesis (Boston University).
- Wallace, S., D. Dill and J.L. Dehmer, 1979, *J. Phys. B* **12**, L417.
- Wallace, S., D. Dill and J.L. Dehmer, 1982, *J. Chem. Phys.* **76**, 1217.
- Wendin, G., 1981, in: *Structure and Bonding*, Vol. 45 (Springer, Heidelberg).
- Werner, A.S., B.P. Tsai and T. Baer, 1974, *J. Chem. Phys.* **60**, 3650.
- West, J.B., A.C. Parr, B.E. Cole, D.L. Ederer, R. Stockbauer and J.L. Dehmer, 1980, *J. Phys. B* **13**, L105.
- West, J.B., K. Codling, A.C. Parr, D.L. Ederer, B.E. Cole, R. Stockbauer and J.L. Dehmer, 1981, *J. Phys. B* **14**, 1791.
- White, M.G., R.A. Rosenberg, G. Gabor, E.D. Poliakoff, G. Thornton, S.H. Southworth and D.A. Shirley, 1979, *Rev. Sci. Instrum.* **50**, 1288.
- White, M.G., K.T. Leung and C.E. Brion, 1981, *J. Electron Spectrosc.* **23**, 127.
- White, M.G., M. Seaver, W.A. Chupka and S.D. Colson, 1982, *Phys. Rev. Lett.* **49**, 28.
- White, M.G., W.A. Chupka, M. Seaver, A. Woodward and S.D. Colson, 1984, *J. Chem. Phys.* **80**, 678.
- Wight, G.R., and C.E. Brion, 1974a, *J. Electron Spectrosc.* **3**, 191.
- Wight, G.R., and C.E. Brion, 1974b, *J. Electron Spectrosc.* **4**, 313.
- Wight, G.R., and C.E. Brion, 1974c, *J. Electron Spectrosc.* **4**, 327.
- Wight, G.R., and C.E. Brion, 1974d, *J. Electron Spectrosc.* **4**, 335.
- Wight, G.R., and C.E. Brion, 1974e, *J. Electron Spectrosc.* **4**, 347.
- Wight, G.R., C.E. Brion and M.J. van der Wiel, 1972/73, *J. Electron Spectrosc.* **1**, 457.
- Wight, G.R., M.J. van der Wiel and C.E. Brion, 1976, *J. Phys. B* **9**, 675.
- Williams, G.R.J., and P.W. Langhoff, 1981, *Chem. Phys. Lett.* **78**, 21.
- Wilson, W.G., K.S. Viswanathan, E. Sekreta and J.P. Reilly, 1984, *J. Phys. Chem.* **88**, 672.
- Winick, H., and S. Doniach, eds, 1980, *Synchrotron Radiation Research* (Plenum, New York).
- Woodruff, P.R., and G.V. Marr, 1977, *Proc. R. Soc. London Ser. A* **358**, 87.
- Wu, C.Y.R., and C.Y. Ng, 1982, *J. Chem. Phys.* **76**, 4406.
- Zimkina, T.M., and V.A. Fomichev, 1966, *Dokl. Akad. Nauk SSSR* **169**, 1304 [*Sov. Phys.-Dokl.* **11**, 726].
- Zimkina, T.M., and A.S. Vinogradov, 1971, *J. Phys. Colloq. (France)* **32**, 3.